Dissertation
submitted to the
Combined Faculties of the Natural Sciences and Mathematics
of the Ruperto-Carola-University of Heidelberg, Germany
for the degree of
Doctor of Natural Sciences

Put forward by

Sergei Kobzak

born in Tiraspol, Moldova
Oral examination: June 24, 2020

Transition from bound to single independent nucleons in strong fields

Referees: **PD Dr. Adriana Pálffy-Buß**
Prof. Dr. Georg Wolschin

Zusammenfassung

Experimentelle Entwicklungen im Bereich der Petawatt-Laser versprechen die Verfügbarkeit von starken Zeptosekunden-Lichtpulsen mit Photonen-Energien von mehreren MeV in der nahen Zukunft. Die Wechselwirkung solcher Pulse mit Atomkernen wird Zugang zu Parameterbereichen mit hoher Kernanregungs-Energie und niedrigem Drehimpuls ermöglichen, welche bisher unerforscht geblieben sind. In dieser Dissertation wird zum ersten Mal das Sudden-Regime der Laser-Nukleus Wechselwirkung, in dem Multi-Photonen-Absorption schneller abläuft als der Atomkern equilibriert, untersucht. Wir konstruieren eine Mastergleichung, die den zeitlichen Ablauf des nuklearen Zustandes beschreibt, basierend auf den folgenden zugrundeliegenden Prozessen: Dipolabsorption, stimulierte Dipolemission, Equilibrierung und Neutronen-Evaporation. Die Equilibrierung wird durch die Berücksichtigung der Kopplung verschiedener Zustände mit unterschiedlicher Teilchen- und Loch-Zahl bei konstanter Energie behandelt. Wir benutzen moderne Matrixexponential-Solver basierend auf der Tschebyschevschen Rational-Näherungsmethode, um die Mastergleichung numerisch zu lösen. Die Ergebnisse zeigen ein Zusammenspiel zwischen Photonenabsorption und nuklearer Equilibrierung, sowie dessen Auswirkungen auf Neutronenemission. Unsere quantitativen Schätzungen sagen den Anregungspfad sowie den Bereich von Atomkernen vorher, der durch Neutronenzerfall zur protonen-reichen Seite der Nuklidkarte erreicht werden kann, und stellen relevante Informationen für die Entwicklung zukünftiger Experimente zur Verfügung.

Abstract

Experimental developments in the field of petawatt lasers promise to provide in the near future strong zeptosecond multi-MeV photon pulses. The interaction of such pulses with nuclei would provide access to regimes so far unexplored of high nuclear excitation energy and low angular momentum. In this thesis we investigate theoretically for the first time the sudden regime of laser-nucleus interaction, in which multiple photon absorption occurs faster than the nucleus has time to equilibrate. We construct a master equation that determines the temporal evolution of the nuclear state starting from the underlying processes: dipole absorption, stimulated dipole emission, equilibration and neutron evaporation. Equilibration is taken into account by considering the coupling of states with different particle-hole numbers at constant energy. We use state-of-the-art matrix exponential solvers based on the Chebyshov rational approximation method to solve numerically the master equation. The results show the interplay between photon absorption and nuclear equilibration and its effects on neutron emission. Our quantitative estimates predict the excitation path and range of nuclei reached by neutron decay towards the proton-rich region of the nuclide table and provide relevant information for the layout of future experiments.

Within the framework of this thesis, the following article has been submitted for publication in peer-reviewed journal:

Laser-Nucleus Interactions: Towards the Sudden Regime
Sergei Kobzak, Hans A. Weidenmüller, and Adriana Pálffy
arXiv:2005.04981 [nucl-th] (2020).

Moreover, the following article is in preparation:
Spreading width for nuclear equilibration
Sergei Kobzak, Adriana Pálffy and Hans A. Weidenmüller

Contents

Introduction

Recent experimental progress in the field of petawatt lasers and relativistic ion beams hold promise to soon produce multi-MeV zeptosecond photon beams. These are pursued at several facilities around Europe, such as the Nuclear Pillar of the Extreme Light Infrastructure (ELI-NP) [1] in Romania, International Center for Zetta- and Exawatt Science and Technology (IZEST) [2] in France, and partially in the development of so-called Gamma Factories [3, 4] at CERN. Once available, such ultra-short and intense MeV photon beams would offer new possibilities to investigate laser-nucleus interactions.

One of the pursued avenues to generate MeV photons at ELI is Compton backscattering of an optical laser pulse on a 'relativistic flying mirror' [5]. In the first step, a petawatt laser pulse hits a thin carbon foil and a bunch of electrons are emitted and accelerated from its surface. These electrons then form a relativistic flying mirror. In the second step, another laser pulse gets Compton backscattered on the electronic mirror [6–13]. That increases the central energy and the energy spread of the photons in the back-scattered pulse by a factor $4/(1-(v_e/c)^2) = 4\gamma_e^2$ [6], where c is the speed of light, v_e is the velocity of the ejected electrons, and γ_e their relativistic Lorentz factor. In principle, photon energies $\hbar\omega_0$ in the MeV range and beyond can be reached, accompanied by corresponding energy spreads σ in the 10 keV range. Allegedly, in practice so far only backscattered photons in the ultraviolet have been achieved. Apparently, an additional step is required in order to boost the photon energy towards the MeV range. The electrons in the relativistic flying mirror must be compressed to a solid-state value mean density [8].

Theoretical predictions show that even without notable coherence properties, such MeV beams could bring the nuclear photoexcitation rate close to MeV values similar to the spreading widths of the Giant Dipole Resonance [14]. The pulse parameters such as number N of MeV photons, pulse energy spread σ, and the opening angle α, define the rate of photon absorption. A short laser pulse with energy spread of 10 keV, opening angle of 10^{-2} rad and 10^8 photons should be sufficient to yield the effective dipole width $N\Gamma_{\mathrm{dip}}$ in the range of several MeV. Gamma photon absorption leads to the excitation of single nucleons. This process is in competition with the nuclear residual interaction, which has no counterpart in atoms and has the tendency to drive the system towards statistical equilibrium [15]. The laser energy absorbed by single nucleons is thereby distributed among all nucleons on a time scale governed by the so-called nuclear spreading width $\Gamma^{\downarrow}$ [16]. The ratio between the effective dipole and the nuclear spreading widths determines the regime of interaction.

In the perturbative regime [17], $\Gamma^{\downarrow} \gg N\Gamma_{\mathrm{dip}}$, the relaxation time is much

shorter than the time between two constitutive photon absorptions. Hence, the nucleus experiences excitations as single-photon absorptions, which lead to collective dipole mode. In the quasi-adiabatic regime [18, 19], $\Gamma^{\downarrow} \approx N\Gamma_{\mathrm{dip}}$, the rate of photon absorption attains values similar to those of nuclear relaxation rate. This allows the nucleus to equilibrate after each consecutive photon absorption. This in turn supports the absorption of the next photon leading to multi-photon excitation and to the formation of a compound nucleus, i.e., a nucleus with many excited nucleons, which has just modest angular momentum. Theoretical studies have shown that multiple photon absorption may produce compound nuclei in the so-far unexplored regime of several hundred MeV excitation energies [18, 19]. Due to successive neutron evaporation, the decay products of the laser-nucleus reaction are expected to be proton-rich isotopes far from the valley of stability. Finally, the sudden regime, so far not addressed, is characterized by fast photoexcitation in comparison to nuclear relaxation, $\Gamma^{\downarrow} \ll N\Gamma_{\mathrm{dip}}$. The nucleus does not have enough time to attain equilibrium between two consecutive photon absorption processes. As a result, the nucleons are excited independently. A laser pulse of sufficiently long duration could lead to the evaporation of the nucleus.

A very important quantity for the compound nucleus excited by MeV photon pulses are the level densities that characterize the nucleus at high excitation energies. Knowledge of the level densities is required to determine all the rates that determine the laser-nucleus interaction: the photon absorption, equilibration or neutron emission rates. Nuclear level densities pose a large interest in nuclear physics and are quantities of high importance. One of the first attempts to calculate them was made by Bethe in 1936 [20]. The calculation of particle-hole densities followed more than 20 years later and was put forward by Ericson in Ref. [21]. A refinement of Ericson's results was presented in the 1980s by Obložinský in Ref. [22]. More recently, the study in Ref. [23] showed for a large number of particles that the densities have Gaussian form and proposed an improvement of this Gaussian distribution. However, the majority of works addressed only constant spacing model, which approximately describes single-particle energy distributions in light-weight nuclei. In Ref. [24] a new transparent method for the calculation of the densities using a more realistic single-particle spacing was proposed. From different single-particle models of single-particle density, including approximations for medium-weight and heavy nuclei, the total level density and the density of accessible states were derived. Also a recipe for the calculation of the densities for different particle-hole classes was presented.

This thesis investigates for the first time the sudden regime of laser-nucleus interaction, following the study of the two other regimes: perturbative [17] and quasi-adiabatic regime [18, 19]. Upon excitation, multiple photon absorptions by a nucleus in its ground state lead to the creation of particle-hole pairs. The energy that is brought into the nucleus via photoexcitation is distributed among the nucleons by means of nucleon-nucleon collisions. This redistribution of energy is of stochastic nature and couples classes of different number of particle-hole pairs. The sudden regime assumes that between consecutive absorptions of single photons the nucleus does not attain full equilibrium.

However, we assume that equilibrium within the same class of particle-hole pairs is instantaneous. Besides photon absorption and nuclear equilibration, processes such as induced photon emission, neutron evaporation, excitation of a nucleon into continuum and induced fission can take place.

Our approach is based on the master equation describing the excitation and relaxation of the nucleus under the influence of the external field provided by the laser. We restrict our investigation to the most important competing processes: photoexcitation (with both absorption and stimulated decay), equilibration and neutron evaporation. Multiple absorption of coherent photons leads to nuclear excitation far above yrast. Setting up the master equation requires, therefore, the knowledge of corresponding rates, which are related to the $n$particles-$n$holes level densities ρ at high excitation energies and for large particle numbers A, expressed in terms of the single-particle level density ρ_1. For this we use the method described in Ref. [24]. We use state-of-the-art matrix exponential solvers based on the Chebyshov rational approximation method to solve numerically the master equation.

The numerical calculation of the occupation probabilities for the nucleus shows that in the absence of neutron evaporation, the excitation reaches saturation. This phenomenon was also predicted for the quasi-adiabatic case. The saturation energy coincides with the maximum of the total level density and marks the point where dipole absorption becomes less probable than stimulated dipole emission. Investigation of occupation probabilities of different particle-hole classes shows that the saturation process can occur at different times in each class, up to reaching the saturation point of the entire nucleus. However, the presence of neutron evaporation changes this picture. Neutron evaporation dominates the photon absorption at energies lower than the saturation point. This leads to production of new daughter nuclei rather than saturation in the target nucleus. Photon absorption is still required for the neutron evaporation to take place in the next generation of nuclei. A long enough laser pulse may result in many neutron evaporations leading to the production of proton-rich nuclei far from the valley of stability. A comparison between the sudden and quasi-adiabatic regime results from Ref. [19] shows that surprisingly, neutron evaporation occurs faster when after each photon absorption, the equilibration takes place instantaneously. Qualitative arguments are presented on why this is the case. They are related to the inherent time required for equilibration of the nucleus when photoabsorption from the ground state commences, as well as with the particular assumptions of our calculation.

We structure the thesis is as follows. In Chapter I, first we explain basic concepts of photoexcitation process and the relevant processes that can occur in the nucleus. We make a parallel to the concept of compound nucleus, explain the nature and how neutron evaporation process works. After that we introduce the master equation and the relevant transition rates of the processes that we consider. Chapter II is devoted to the densities of states, including the densities for different particle-hole numbers and densities of accessible states for two models of single-particle density, corresponding to constant spacing and more realistic linear model for medium-weight nuclei. Then Chapter III

provides details on the calculation of spreading width which is required for the nuclear equilibration rates. Finally, in Chapter IV we present and discuss our numerical results. The thesis concludes with Summary and Outlook.

CHAPTER I
Photoexcitation

The laser-nucleus reactions are not a typical subject in nuclear physics. An interaction that differs from the atomic physics scenario is expected. Strong nuclear interaction is dominant in nuclei. As a result even the strong laser pulse described in Introduction perturbs the nucleus fairly weakly [19]. We consider sequential multi-photon absorption process of single photons with energies in MeV range. Photoexcitation of a nucleus via MeV photons allows us to apply the dipole approximation. Photon energy of, e.g. $E_L = 5$ MeV, correspond to wavenumber $k \sim 0.03$ fm^{-1}, while a nucleus of mass number $A \sim 100$ has radius $r \approx r_0 A^{1/3} \sim 7$ fm ($r_0 \sim 1.5$ fm being an empirical constant [25]), hence dipole approximation is justified: $kr \ll 1$.

We start with the description of the photoexcitation mechanism and how it results in the formation of a system similar to a compound nucleus. We then talk about the consequences it brings and in the last two sections develop a way to calculate evolution of the system and describe the processes taking place under laser-nucleus interaction.

I.1 Basic concepts of photoexcitation

In this section we discuss photoexcitation and introduce the different regimes of laser-nucleus interaction.

Each time a photon is absorbed by a target nucleus, a unit of spin is transfered and some nuclear state is populated by this absorption. Further in this paragraph we shall follow reasoning from Ref. [19]. Absorbing a single photon propagating in z–direction leads to population of nuclear states with $J_z = \pm 1$, changing the total spin of the nucleus with spin zero to $J = 1$. Absorbing two such photons produces nuclear states with $J_z = \pm 2$ and $J_z = 0$. This will give total spins $J = 2$ and $J = 0$ respectively. If we carry on and the nucleus absorbs n such photons then states with $J_z = \pm n, \pm(n-2), \pm(n-4), \ldots$ will be populated. The multiplicity of states with given $|J_z|$ can be expressed as $\binom{n}{k}$[1] with $2k = |J_z| + n$ or as $k = n/2, n/2+1, \ldots, n$ for n even and $k = (n+1)/2, (n+3)/2, \ldots, n$ for n odd. We note that for n even (odd) only even (odd) values of J_z and, thus, of total spin J can occur. The partition function $Z(J) = \binom{n}{k} - \binom{n}{k+1}$, with $2k = J + n$, is then approximated by the

[1] A combination, number of ways an unordered subset of k distinct elements can be chosen from a set of n elements, also known as binomial coefficient: $\binom{n}{k} = \frac{n(n-1)\cdots(n-k+1)}{k(k-1)\cdots 1}$.

negative derivative of a combination $\binom{n}{k+1}$ with respect to k. Applying Stirling's formula we obtain

$$\begin{aligned} Z(J) &= -\frac{\mathrm{d}}{\mathrm{d}k}\binom{n}{k}\Big|_{k=(n+J)/2} \\ &\approx \ln\frac{n+J}{n-J}\exp\{n\ln n-(1/2)(n+J)\ln(n+J)/2 \\ &\qquad -(1/2)(n-J)\ln(n-J)/2\}\,. \end{aligned} \tag{I.1}$$

$Z(J)$ is positive and has a single maximum (see Fig. I.1). When J approaches n from the left[2] this function drops to small values in comparison to the maximum, which is around

$$J_0 \approx \sqrt{n}\,. \tag{I.2}$$

This shows that the average spin J_0 grows slowly (Eq. (I.2)), resulting in small spin values of the nucleus in comparison to total number of absorbed photons, e.g., even for a thousand of absorbed photons, the total spin is just around thirty spin units. Based on this justification further on we consider states and densities without spin [19].

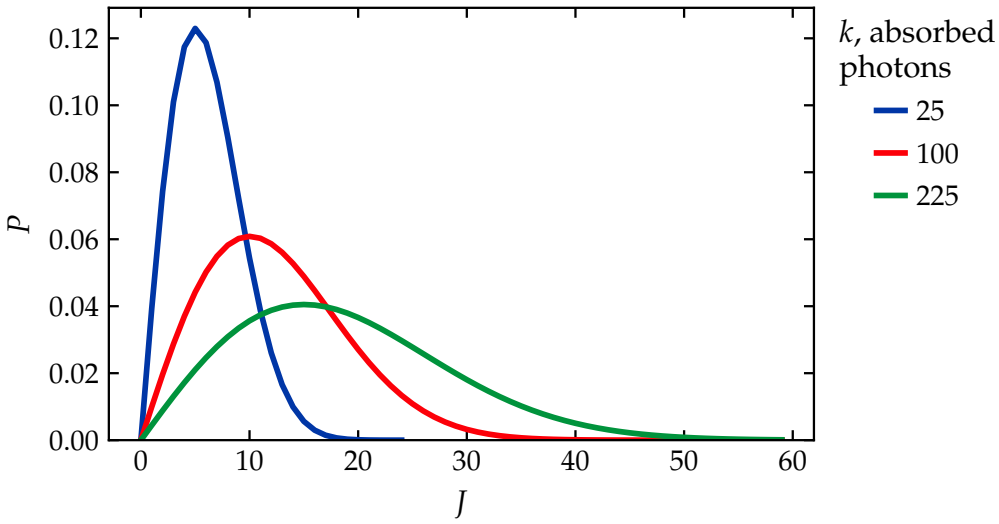

FIGURE I.1: Total spin distribution of a nucleus for different number of absorbed photons.

Definition 1. A yrast state is a state closest to the ground state of a nucleus with a given angular momentum. A collection of yrast states at different angular momenta forms a yrast line.

In excitation of isotopes via heavy ion collisions, the reaction products usually lie close to the yrast line. In contrast to this picture, photoexcitation allows small angular momentum transfer. Multiple photon absorption brings a nucleus to high excitation energies far above the states produced by heavy ion collisions at low angular momenta.

[2] $J \to n-\delta, \delta > 0, \delta \to 0$.

Further on we treat many aspects of nuclear structure in the framework of nuclear shell model. An extensive description of the model was given by M. Goeppert Mayer and J. H. D. Jensen in Ref. [26]. The model is analogous to Bohr atomic model in which electrons occupy energy levels. The shell model is a mean-field approach that leads to a central potential (later introduced as U_0), additionally residual nucleon-nucleon interactions are included. The potential U_0 determines quantized energy levels occupied by the nucleons. And the residual interactions cause nuclear equilibration. The nuclear shell model has a prominent impact on the nuclear physics by accurately predicting many nuclear properties of stable nuclei, such as magic numbers, total angular momentum, parity.

Further on we consider a nucleus as system of nucleons occupying energy levels of different shells, see Fig. I.2. For explanation of some of the processes taking place under laser-nucleus interaction we consider the nucleus as a Fermi-gas of protons and neutrons in finite single-particle potential. We draw a schematic analogy to a 'gas' stored in a vessel. The depth of this vessel corresponds to the depth of the potential well, which we denote as V. The gas occupies a volume up to the Fermi level F. This situation corresponds to a nucleus in the ground state. Photon absorption from this state leads to excitation of a particle to a single-particle state above the Fermi level, see Fig. I.3. Meanwhile the vacant spot below the Fermi level becomes a 'hole'. The particle and the hole form a particle-hole pair, following the notation in semiconductors physics.

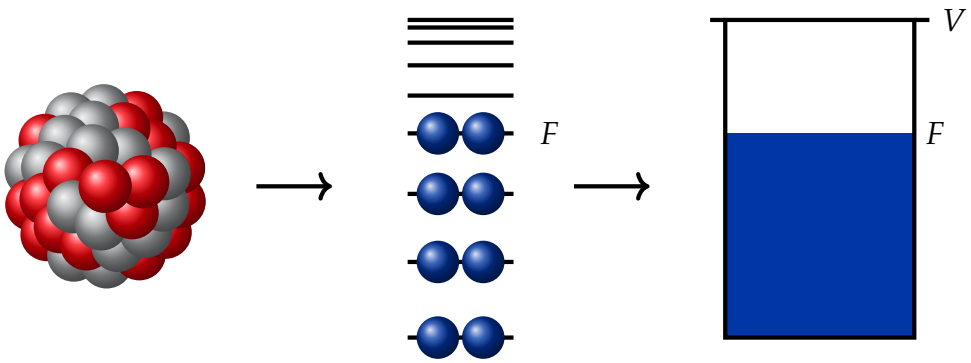

FIGURE I.2: Simplified representation of a nucleus.

In our investigation we shall consider the excitation of a nucleus via an intense zeptosecond photon beam. Upon absorption of one photon, a particle-hole pair is produced, see Fig. I.4. The energy of this pair is redistributed among the nucleons by means of the nuclear equilibration process. This produces more particle-hole pairs, each at lower energy than the initial pair, such that the total energy of the nucleus is conserved. Equilibration process occurs due to the interaction between the nucleons and has stochastic nature. If the photoexcitation rate is sufficiently large the nucleus may not have enough time to equilibrate. An interplay between characteristic timescales of nuclear equilibration and photoexcitation define the future evolution and behavior of the system.

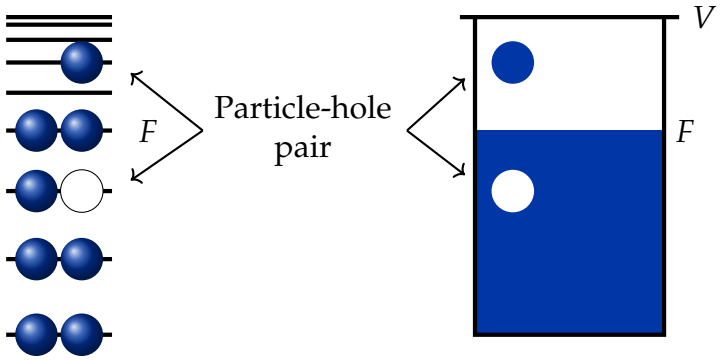

FIGURE I.3: A particle-hole pair.

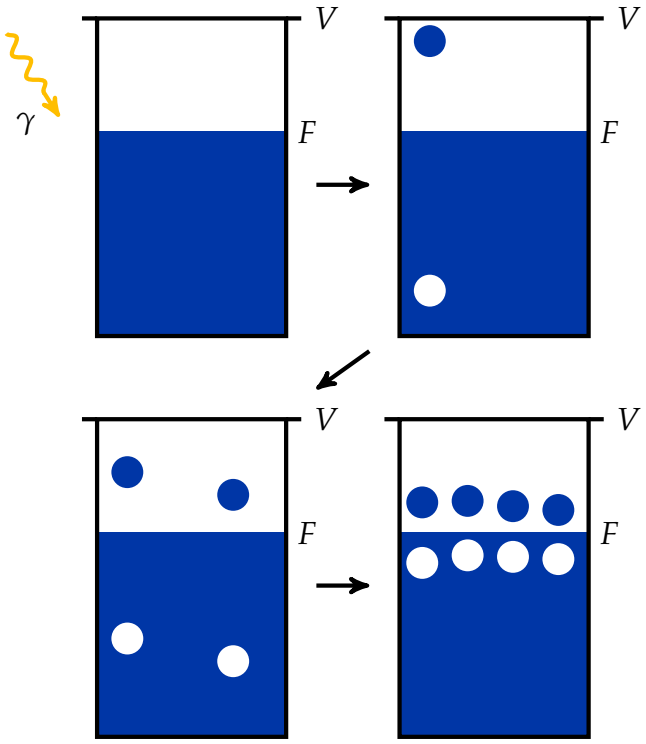

FIGURE I.4: Nuclear equilibration scheme after photon absorption.

Nuclear multi-photon excitation by laser pulses with $N \gg 1$ photons of several MeV and pulse duration of several hundreds zeptoseconds can lead to the following scenarios:

i) nuclear equilibration is much faster compared to excitation of a single nucleon,

ii) nuclear equilibration is comparable to excitation of a single nucleon,

iii) nuclear equilibration is much slower compared to excitation of a single nucleon.

Theoretical investigations of the first two scenarios were conducted before previously in Ref. [17, 19], respectively. Scenario i) corresponds to perturbative regime of laser-nucleus interaction. It is assumed that nuclear equilibration takes place after each photon absorption such that each photoexcitation is essentially a single-photon absorption. This induces collective dipole mode. In quasi-adiabatic regime, scenario ii), the photons excite the nucleons at such a rate that the nucleus equilibrates after each photon absorption which supports the consecutive photoexcitation. This causes to multi-photon excitation and the formation of a compound nucleus, a low angular momentum system of many excited nucleons. Scenario iii) is the topic of the thesis. It describes sudden regime, which was not addressed so far. In this scenario multiple photon absorption occurs faster than the nucleus equilibrates. The photons come at such rate that the nucleus does not have time to redistribute the excitation energy and, hence does not equilibrate. Long enough laser pulse leads to neutron decay and induced nucleon emission. This regime gives rise to several exciting questions related to the nuclear equilibration process, nuclear structure, decay mechanisms, etc.

These scenarios can be quantitatively expressed via relations between two quantities: the width $\Gamma^{\downarrow}$ (so called 'spreading width') of the Giant Dipole Resonance and effective dipole width $N\Gamma_{\mathrm{dip}}$. The latter determines the dipole excitation in the case of large number of photons $N \gg 1$. Furthermore, Γ_{dip} is the standard nuclear dipole width. This dipole width divided by the Planck constant yields the rate for nuclear dipole absorption. This in turn was explicitly deduced in Ref. [14]. The pulse parameters such as number N of MeV photons, pulse energy spread σ, and the opening angle α, define the rate of photon absorption. A short laser pulse with energy spread of 10 keV, opening angle of 10^{-2} rad and 10^8 photons should be sufficient to yield the effective dipole width $N\Gamma_{\mathrm{dip}}$ in the range of several MeV. The rates for photon absorption and nuclear equilibration can be expressed through the characteristic time scales for these processes which are connected with rates via $\hbar$:

$$\tau_{\mathrm{dip}} = \hbar / \left(N\Gamma_{\mathrm{dip}}\right) ; \tau_{\mathrm{eq}} = \hbar / \Gamma^{\downarrow} .$$

For scenario i) we shall have $\tau_{\mathrm{dip}} > \tau_{\mathrm{eq}}$ which defines the perturbative regime of excitation, for scenario ii) we have the adiabatic regime: $\tau_{\mathrm{dip}} \approx \tau_{\mathrm{eq}}$, and iii) is the sudden regime defined by $\tau_{\mathrm{dip}} < \tau_{\mathrm{eq}}$. It is clear that the greater the number of coherent MeV photons, the more efficient excitation

process takes place. This leads to eventual escape of the particles from the common potential. For reference, the characteristic timescale of a nucleon traversing a nucleus, and hence interacting with other nucleons, is on the order of zeptosecond, i.e., 10^{-21} s and we shall consider time scales up to several hundreds of zeptoseconds.

I.2 Compound nucleus

The residual interaction of the shell model in the long-time limit results in an equilibrated system, which is called compound nucleus.

In this section a description of a compound nucleus and a mechanism of nuclear equilibration is given. In the end of the section we draw a parallel between a system formed by photoexcitation and a compound nucleus.

Definition 2. A compound nucleus represents an excited system of a target nucleus and a bombarding particle formed after the bombarding particle lost its energy to the target nucleus. This system shows relatively long lifetime of about 10^{-19} s in comparison to the formation time of about 10^{-21} s.

Although N. Bohr [27] initially suggested the idea of the formation of a compound nucleus in the reaction of neutron capture by a heavy nucleus, the concept has been generalized for an arbitrary particle a that gets within the range of nuclear forces of a particle X. From this moment the actual nuclear process starts and a compound system is formed. After that a break up of the system is possible via emission.

The interaction between nucleons is described via the strong force which binds the nucleons. Due to this strong interaction, as soon as particle a gets captured, the extra energy it has brought in is quickly distributed among all nucleons. This mixing of energy is so efficient, that at some time later none of the constituents of the compound system have enough energy to escape. But re-emission is possible. As energy is exchanged between the constituents via collisions, it will require a multiple of such collisions for the energy to be concentrated again on one of the nucleons close to the surface of the nucleus. This may lead to an excess of energy sufficient enough to liberate such a particle. This is a complicated process of rearrangement of energy by means of which the system 'forgets' the way it was formed. Thus the disintegration process is being determined by conserved quantities such as energy, angular momentum and parity. These are the only 'recollections' that the system has about the way it was formed. Hence we should separate formation of a compound system from its break up and treat them as independent from each other.

This was the main idea of Bohr's assumption, which states that there is no simple analogy to the well-known excitation mechanism in atomic physics. However this assumption has a main limitation: it does not work well for very light nuclei. The less nucleons are in the given nucleus, the less distinction there is between the mixing of energy and escape of a particle. The other limitation is that mechanisms may exist that prevent thorough mixing of energy,

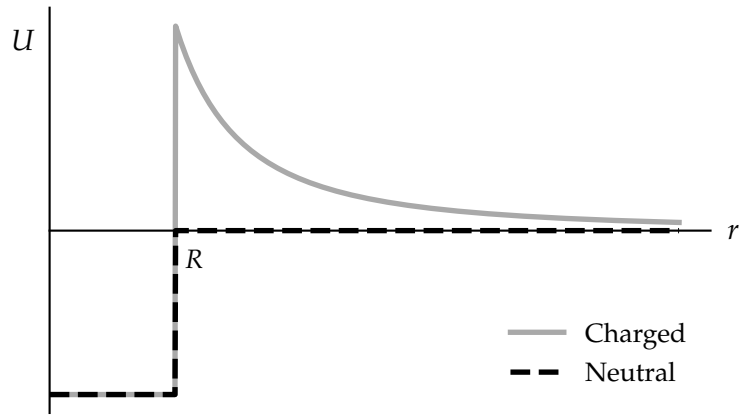

FIGURE I.5: Qualitative illustration of nuclear potential for charged and neutral particles with angular momentum $l = 0$.

such as Pauli's exclusion principle. The nucleons can occupy only available states, and Pauli's principle limits this number. The division of energy between all the constituents will not be as efficient as if there were no forbidden states.

As follows, the compound system does not keep track of the way it was formed, it does not matter what kind of particles bombard the target nucleus. Usually the naive picture of scattering is one where the bombarding particle is massive, e.g., a neutron or a proton. However, in our study we consider formation of a compound nucleus via photoexcitation.

I.3 Overcoming barriers. Neutron evaporation

During the course of laser-nucleus interaction neutron evaporation can take place. In this section we give a brief description of how this process can occur in a compound nucleus.

In general the effective approximate potential of the nucleus for a particle with angular momentum l and mass M is considered to be of the following [25]

$$\begin{aligned} U_l(r) &\cong -U_0 \quad (\text{ for } r < R), \\ U_l(r) &= V(r) + \frac{\hbar^2 l(l+1)}{2Mr^2} \quad (\text{ for } r > R)\,. \end{aligned} \tag{I.3}$$

A simplistic description assumes constant potential $-U_0$ inside the nucleus. However outside the nucleus an effective potential can be introduced which would be a sum of Coulomb $V(r)$ and centrifugal potential $\frac{\hbar^2 l(l+1)}{2Mr^2}$.

The probability for protons to escape the nucleus is much lower than for neutrons, since an additional Coulomb barrier for charged particles is present while there is none for neutral ones, the corresponding potentials are presented in Fig. I.5. In fact, to some extent the richer with protons the nucleus the harder it is for the protons to escape since the Coulomb barrier is higher.

The photon absorption leads to a creation of an excited states with several particle-hole pairs. After that via the nucleon-nucleon collisions nuclear equilibration process occurs. Photon absorption and nuclear equilibration alternate each other. Eventually the collisions lead to a situation where one of the high-energy nucleons receives enough excess energy to overcome the potential barrier and leaves the common potential. This produces a daughter nucleus in which the alternating processes restart and another neutron escapes.

As follows from Section I.2, a stochastic process is involved in the liberation of a neutron when significant energy is concentrated on it after many recollisions, i.e., many exchanges of initial excitation energy between constituents. In Fig. I.6 a scheme for neutron evaporation is presented. The process of neutron escape via this stochastic mechanism is sometimes called 'neutron evaporation'. This scenario cannot be initialized unless some excitation energy is already deposited into the system. The higher the excess of energy available, the higher the probability for neutron evaporation. After a neutron escapes a nucleus with mass number A, a daughter nucleus of mass number $A-1$ is formed. The escaped neutron will not carry away all the excitation energy. This results in an excited daughter nucleus. If the laser pulse continues, the initialization of yet another neutron evaporation in the daughter nucleus is possible and depends on the degree of excitation. This process can carry on if the laser pulse is not terminated and possesses significant number of photons, resulting in a chain of reactions producing proton-rich nuclei at high excitation energy far from the valley of stability.

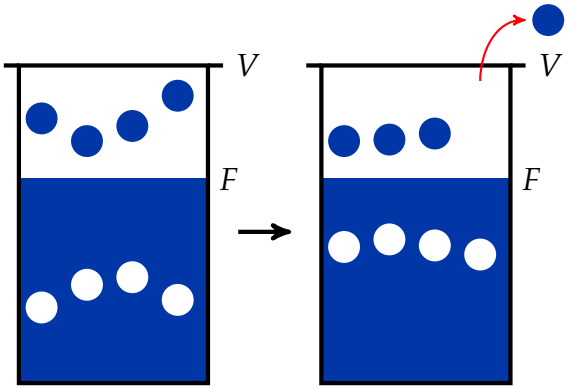

FIGURE I.6: Neutron evaporation scheme.

In the process of excitation by a laser pulse, additionally induced nucleon emission is possible. The height of the potential barrier is equal to the binding energy, which amounts to around 8 MeV above the Fermi level. In the course of excitation the occupation of states above the Fermi level grows, and so does the probability for direct excitation into continuum via photons of several MeV. However in the scenario of dipole excitation of nuclei and the timescales that we are going to consider ($A \sim 100$, $\tau \sim 100$ zs), the neutron evaporation is a dominant process [18] and we shall neglect induced emission of single nucleons completely.

I.4 Master equation for the sudden regime

In this section we construct the master equation accounting for photo-absorption, induced photon emission, nuclear equilibration and neutron evaporation with a brief description of these processes. The section concludes with the corresponding transition rates. For the derivation of the master equation we shall use the recipe from Ref. [28].

The time evolution of the compound nucleus will be described in terms of occupation probabilities with help of the master equation. We consider only cases with equal number of particles and holes. The occupation probability $P_m(i,k,t)$ depends on the variables:

- m—the number of particle-hole pairs or particle-hole class
- i—the nuclear species or generation, tells the number of lost neutrons
- k—the number of absorbed photons, tells what is the total excitation energy as the photon energy is fixed and denoted by E_L, i.e. $P_m(i,k,t) \equiv P_m(i,kE_L,t)$
- t—time.

The three main processes which define the dynamics of the system are:

i) nucleon-nucleon interaction, denoted by a mean squared matrix element $V^2_{m,m'}(i,k)$

ii) laser-nucleus interaction, denoted by a mean squared matrix element $W^2_{m,m'}(i,k,k')$

iii) neutron evaporation, denoted by neutron decay width $\Gamma_N(i,k,m)$,

The master equation for quasi-adiabatic regime differs by the absence of nuclear equilibration rates because the nuclear equilibration occurs almost instantaneously after each photon absorption in that regime.

However, the sudden regime implies that between consecutive absorptions of single photons the nucleus does not attain full equilibrium. However, we assume that equilibrium within the same class of particle-hole pairs is instantaneous. Our nucleon-nucleon interaction describes equilibration between classes with different number of particle-hole pairs. It will correspond to transitions between classes with m and m' particle-hole pairs. In such a process the energy of the system is conserved. The laser-nucleus interaction will be described by dipole absorption rate, while emission of photons by dipole emission rate, both responsible for population and depopulation of states at energies kE_L. Furthermore, the neutron evaporation will result in population of states of neighboring nuclei (which in turn undergo all aforementioned processes) with mass numbers $A-i$, where $i = 1,2,\ldots$ corresponds to the number of emitted neutrons from the target nucleus (target nucleus) with mass number A.

We start with the master equation for the target nucleus, i.e. $i = 0$, taking into account only nucleon-nucleon interaction. We consider a mean squared

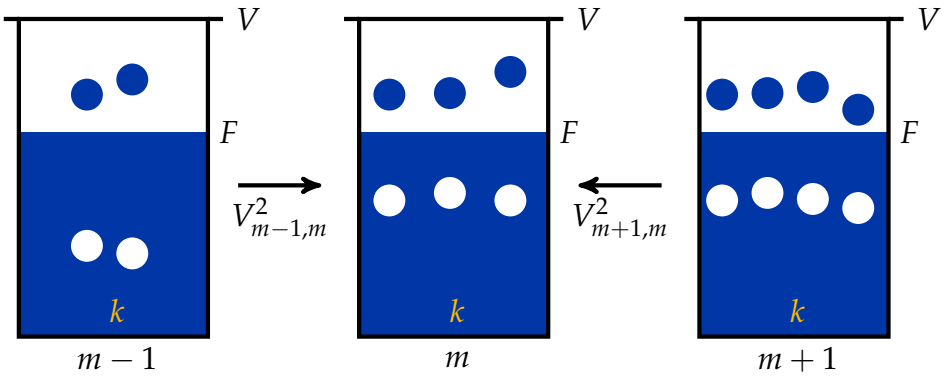

FIGURE I.7: Transitions into class m from neighboring classes $m-1$ and $m+1$ under nucleon-nucleon interaction.

matrix element $V^2_{mm'}(0,k)$, which couples class m with class m'. Such matrix elements satisfy: $V^2_{mm'}(0,k) = V^2_{m'm}(0,k)$ and $V^2_{mm}(0,k) = 0$. Introducing $\rho_m(i,k)$ (see Chapter II) as the mean density of states in class m in nucleus i at excitation energy kE_L and putting $\hbar = 1$ (so that further on we shall use terms 'rate' and 'width' interchangeably) we can write down our first master equation for the occupation probability. For target nucleus $i = 0$, hence for $P_m(0,k,t)$ we arrive to the following equation

$$\begin{aligned}\dot{P}_m(0,k,t) = &\sum_{m'\neq m} V^2_{m'm}(0,k)\rho_m(0,k)P_{m'}(0,k,t) \\ &- \sum_{m'\neq m} V^2_{mm'}(0,k)\rho_{m'}(0,k)P_m(0,k,t)\ .\end{aligned} \tag{I.4}$$

Here the positive terms describe gain of occupation probability due to feeding into class m from different classes (see Fig. I.7 for neighboring classes). The negative terms describe loss of occupation probability due to depletion from class m into different classes (considering only neighboring classes, it corresponds to reversing arrows in Fig. I.7). Altogether we consider only processes that couple neighboring classes $|m - m'| = 1$.

For photon absorption (stimulated emission) we shall consider only transitions from state k in class m to state $k+1$ ($k-1$) in class $m+1$ ($m-1$) and the inverse processes. The process involving photon absorption leads to a particle-hole pair creation while the stimulated emission leads to a particle-hole pair annihilation. We arrive to our second master equation, that modifies Eq. (I.4),

by inclusion of laser-nucleus interaction terms

$$\begin{aligned}\dot{P}_m(0,k,t) = &\sum_{m'\neq m} V^2_{m'm}(0,k)\rho_m(0,k)P_{m'}(0,k,t)\\ &- \sum_{m'\neq m} V^2_{mm'}(0,k)\rho_{m'}(0,k)P_m(0,k,t)\\ +\Theta(1/\sigma - t)\sum_{m'}\Big\{ &W^2_{m'm}\rho_m(0,k)P_{m'}(0,k-1,t)\\ &+W^2_{m'm}\rho_m(0,k)P_{m'}(0,k+1,t)\\ &-W^2_{mm'}\rho_{m'}(0,k+1)P_m(0,k,t)\\ &-W^2_{mm'}\rho_{m'}(0,k-1)P_m(0,k,t)\Big\}\,.\end{aligned} \tag{I.5}$$

Here the Heaviside step function $\Theta(1/\sigma - t)$ terminates the laser pulse at time $1/\sigma$. Similarly to Eq. (I.4) positive terms correspond to population of state k from neighboring energetic states $k-1$ and $k+1$ (see Fig. I.8) while negative terms correspond to the opposite process. Transitions with increasing k correspond to photon absorption process while transitions decreasing k correspond to stimulated photon emission.

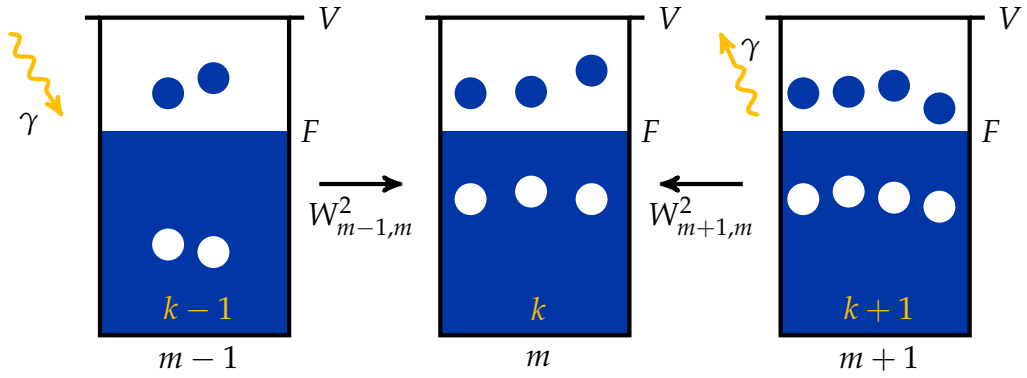

FIGURE I.8: Transitions into state k in class m from neighboring states at $k-1$ and $k+1$ in classes $m-1$ and $m+1$, respectively under laser-nucleus interaction.

At this point we are ready to introduce the last transition rate that will correspond to neutron decay. Denoting $\Gamma_N(0,k,m)$ as average neutron decay width of class m at excitation energy kE_L in target nucleus $i=0$ we arrive to

the following equation

$$\begin{aligned}\dot{P}_m(0,k,t) = &\sum_{m'\neq m} V^2_{m'm}(0,k)\rho_m(0,k)P_{m'}(0,k,t)\\ &- \sum_{m'\neq m} V^2_{mm'}(0,k)\rho_{m'}(0,k)P_m(0,k,t)\\ +\Theta(1/\sigma - t)\sum_{m'}\Big\{ &W^2_{m'm}\rho_m(0,k)P_{m'}(0,k-1,t)\\ &+W^2_{m'm}\rho_m(0,k)P_{m'}(0,k+1,t)\\ &-W^2_{mm'}\rho_{m'}(0,k+1)P_m(0,k,t)\\ &-W^2_{mm'}\rho_{m'}(0,k-1)P_m(0,k,t)\Big\}\\ &-\Gamma_{\mathrm{N}}(0,k,m)P_m(0,k,t)\ .\end{aligned} \tag{I.6}$$

As noted in Section I.3 neutron decay is not initialized unless several photons have been absorbed by the nucleus. Neutron evaporation in the target nucleus $i = 0$ populates a continuum of states in the daughter nucleus $i+1$. We cannot address a continuum of master equations. We turn to a simplification of the description to account for all the described processes in the nuclei with $i \geq 1$. We introduce a sum of occupation probabilities $P_m(i, E^*, t)$ over the energy interval $[(k-1/2)E_L, (k+1/2)E_L]$

$$\Pi_m(i,k,t) = \int_{(k-1/2)E_L}^{(k+1/2)E_L} \mathrm{d}E^* \rho_m\left(i,E^*\right) P_m\left(i,E^*,t\right)\ , \tag{I.7}$$

with $E^* = kE_L$ being the excitation energy of the nucleus. We simplify this expression even further by assuming smoothness of the densities and considering them approximately constant within intervals $[(k-1/2)E_L, (k+1/2)E_L]$. Within each such interval we introduce a number of states in class m

$$N_m(i,k) = \int_{(k-1/2)E_L}^{(k+1/2)E_L} \mathrm{d}E^* \rho_m\left(i,E^*\right) \approx \rho_m(i,k)E_L\ . \tag{I.8}$$

This finally brings us to a simplified expression for the sum of the probabilities

$$\Pi_m(i,k,t) \approx N_m(i,k)P_m(i,k,t)\ . \tag{I.9}$$

We generalize our master Eq. (I.6) to an arbitrary species i and take the sum over the energy interval $[(k-1/2)E_L, (k+1/2)E_L]$

$$\begin{aligned}
\dot{\Pi}_m(i,k,t) = &\sum_{m'\neq m} V^2_{m'm}(i,k)\rho_m(i,k)\Pi_{m'}(i,k,t)\frac{\rho_m(i,k)}{\rho_{m'}(i,k)} \\
&- \sum_{m'\neq m} V^2_{mm'}(i,k)\rho_{m'}(i,k)\Pi_m(i,k,t) \\
+\Theta(1/\sigma - t)\sum_{m'}\Big\{ &W^2_{m'm}\rho_m(i,k)\Pi_{m'}(i,k-1,t)\frac{\rho_m(i,k)}{\rho_{m'}(i,k-1)} \\
&+W^2_{m'm}\rho_m(i,k)\Pi_{m'}(i,k+1,t)\frac{\rho_m(i,k)}{\rho_{m'}(i,k+1)} \\
&-W^2_{mm'}\rho_{m'}(i,k+1)\Pi_m(i,k,t) \\
&-W^2_{mm'}\rho_{m'}(i,k-1)\Pi_m(i,k,t)\Big\} \\
+\sum_{k'm'} &\Gamma_N(i-1,k'\to k,m'\to m)\Pi_{m'}(i-1,k',t)\frac{\rho_m(i,k)}{\rho_{m'}(i-1,k')} \\
-&\Gamma_N(i,k,m)\Pi_m(i,k,t)\ ,
\end{aligned} \tag{I.10}$$

with $\Gamma_N(i-1,k'\to k,m'\to m)$ being the partial neutron decay width from species $i-1$, class m, state with k' absorbed photons to class m, state k in species i, so that the total width is $\Gamma_{\rm N}(i,k,m) = \sum\limits_{k'm'} \Gamma_{\rm N}\,(i,k\to k',m\to m')$. We consider a finite chain of reactions, hence in the final nucleus i_f the neutron decay is switched off ($\Gamma_{\rm N}(i_f,k,m)=0$). In our calculations the last daughter becomes a dump nucleus, where the flow of probability terminates after traveling from initial condition in target nucleus through all the intermediate species. We symmetrize and generalize the master equation in Appendix D. Eq. (D.6) has a more convenient and memorable form.

The master equation exhibits property of detailed balance, hence we have conservation of total probability

$$\sum_{i,k,m} \dot{P}_m(i,k,t) = 0\ . \tag{I.11}$$

We have constructed the master equation, however, ingredients are missing. In order to obtain the occupation probabilities $P_m(i,k,t)$ transition rates $V^2_{m,m'}$, $W^2_{m,m'}$, Γ_N are required. They in turn depend on the densities of states $\rho_m(i,k)$. We discuss the densities of states in Chapter II, while transition rates are discussed in the following section.

I.5 Transitions rates

I.5.1 Dipole absorption rate

For the dipole absorption rate in nuclear species i in a given class m at a given energy kE_L we consider transitions changing $m \to m+1$, $k \to k+1$. We note that the excitation of an already excited particle (hole) is possible but taking into account large number of particles (holes) available for excitation these possibilities are for a large range of energies unlikely, hence we neglect them altogether. We utilize the definition for the dipole absorption rate from Ref. [19], so that the effective dipole rate $N\Gamma_{\rm dip}$ is equated with $W^2_{01}(i,1)\rho_1(0,1)$. All the high-energy rates are calculated via densities of accessible states $\rho_{{\rm acc},m}(i,k)$ (see Ref. [24] and Section II.3) and $W^2_{01}(i,1)$

$$W^2_{mm+1}(i,k+1)\rho_{m+1}(i,k+1) = W^2_{01}(i,1)\rho_{{\rm acc},m+1}(i,k+1)\ . \tag{I.12}$$

Assuming that the matrix elements $W^2_{mm'}$ are symmetric under exchange of indices m, m', we can write a rate for dipole induced emission

$$W^2_{mm-1}(i,k-1)\rho_{m-1}(i,k-1) = W^2_{01}(i,1)\rho_{{\rm acc},m}(i,k)\frac{\rho_{m-1}(i,k-1)}{\rho_m(i,k)}\ . \tag{I.13}$$

I.5.2 Neutron evaporation rate

The neutron evaporation rates are simply expressed via the Weisskopf estimate [19]

$$\begin{aligned}\Gamma_N(i,k,m) &= \frac{1}{2\pi\rho(i,k)}\int_0^{(k+1/2)E_L-(V-F)} dE^*\rho_m\left(i+1,E^*\right)\\ \Gamma_N\left(i,k\to k',m'\right) &= \frac{1}{2\pi\rho(i,k)}\int_{(k'-1/2)E_L}^{(k'+1/2)E_L} dE^*\rho_{m'}\left(i+1,E^*\right)\ ,\end{aligned} \tag{I.14}$$

where $V-F$ is the binding energy of the neutron and only neutrons with excess energy can leave the compound nucleus i. The first expression is the rate for depletion of occupation probability of species i in class m at energy kE_L. The probability is transfered into a continuum of states up to the energy $(k+1/2)E_L-(V-F)$ in class m of species $i+1$, where $V-F$ is the energy needed to escape the common potential. The second expression is a partial feeding term into states in energy interval $[k'-1/2, k'+1/2]$ in class m of nuclear species $i+1$. After a particle leaves the nucleus Fermi level moves down. If prior to the shift of the Fermi level there was a particle at F then this particle will go above it. If there was hole at the Fermi level it will go above it and disappear. So that the class number will not change. Hence we consider neutron evaporation only within the same classes. However we assume the

values of F and V to be the same in a chain of several neighboring nuclear species and therefore disregard the odd-even staggering [29].

I.5.3 Nuclear equilibration rate

For the nuclear equilibration to happen, transitions coupling different particle-hole classes have to occur. Nuclear equilibration involves only mixing of states in different classes and with the total energy being conserved. Hence the transition rate $V^2_{mm'}(i,k)\rho_{m'}(i,k)$ characterizes a process at the same number k but between different m's: $m \neq m'$. As mentioned previously, we consider only processes that couple neighboring classes $|m - m'| = 1$. Another assumption is that within the same particle-hole class the equilibration is instantaneous.

A quantity extracted from the experiments that accounts for the nuclear equilibration is spreading width $\Gamma^{\downarrow}$ of the Giant Dipole Resonance. We equate $\Gamma^{\downarrow}_m$, the average spreading width of states in class m, with a sum of mean-squared matrix elements coupling states of class m with states of neighboring classes $m-1$ and $m+1$

$$\Gamma^{\downarrow}_m(i,k) = 2\pi \left[V^2_{mm-1}(i,k)\rho_{m-1}(i,k) + V^2_{mm+1}(i,k)\rho_{m+1}(i,k) \right] . \tag{I.15}$$

Then, we evaluate the terms on the r.h.s. of Eq. (I.15) separately. From the first term we get the averaged squared matrix element for transition $m \to m+1$

$$V^2_{mm+1} = \frac{1}{2\pi} \frac{\Gamma^{\downarrow}_{m\to m+1}}{\rho_{m+1}(i,k)} , \tag{I.16}$$

where $\Gamma^{\downarrow}_{m\to m+1}$ is calculated in Chapter III. Assuming the symmetry of matrix elements ($V^2_{m,m'} = V^2_{m',m}$) we arrive at an expression for the rate of an inverse process $m \to m-1$

$$V^2_{mm-1}(i,k)\rho_{m-1}(i,k) = \frac{1}{2\pi}\Gamma^{\downarrow}_{m-1\to m} \frac{\rho_{m-1}(i,k)}{\rho_m(i,k)} . \tag{I.17}$$

This symmetry is required by the detailed balance of the master equation.

All the transition rates are expressed through the level densities and/or the densities of accessible states. We present calculation of the required densities in the following chapter.

CHAPTER II
Densities of states

Definition 3. Density of states is the number of states available for occupation at a given energy or energy interval.

As one may have already noticed, the density of states $\rho_m(i,k)$ plays an important role in our approach. It enters both master equation (Eq. (I.10)) and transitions rates (Eqs. (I.12), (I.14) and (I.16)). The quantity $\rho_m(i,k)$ denotes a mean density of states in class m in nucleus i in energy interval $[(k-1/2)E_L,(k+1/2)E_L]$ and it is measured in number of configurations (states) per unit energy. We are going to conduct all our reasoning in the framework of nuclear shell model [26], where the nucleons are distributed over energetic levels. Here a parallel to atomic shell model can be drawn, where different atomic shells are occupied by electrons.

We start from a general picture of total nuclear level density and conclude with a more detailed picture for particle-hole level densities. Alongside we shall obtain the densities which are required for the description of population of accessible states in the dipole laser-nucleus interaction.

II.1 Total level density

Canonically in nuclear physics one describes the *nuclear level density* which is the number of nuclear levels per unit energy at given excitation energy E. Here 'nuclear levels' are understood as the energy levels that a given nucleus as a whole can occupy, and should not be confused with energy levels which a single nucleon of the nucleus can occupy. The latter will be addressed as *single-particle levels*.

One of the first attempts to calculate the nuclear level density was done by Hans Bethe [20]. In his work he derived nuclear level density for a system of unbound nucleons as a function of excitation energy E, considering the continuous approximation of independent particle energy levels

$$\rho(E) = \frac{1}{\sqrt{48}E} e^{\sqrt{\frac{2}{3}Ed}}, \tag{II.1}$$

where d is average spacing around Fermi level, which is assumed to be constant.

In Ref. [30] a system of A noninteracting fermions with given angular momentum J at excitation energy E is considered. The general expression for

total level density is given as

$$\rho_{\mathrm{tot},A}(E,J) = \rho_{\mathrm{tot},A}(E)\frac{2J+1}{2\sigma^3\sqrt{2\pi}}\exp\left\{-\frac{(J+1/2)^2}{2\sigma^2}\right\}, \tag{II.2}$$

where σ determines a spin cut-off factor. As can be seen the dependence on total angular momentum is factored out. As mentioned previously in Section I.1, we disregard spin and consider only $\rho_{\mathrm{tot},A}(E)$. This quantity describes how many configurations a system of A nucleons at a given excitation energy E can have, assuming that each nucleon can occupy a single-particle state with energy ε_i, so that the total energy of the system is a sum of all energies of occupied states, i.e. $E = \sum_i \varepsilon_i$. Further on we derive the level density, making the following assumptions:

- The nucleons are non-interacting.
- The potential well is constant. Each single nucleon sees a common potential formed by $A-1$ nucleons. This potential depends on a particular arrangement of the particles and excitation energy E. We expect this dependence to vary slowly with E;
- The potential well is of finite depth. This, in turn, causes the level density to have a bell-shape form (see Fig. II.2). Starting from the ground state it will grow with excitation energy à la Bethe's formula in Eq. (II.1), reaching a maximum and further on, representing inverse occupancy, it goes down towards the threshold state, a state in which all the particles are concentrated under the level with threshold energy of the potential.

One of the challenges in constructing level densities is that the range of values for number of states is quite drastic, going from 1 state (ground state) to $\sim 10^{30}$ for $A \approx 100$, for instance. It is hard to find a proper approximation, that will work throughout the spectrum of the level density. Our consideration of the density of states in this chapter will be strongly based on the results from Ref. [24]. Some derivations are rather lengthy, and we put them into Appendix A. Summarizing, A noninteracting spinless fermions with total excitation energy E are distributed over a finite number of single-particle levels B, which are described by a single-particle density $\rho_1(\varepsilon)$. An exact form for the level density $\rho_{\mathrm{tot},A}(E)$ is considered. Then a Fourier transform of $\rho_{\mathrm{tot},A}(E)$ with respect to E and alongside a Laplace transform with respect to A are performed. This results in analytical expressions for low cumulants of the single-particle densities $\rho_1(\varepsilon)$. On the other hand $\rho_{\mathrm{tot},A}(E)$ is expanded in orthogonal polynomials. Coefficients of this expansion are matched with approximation of Fourier transform of the level density in terms of cumulants. The calculation of cumulants is more convenient considering not a discrete single-particle density $\rho_1(\varepsilon)$ but rather a continuous one $\bar{\rho}_1(\varepsilon)$. We consider different continuous single-particle densities $\bar{\rho}_1(\varepsilon)$, namely:

- constant spacing $\bar{\rho}_1(\varepsilon) \propto \mathrm{const}$
- linear dependence $\bar{\rho}_1(\varepsilon) \propto \varepsilon$

- quadratic dependence $\bar{\rho}_1(\varepsilon) \propto \varepsilon^2$.

The constant spacing corresponds to light nuclei, the linear and quadratic cases to medium and heavy weight nuclei, respectively.

II.2 Level density of a particle-hole class

Inclusion of residual interaction in the description of laser-nucleus interaction requires distinction between different particle-hole classes, since equilibration happens via consecutive changes of classes. Particle-hole level density distinguishes between classes with different number of particles and holes.

A particular particle-hole class assumes a picture of an excited nucleus where some particles can be found above the Fermi level as well as some holes left behind due to excitations of single particles. In general, the number of particles and holes can be different from each other. For example, for neutron capture, the excitation brought by the neutron is shared to create a particle-hole pair, but the captured neutron adds to the number of particles above the Fermi level. If the system has in total A particles, then a class with h holes assumes that there are $A - h$ particles below the Fermi level. We shall interchangeably use a picture of h holes and $A - h$ particles below the Fermi level.

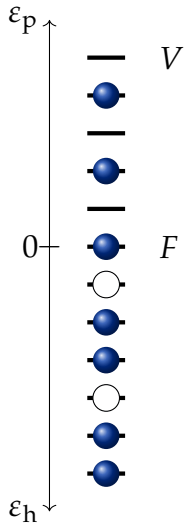

FIGURE II.1: Level scheme for a nucleus with constant spacing. Single-particle energies for particles and holes are counted on the axes labeled with ε_p and ε_h, respectively.

The level density of a class with p particles and h holes of a system at total excitation energy E can be expressed in the following way

$$\rho_{p,h}(E) = \sum_{E_p,E_h} \delta_{E_p+E_h,E}\ \rho_{\mathrm{tot},p}(E_p)\rho_{\mathrm{tot},h}(E_h)\ , \tag{II.3}$$

where $\rho_{\mathrm{tot},p}(E_p)$ is the level density at energy E_p of p particles with single-particle energies ranging from Fermi level F to the threshold level V, i.e.

absolute value of the depth of the potential, see Fig. II.1. In the same manner $\rho_{\mathrm{tot},h}(E)$ is the level density at energy E_h for h holes with single-particle energies ranging from 0 to F. In many parts of our work we shall consider only classes with equal number of particles and holes, i.e. integer number of particle-hole pairs, and denote level density for a class with m particles and m holes as: $\rho_{m,m} \equiv \rho_m$, for brevity. In this chapter we consider only one nuclear species, hence we omit the dependence on nuclear species i for brevity reasons as well.

According to Eq. (II.3), the level density which distinguishes between classes is just a convolution of two level densities at such energies that their sum is the total energy of the system. Hence we need the same method from Ref. [24] to calculate the particle-hole level density.

II.2.1 Constant spacing

Here we present the level densities for constant spacing, with the single-participle level spacing $d = V/B = F/A$, calculated using the method of Ref. [24]. The method proved to work very well in the center of the spectrum but fails in the tails. We present the calculation following this method in Appendix B. To obtain the values of the level density in the tails we use interpolation. The furthermost points in the tails of level densities in each class are approximated by the inverse of the single-particle level spacing. Fig. II.2 shows an example of such calculation for a system with mass number $A = 42$ with $B = 51$ single-particle states, $F = 37$ MeV, $V = 45$ MeV. In the following we consider a combinatorial calculation to see how well the method works for different number of particle-hole classes. The calculation is straightforward in

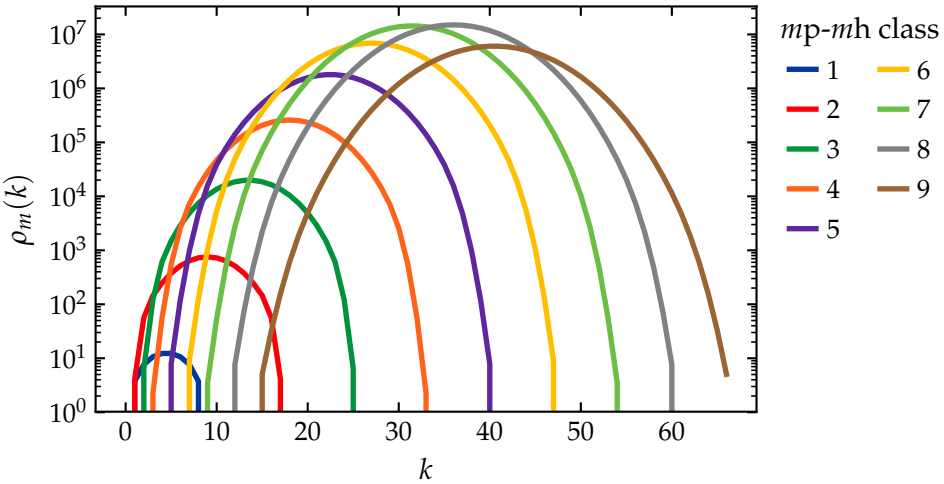

FIGURE II.2: Level density of different particle-hole classes for $A = 42$, constant spacing.

the case of equidistant constant spacing, however, two other cases (linear and quadratic dependence models) display increasing complexity.

We consider equidistant non-degenerate energy levels which start from level with number 1 and go up to level B. Each energy level can be occupied by only one particle. So 'energy level' and 'single-particle state' are the same

thing in the case of constant spacing. Because the spacing d is constant, the total energy of the system can be expressed as integer multiple of it: $E = \mathcal{E}d$. Now, the density of states $\rho_{\mathrm{tot},A}(E)$ will be the number of ways to distribute A particles over B levels so that the total energy of the system is equal to E. In other words it is the number of ways to sum up exactly A distinct numbers from the interval 1...B to get number $\mathcal{E}$, which is called *partition* in number theory and has the following generating function

$$\prod_{j=1}^{B}(1+yx^j) = \sum_{A,\mathcal{E}} C_{A,\mathcal{E}} y^A x^{\mathcal{E}} \ . \tag{II.4}$$

In this expression $C_{A,\mathcal{E}}$ is the partition of $\mathcal{E}$ into A distinct parts each not exceeding B. The power of y controls the number of parts (particles or occupied levels) and the power of x is the sum of the parts, i.e. corresponds to the 'energy' $\mathcal{E}$ (sum of the energies of each particle). So $C_{A,\mathcal{E}} = \rho_{\mathrm{tot},A}(E)$, with $E = \mathcal{E}d$.

In the same manner, the level densities for particles and holes in Eq. (II.3) are the corresponding coefficients in the sums on the right hand side the following equations

$$\prod_{j=A+1}^{B}(1+yx^j) = \sum_{p,E} C_{p,E} y^p x^E, \quad \prod_{j=1}^{A}(1+yx^{A-j+1}) = \sum_{p,E} \tilde{C}_{p,E} y^p x^E \ . \tag{II.5}$$

Then,

$$\prod_{j=1}^{A}(1+zx^{A-j+1}) \times \prod_{k=A+1}^{B}(1+yx^k) = \sum_{p,h,E_p+E_h} C_{p,h}^{E_p+E_h} y^p z^h x^{E_p+E_h} \ . \tag{II.6}$$

Only states with equal number of holes and particles are considered, so only coefficients at $y^p z^p$ (p particles, p holes) are of interest. Therefore the level density density of a class with p particles and p holes is

$$\rho_{p,p}(E) = C_{p,p}^{E} \ , \tag{II.7}$$

where $E = E_p + E_h$. Using this procedure it is very easy to calculate the densities.

Fig. II.3 shows a comparison between the calculation following the method in Ref. [24] and the combinatorial calculation. For both calculations we considered a nucleus with mass number $A = 42$ with $B = 51$ single-particle levels, the Fermi level $F = 37$ MeV, the depth of the potential well $V = 45$ MeV. The results show a good agreement between the two methods.

The results display for the particular case of 1p-1h states a peculiar plateau. This can be explained in a following way. The level density for this class has some maximum. But what puts an upper limit for the level density of 1p-1h class? The freedom of combinations is governed either by the number of possible states for the particle above the Fermi level or by the number of possible states for the hole below the Fermi level. To be more precise it is the minimum of two of these numbers. Indeed, for a given energy we can move

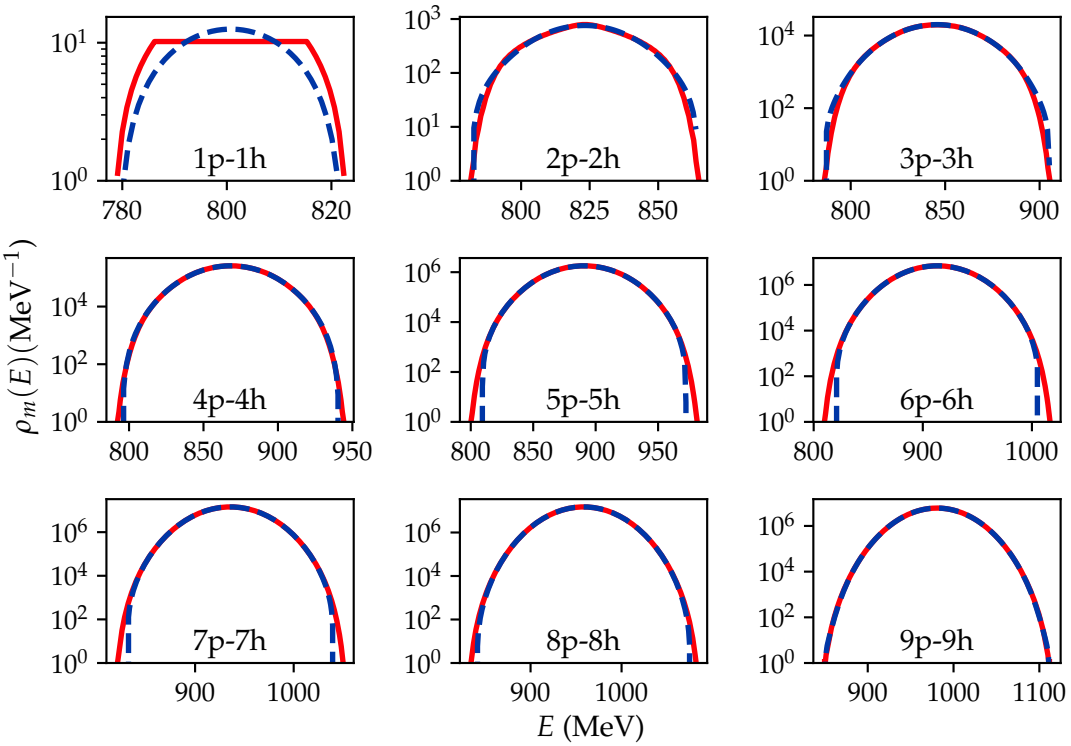

FIGURE II.3: ip-ih ($i = 1...9$) level density for constant spacing calculated via the exact combinatorial (red solid line) and and according to formalism in Ref. [24] (blue dashed line). The used parameters are $B = 51$, $A = 42$, $V = 45$ MeV, $F = 37$ MeV, $d = V/B = 0.88$ MeV.

particles and holes up and down the energy levels, simultaneously ensuring that the total energy remains unchanged. This is where the number of possible states plays a role for the boundary of the maximum of the density. We consider a system with B levels and A particles, where the number of single-particle states above the Fermi level is less than the number of single-particle states below the Fermi level ($B - A < A$). Let us start, for example, from the state in which 1 particle is 1 level higher than the Fermi level (which is denoted by level A since it is the highest occupied single-particle state for the ground state configuration), i.e. it is at level $A + 1$, and the hole is at least $B - A$ levels lower than the Fermi level, i.e. at least at level $A - (B - A) + 1$. Then we move this particle-hole pair up, keeping the same total energy, and count the number of possible states for this pair, and this number will be the number of possible states for the particle above the Fermi level. If at the start we put the hole deeper than $B - A$ levels below the Fermi level we shall still have the same exact number of possible states though the total energy will be greater than in previous case. And we can continue so until the hole is in the single-particle level 1. This way the number of single-particle states above the Fermi level defines the maximum of the 1p-1h level density when $B - A < A$. Also we can conclude that the length of the plateau for a fixed number of single-particle states above the Fermi level is governed by the number of single-particle states

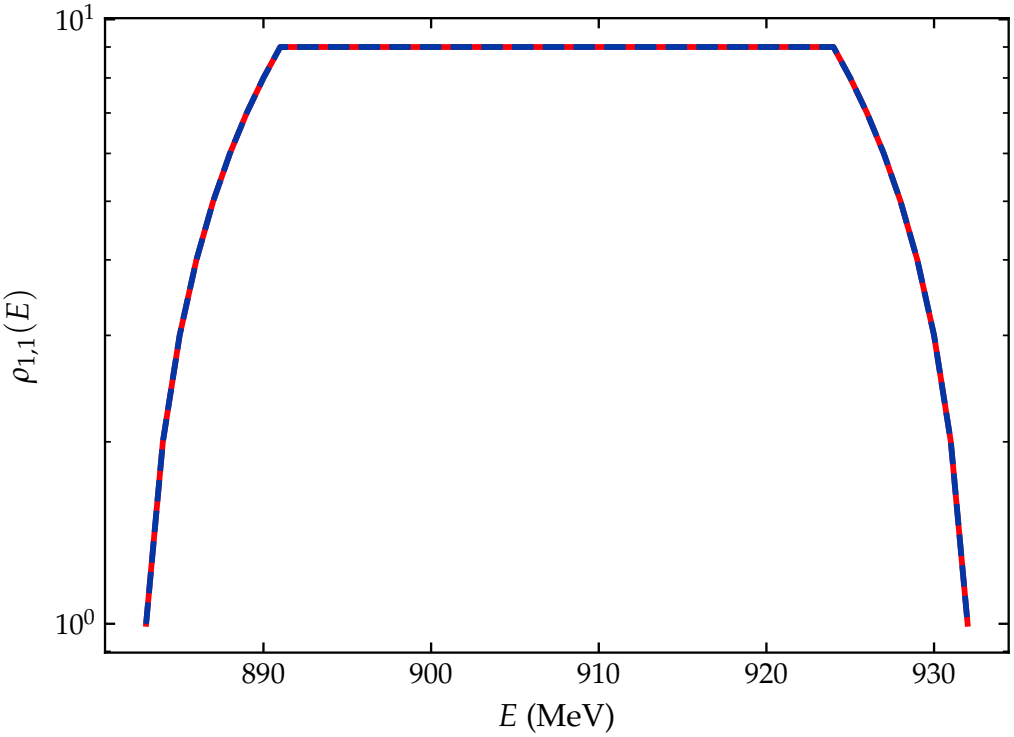

FIGURE II.4: Comparison of 1p-1h level density for constant spacing using exact combinatorial calculations (red solid line) and the method proposed by Obložinský [22] (blue dashed line). $B = 51$, $A = 42$, dimensionless spacing between levels is 1 energy unit.

below the Fermi level. This logic can be applied to the case when $B - A > A$, too, so that the length of plateau will be determined by the number of single-particle states above the Fermi level and the maximum of the density by the number of single-particle states below the Fermi level.

To check our results, we compare in Fig. II.4 our 1p-1h level densities to the results from [22], where the level density has the following form

$$\begin{aligned}\rho_{p,h}(E) =& \frac{g^{p+h}}{p!h!(p+h-1)!}\sum_{i=0}^{p}\sum_{j=0}^{h}(-1)^{i+j}\binom{p}{i}\binom{h}{j} \\ &\times \Theta\left(E-\alpha_{\mathrm{ph}}-i(V-F)-jF\right) \\ &\times \left(E-A_{\mathrm{ph}}-i(V-F)-jF\right)^{p+h-1} ,\end{aligned} \tag{II.8}$$

with

$$\begin{aligned}A_{\mathrm{ph}} &= \frac{1}{4}\frac{p^2+p}{g}+\frac{1}{4}\frac{h^2-3h}{g} , \\ \alpha_{\mathrm{ph}} &= \frac{1}{2}\frac{p^2+p}{g}+\frac{1}{2}\frac{h^2-h}{g} , \\ g &= 1/d .\end{aligned} \tag{II.9}$$

The agreement is excellent. The plateau appears at $B - A = 9$ states which is precisely the number of single-particle states above the Fermi level and it is less than the number of single-particle states below the Fermi level ($A = 42$). The length of the plateau is $A - (B - A) + 1 = 42 - 8 = 34$.

For the 2p-2h case there is also a small plateau. However, 2p-2h states with same energy can be achieved in more complex ways, such that our simple argument can no longer be applied to a general case of arbitrary number of particles and holes.

II.2.2 The case of linear dependence of single-particle density on the energy

The calculation of the level densities assumes that the single-particle density depends linearly on the single-particle energy

$$\bar{\rho}_1(\varepsilon) = \frac{2A}{F^2}\varepsilon \,. \tag{II.10}$$

The method presented in Ref. [24] is not confined to constant spacing. We follow this method again to calculate the level densities of particle-hole classes with a more realistic energy-dependent form $\bar{\rho}_1(\varepsilon) = \frac{2A}{F^2}\varepsilon$. We repeat the same steps that are carried out for the constant particle-hole level density up to replacement of the mass number A, the number B of single-particle levels the single-particle density $\bar{\rho}_1(\varepsilon)$. The calculation is carried out in Appendix C. The tails of the spectrum interpolated by taking the furthermost points as the inverse of the level spacing at those energies. Fig. II.5 shows a result for a system with mass number $A = 100$ with $B = 148$ single-particle states, $F = 37$ MeV, $V = 45$ MeV.

II.3 Density of accessible states

In this section we address the density $\rho_{\mathrm{acc}}(E)$ of accessible states, an important quantity which governs the transition rates in the process of dipole absorption resulting in a creation of a new particle-hole pair. The density $\rho_{\mathrm{acc}}(E)$ is defined for a process of excitation of a single nucleon from a many-body state at excitation energy E to another state at $E + \Delta E$. In both of these states the nucleus is assumed to be in thermal equilibrium. For a nucleus in a state with p-particles and p-holes at energy E we apply the Fermi-gas model for the particles and the holes, following the procedure from Ref. [24]. Then 2 Fermi-gases at thermal equilibrium are described by the following Fermi-distributions

$$n_{A-p,E_1}(\varepsilon) = \frac{\Theta(F-\varepsilon)}{1+\exp\{\beta_{E_1}\varepsilon + \alpha_{A-p,E_1}\}} \,, \tag{II.11}$$

$$n_{p,E_2}(\varepsilon) = \frac{\Theta(\varepsilon-F)}{1+\exp\{\beta_{E_2}\varepsilon + \alpha_{p,E_2}\}} \,, \tag{II.12}$$

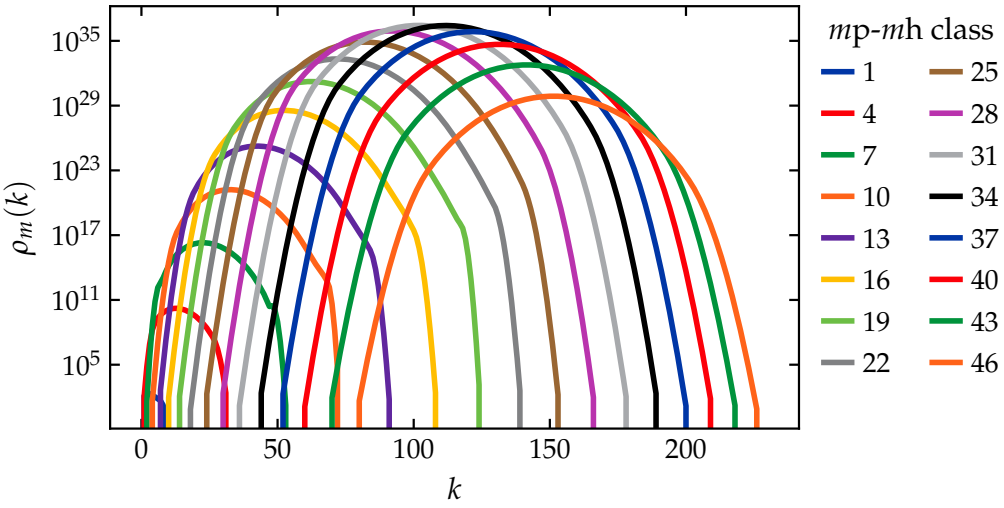

FIGURE II.5: Level density of different particle-hole classes for $A = 100$. Every third particle-hole class is presented. Colors correspond to different particle-hole classes. First blue line (lower left corner) corresponds to the class 1-particle – 1-holes. The class number grows with number of absorbed photons. Each 12 classes the color of the lines repeats and the last orange line (starts around $k = 80$) corresponds to the class 46-particles – 46-holes.

One gas represents the $A - p$ particles below the Fermi level and the other p particles above F. The total energy of the two gases is the sum of the particle and hole energies and equals to the total energy of the nucleus: $E = E_1 + E_2$. The parameters $\beta, \alpha_{A-p}, \alpha_p$ are deducted from the following conditions on numbers of particles and total energy of the system

$$\begin{aligned} A - p &= \int_0^F \mathrm{d}\varepsilon \, n_{A-p,E_1}(\varepsilon)\bar{\rho}_1(\varepsilon) \, , \\ p &= \int_F^V \mathrm{d}\varepsilon \, n_{p,E_2}(\varepsilon)\bar{\rho}_1(\varepsilon) \, , \\ E &= \int_0^V \mathrm{d}\varepsilon \, \varepsilon \left(n_{p,E_2}(\varepsilon) + n_{A-p,E_1}(\varepsilon) \right) \bar{\rho}_1(\varepsilon) \, . \end{aligned} \tag{II.13}$$

We consider a process which leads from a p-particles – p-holes state to a $(p+1)$-particles – $(p+1)$-holes state. This happens due to photon absorption by a particle below Fermi level leading to excitation of it above Fermi level, hence creation of a new particle-hole pair while the energy of the system increases by the energy of absorbed photon.

We take into account only configurations from which particles below Fermi level are excited above Fermi level (but not into the continuum) leaving a hole behind. If the system is in a p-particles – p-holes state with energy E and a

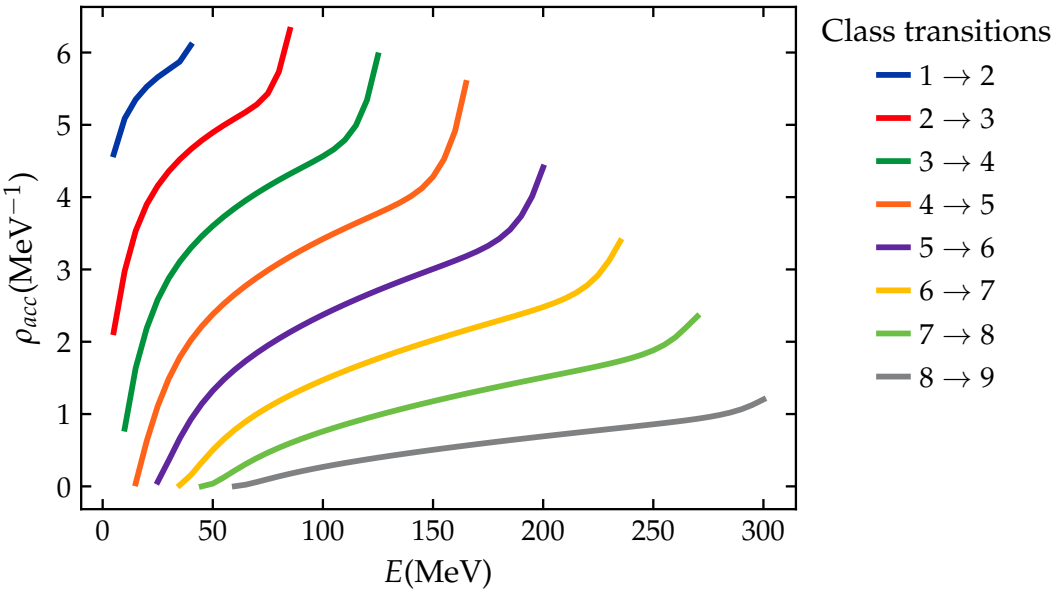

FIGURE II.6: Density of accessible states for dipole absorption in the constant spacing model as a function of excitation energy E. We use $A = 42$ particles, $B = 51$, $V = 45$ MeV, $F = 37$ MeV, $E_L = 5$ MeV. Colors correspond to different transitions between particle-hole classes.

photon with energy E_L excites a nucleon below Fermi level to a state above Fermi level then the system changes its state to $(p+1)$-particles – $(p+1)$-holes state with energy $E + E_L$. In this case the energy of the incoming photon should be large enough to excite a nucleon to a state above Fermi level but not as large as to excite it into the continuum. Thus, before absorbing a photon the yet to be excited particle under the Fermi level should be on such a single-particle level ε, that $F - E_L < \varepsilon < F$.

In the considered processes the probability of finding an occupied single-particle state at energy ε below Fermi level in the system with energy E_1 is $n_{A-p,E_1}(\varepsilon)$. Respectively, the probability of finding an unoccupied single-particle state with energy $\varepsilon + E_L$ above Fermi level is $(1 - n_{p,E_2}(\varepsilon + E_L))$. Denoting the single-particle densities of states below and above Fermi level as

$$\bar{\rho}_{1,<}(\varepsilon) = \Theta(F - \varepsilon)\bar{\rho}_1(\varepsilon), \quad \bar{\rho}_{1,>}(\varepsilon) = \Theta(\varepsilon - F)\bar{\rho}_1(\varepsilon)\ , \tag{II.14}$$

we can write the total density of accessible states

$$\rho_{\mathrm{acc},p}(E) = \int_{F-E_L}^{F} \mathrm{d}\varepsilon\, n_{A-p,E_1}(\varepsilon)(1 - n_{p,E_2}(\varepsilon + E_L))\bar{\rho}_{1,<}(\varepsilon)\bar{\rho}_{1,>}(\varepsilon + E_L)\ . \tag{II.15}$$

The numerical results for constant spacing (with $A = 42$ particles and $B = 51$ single-particle levels) and $\bar{\rho}_1(\varepsilon) \propto \varepsilon$ (with $A = 100$ and $B = 148$) with photon energy $E_L = 5$ MeV are presented in Figs. II.6 and II.7 As can be seen from the plots for different particle–hole classes, accessible densities

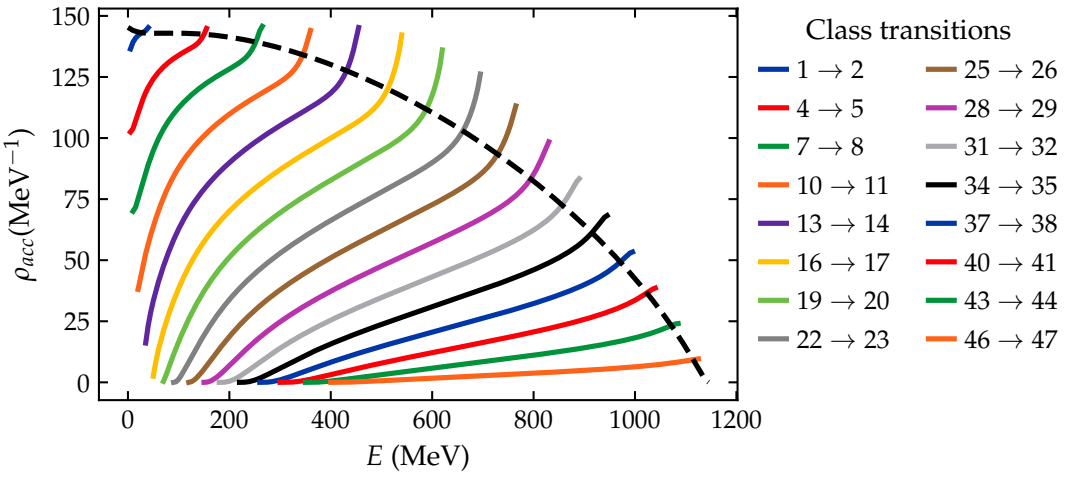

FIGURE II.7: Same as Fig. II.6 but $A = 100$ particles, $B = 148$ and every third particle-hole class is presented. Colors correspond to different transitions between particle-hole classes, the shorter the line the smaller the number of a class it represents. First blue line (upper left corner) corresponds to a transition into the 2-particles – 2-holes class. Each 12 classes the color of the lines repeats and the last orange line (bottom) corresponds to the transition into the 47-particles – 47-holes class. The black dashed line corresponds to calculation according to Eq. (II.16).

are monotonically increasing functions of energy. This can be understood if one takes into consideration two extreme cases of low and high energy in a given class. At low energy one would face a configuration where p particles occupy states right above the Fermi level, and below Fermi-level there are p vacant spots. This is a challenging big range to overcome for a yet to be excited particle, which has to 'hop' not only p vacant spots below Fermi-level, but also p occupied single-particle levels above Fermi-level. Going from this extreme case to high occupancy above Fermi level vacates some single-particle states which gives more freedom for transitions. However, keeping p levels occupied above Fermi level and increasing occupancy right below Fermi-level does not necessary allow more transitions, since at high p a yet to be excited particle has to go over at least p occupied single-particle levels, and in fact is lower than for low p. The complete opposite picture is obtained when the top-most levels below Fermi-level and top-most levels above it are occupied, hence there are some vacant spots right above Fermi level, which makes it very easy for the particles right below the Fermi level to emerge and create a new particle–hole pair.

More to that, excitations within the same particle-hole class are not considered. This means that we neglect such transitions triggered by a photon absorption, in which a particle below (above) the Fermi level is excited to another state below (above) the Fermi level, i.e. do not produce an additional particle-hole pair. However, such transitions lead to the increase of excitation energy of the nucleus. Hence, this limitation lowers the efficiency of brining the system as a whole to high excitation energy. The impact of this restriction

we shall observe further in our investigation while comparing occupation probabilities between the sudden regime and the quasi-adiabatic regime.

For the quasi-adiabatic regime the density of accessible states is taken from Ref. [24] (black dashed line in Fig. II.7)

$$\rho_{\mathrm{acc}}(E) = \int_0^{V-E_L} \mathrm{d}\varepsilon n_{A,E}(\varepsilon)\left(1 - n_{A,E+E_L}(\varepsilon + E_L)\right)\bar{\rho}_1(\varepsilon)\bar{\rho}_1(\varepsilon + E_L)\ . \tag{II.16}$$

It considers the transitions of a single nucleon from a many-body state at energy E to another such state at energy $E + E_L$. Some of these transitions may correspond to, e.g. excitation of a particle above the Fermi level to another single-particle state above F. For which Eq. (II.15) does not account. Eq. (II.16) accounts only for such transitions that start from a state of Fermi gas with distribution $n_{A,E}(\varepsilon)$. These states belong to a particular class. In the sudden regime we must account for the transitions from all the classes. In order to relate the formulae Eqs. (II.15) and (II.16) we compare compare parts of their integrands which differ, namely

$$n_{A-p,E_1}(\varepsilon)(1 - n_{p,E_2}(\varepsilon + E_L))\ , \tag{II.17}$$

$$n_{A,E}(\varepsilon)\left(1 - n_{A,E+E_L}(\varepsilon + E_L)\right) \tag{II.18}$$

in the same single-particle energy domain from $F - E_L$ to F for different excitation energies of the whole system. Figs. II.8 to II.10 show that for each

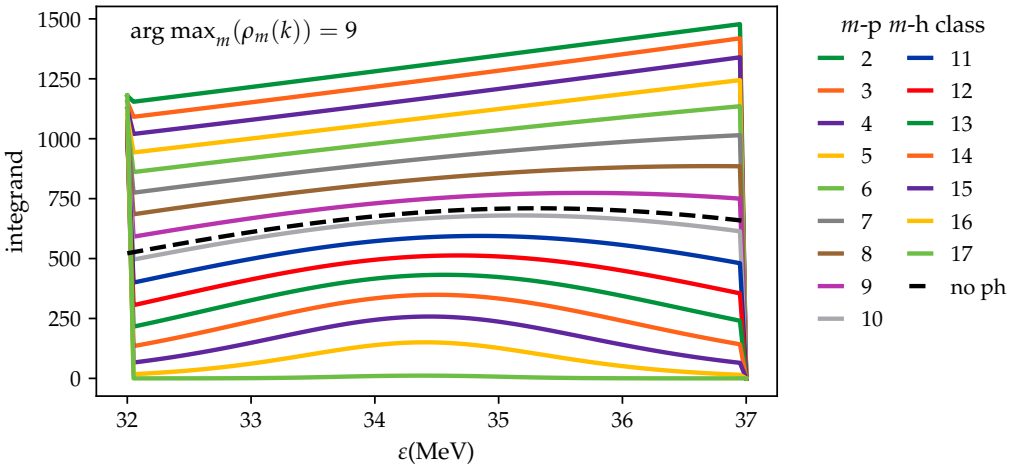

FIGURE II.8: The integrands of Eq. (II.17) at excitation energy $k = 11$ absorbed photons. Color lines correspond to the integrand for different particle-hole classes. Black dotted line corresponds to the integrand which does not specify number of particle-hole pairs. We use $A = 100$, $B = 148$.

total excitation energy kE_L the integrand from Eq. (II.16) lies close to the integrand from Eq. (II.15) for a particular p. This p corresponds approximately to the particle-hole class with the largest level density at energy kE_L (arg max$_m(\rho_m(k))$ in the figures), i.e. the most probable class to occupy.

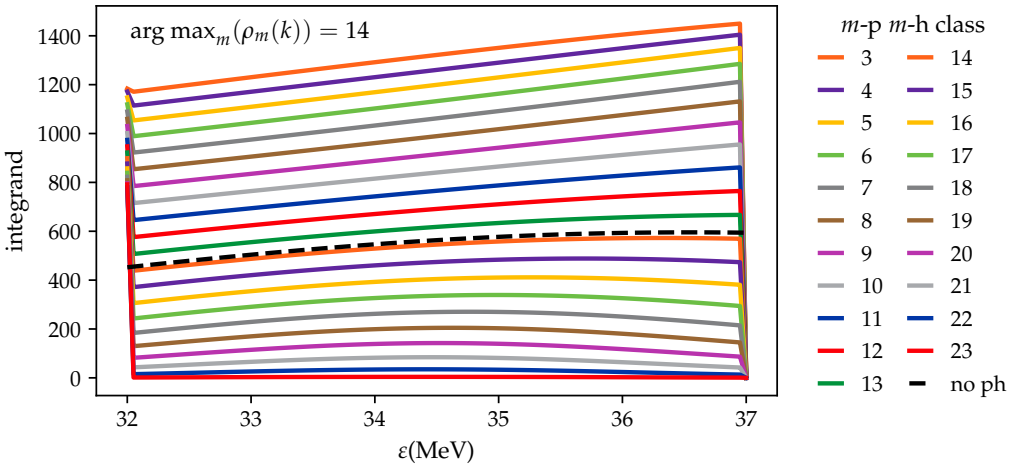

FIGURE II.9: Same as Fig. II.8, but at excitation energy $k = 21$ absorbed photons.

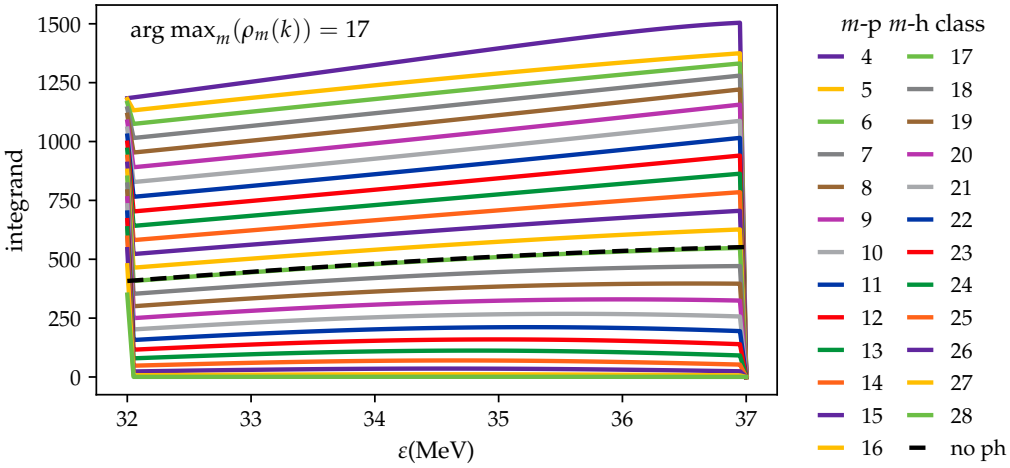

FIGURE II.10: Same as Fig. II.8, but at excitation energy $k = 31$ absorbed photons.

In Fig. II.7 the accessible densities $\rho_{\mathrm{acc},p}(E)$ for the most probable class lie lower than the accessible densities $\rho_{\mathrm{acc}}(E)$ because the later accounts for greater integration limits of positive integrands. However, the right most ends of $\rho_{\mathrm{acc},p}(E)$ attain higher values than $\rho_{\mathrm{acc}}(E)$ because they correspond to the integrands in Eq. (II.15) which attain higher values than the integrands in Eq. (II.16) (see Figs. II.8 to II.10). Despite the different integration limits, $\rho_{\mathrm{acc}}(E)$ lies lower than the ends of $\rho_{\mathrm{acc},p}(E)$ for some p.

Summarizing, the disregard of dipole transitions within the same particle-hole class in Eq. (II.15) and transitions only from the most probable configurations in Eq. (II.16) result in such drastic difference between them in Fig. II.7.

CHAPTER III
Spreading width

We devote a separate chapter to the spreading width since it plays an important role in our investigation. It governs the way the nucleus attains equilibrium, and defines the squared matrix elements $V^2_{m,m+1}$ entering the matrix M in the master equation Eq. (D.3), hence the solution of this equation depends on it.

In the following derivations we adapt calculations from Ref. [16]. As mentioned in Section I.5.3, within one class the equilibration is considered to be instantaneous, hence the average spreading width $\Gamma^{\downarrow}_m$ represents the decay of states in class m into states in other classes. This spreading width is equated with a sum of mean-squared matrix elements $V^2_{mm'}$

$$\Gamma^{\downarrow}_m(i,k) = 2\pi \sum_{m'} V^2_{mm'}(i,k)\rho_{m'}(i,k) \ . \tag{III.1}$$

We assume that states in class m only couple to states in neighboring classes

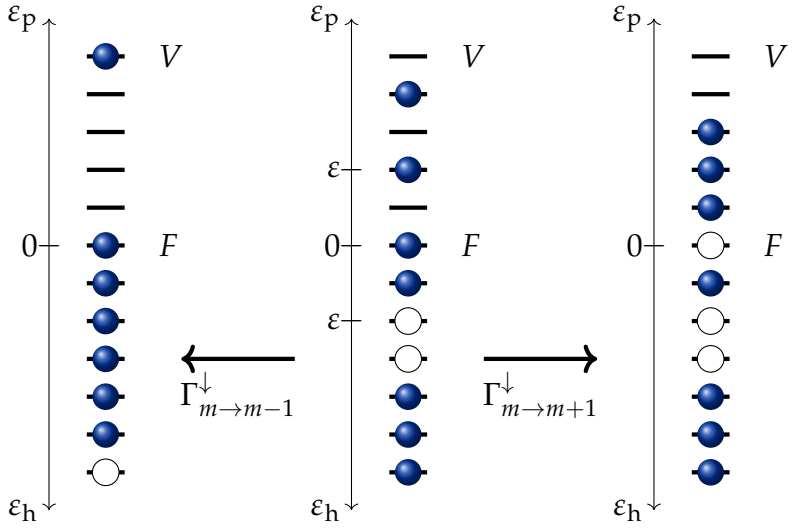

FIGURE III.1: Example of coupling between neighboring classes. At a fixed energy, a configuration in class 2p-2h is coupled only to configurations in the classes 1p-1h and 3p-3h. Here a single example is shown from a large number of combinatorial possibilities.

m' with $|m - m'| = 1$, see Fig. III.1. As mentioned previously, the equilibration

process is conserving energy. In the following derivations we omit the dependence on number of absorbed photons k and nuclear species i for brevity. We can write Eq. (III.1) as a sum of two spreading widths corresponding to the annihilation and production of particle-hole pairs

$$\Gamma^{\downarrow}_{m} = \Gamma^{\downarrow}_{m\to m-1} + \Gamma^{\downarrow}_{m\to m+1} \,. \tag{III.2}$$

This shows that both of these process take part in the attainment of equilibrium.

First, let us address the average spreading width $\Gamma^{\downarrow}_{m\to m+1}$ coupling states in class m with states in class $m+1$. The spreading width of a single exciton at energy ε (either a particle above Fermi level or a hole below it) is expressed as twice the imaginary part of the optical potential: $2W(\varepsilon)$ [31]. We take the potential to be $W(\varepsilon) = 0.003\ \varepsilon^2$, where both $W(\varepsilon)$ and ε are given in MeV [32]. The average width of transition $m \to m+1$ is given by a sum of the spreading widths of all the particles and holes in class m

$$\Gamma^{\downarrow}_{m\to m+1} = 2m \int_{0}^{V-F} P_{\mathrm{p}}(m,\varepsilon) W(\varepsilon) \mathrm{d}\varepsilon + 2m \int_{0}^{F} P_{\mathrm{h}}(m,\varepsilon) W(\varepsilon) \mathrm{d}\varepsilon \,, \tag{III.3}$$

where V is the threshold energy of the single-particle potential and F is the Fermi level. The optical potential is averaged over the following distributions of exciton energies,

$$\begin{aligned} P_{\mathrm{p}}(m,\varepsilon) &= K_{\mathrm{p}} \frac{\tilde{\rho}_{m-1,m}(i, E-\varepsilon)}{\rho_m(i,E)} \,, \\ P_{\mathrm{h}}(m,\varepsilon) &= K_{\mathrm{h}} \frac{\tilde{\rho}_{m,m-1}(i, E-\varepsilon)}{\rho_m(i,E)} \end{aligned} \tag{III.4}$$

for particles and for holes respectively. K_{p} and K_{h} are normalization constants. The density $\tilde{\rho}_{p,h}(i,E)$ (see Chapter II) corresponds to the density of states with p particles, h holes (we note that $p \neq h$ in this expression) at the excitation energy E. This distribution represents how probable it is to occupy a single-particle state at energy ε when $p-1$ particles ($h-1$ holes) are distributed over single-particle states, such that the system is at energy $E-\varepsilon$. The $p-1$ particles ($h-1$ holes) may or may not occupy the single-particle state at energy ε. Ref. [16] exclusion is taken into account. We make a comparison of two following cases in Fig. III.2. In one case we prohibit occupation of the single-particle state at energy ε (this level is blocked), in another we keep it available for occupation. We perform calculation of the spreading width $\Gamma^{\downarrow}_{m\to m+1}$ for both cases and make the comparison, which shows that the difference is insignificant.

Using the symmetry of matrix elements ($V^2_{m,m'} = V^2_{m',m}$), we can calculate $\Gamma^{\downarrow}_{m\to m-1}$

$$\Gamma^{\downarrow}_{m\to m-1} = 2\pi V^2_{m\to m-1}\rho_{m-1} = 2\pi V^2_{m-1\to m}\rho_{m-1} = \frac{\Gamma^{\downarrow}_{m-1\to m}}{\rho_m}\rho_{m-1} \,. \tag{III.5}$$

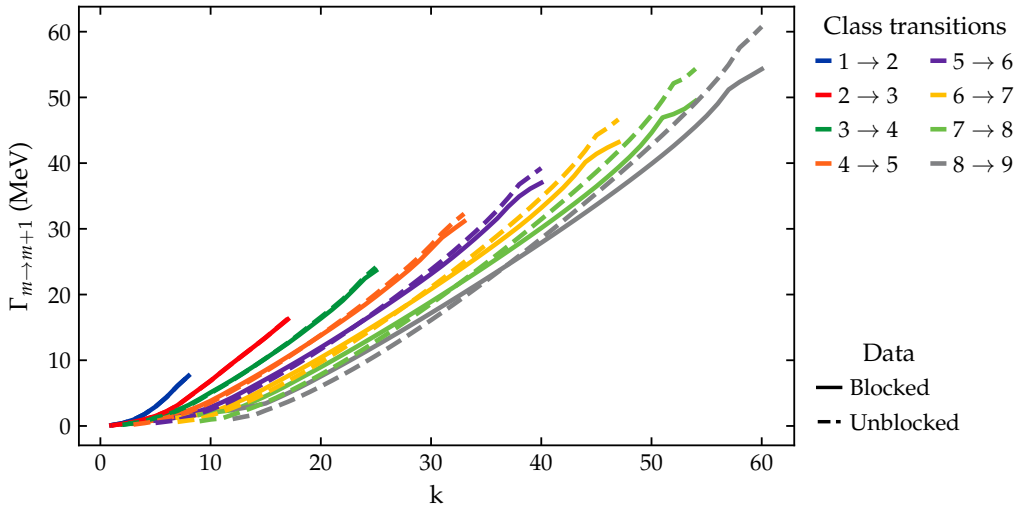

FIGURE III.2: Comparison of spreading widths $\Gamma^{\downarrow}_{n\to n+1}$ for the case of blocked level (solid line), and available for occupation (unblocked, dash line), as functions of the number of absorbed photons k. Colors correspond to spreading widths from different classes. $A = 42, B = 51$.

Fig. III.3 shows a particular case of spreading width $\Gamma^{\downarrow}_{m}$ from Ref. [16]. For this calculation, the level density from Ref. [22] was used with constant spacing $d = 0.13$ MeV. For such small spacing between single-particle states, many particle-hole classes exist in the excitation energy domain of $10 - 20$ MeV. We compare this case with our calculation using the level density from Section II.2. In Fig. III.4 constant spacing $d = 0.81$ MeV is used, hence in the domain of $10 - 20$ MeV (i.e. $2 - 4$ absorbed photons) only a few classes exist. We present results for such an excitation energy that states from many classes are available for occupation. The figures demonstrate qualitatively similar behavior between our calculation and the case from Ref. [16]. The sum of corresponding spreading widths results in the total spreading width $\Gamma^{\downarrow}$ (Eq. (III.2)). Both calculations show competing processes of creation and annihilation of particle-hole pairs. The intersection of curves for $\Gamma^{\downarrow}_{m\to m-1}$ and $\Gamma^{\downarrow}_{m\to m+1}$ happens at some value m_0. If $m > m_0$, then the nucleus is driven back to m_0 by the annihilation of a particle-hole pair. If $m < m_0$, then the nucleus is driven towards m_0 via the production of a particle-hole pair. This feature governs the equilibration process. Our calculation results in much greater values for the spreading widths than the particular case of spreading width from Ref. [16] due to the fact that the level densities attain large values at high excitation energies. This also explains the strong growth of the spreading widths with increasing excitation energy.

In Ref. [33] a statistical analysis of nineteen nuclear reactions induced either by an alpha-particle or a proton was conducted. As a result, the effective matrix element for particle-hole pair creation was obtained. A common trend

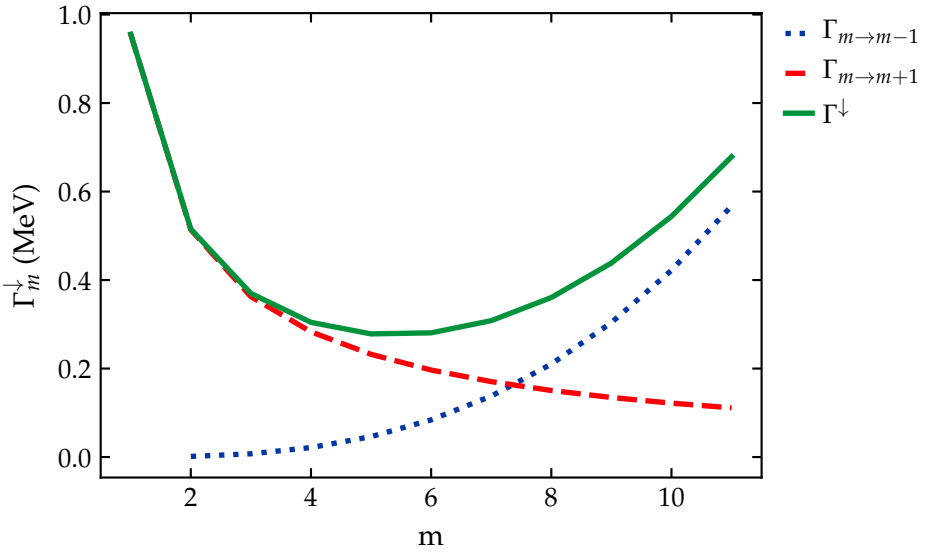

FIGURE III.3: Spreading width $\Gamma^{\downarrow}_{m\to m+1}$ as a function of class number. $\Gamma^{\downarrow}_m$ (solid line), $\Gamma^{\downarrow}_{m\to m+1}$(dashed line), and $\Gamma^{\downarrow}_{m\to m-1}$(dotted line) are calculated according to Ref. [16] for ^{93}Nb at excitation energy $E = 14.6$ MeV for constant spacing $d = 0.13$ MeV between single-particle energy levels.

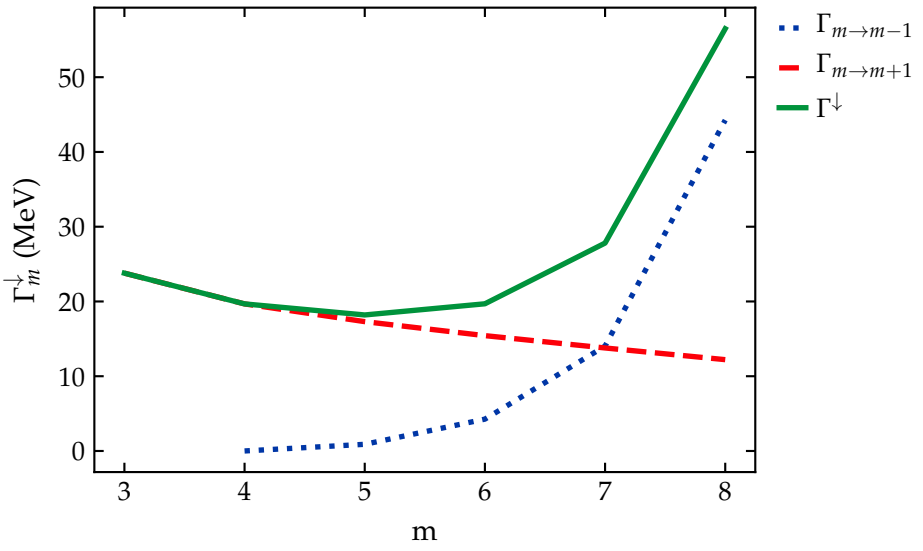

FIGURE III.4: Spreading width $\Gamma^{\downarrow}_{m\to m+1}$ as a function of class number. $\Gamma^{\downarrow}_m$ (solid line), $\Gamma^{\downarrow}_{m\to m+1}$(dashed line), and $\Gamma^{\downarrow}_{m\to m-1}$(dotted line) are calculated in this work at excitation energy $E = 125$ MeV for constant spacing $d = 0.81$ MeV between single-particle energy levels.

for this matrix element at low excitation energies $E \leq 10(p+h+1)$ MeV is

$$V^2 \propto E^{-1} A^{-3} (p+h+1) \ . \tag{III.6}$$

Based on this assumption, we calculated corresponding spreading widths and compared with Eq. (III.1) in Fig. III.5. With increasing excitation energy the results based on Ref. [33] show disagreement with ours. The experimental data are available only for the low excitation energy region. Our investigation involves the high excitation energy domain, as well, which is unexplored so far. Hence, Ref. [33] cannot describe well the behavior of highly excited nuclei.

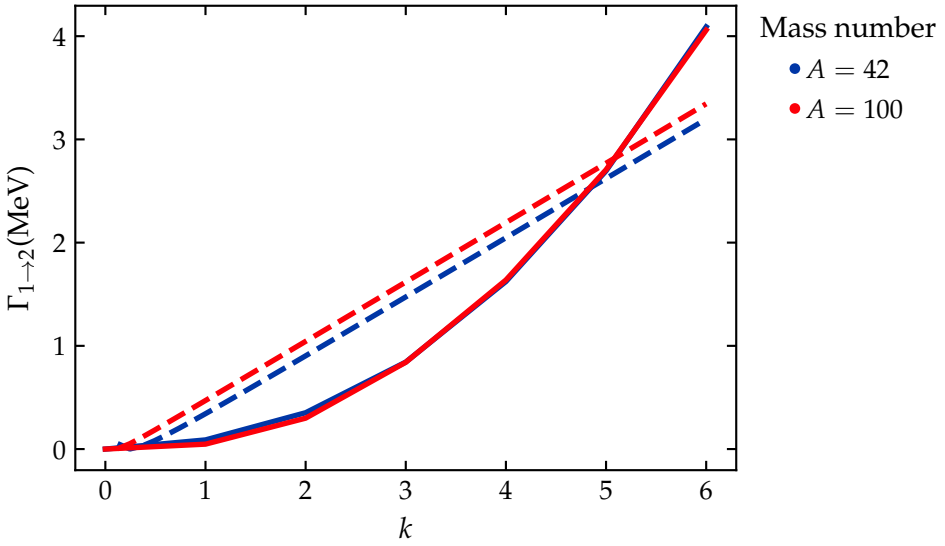

FIGURE III.5: Spreading widths $\Gamma^{\downarrow}_{1\to 2}$ as functions of the number of absorbed photons k. Comparison between our calculation (solid lines) and the calculation from Ref. [33] (dashed lines).

Finally, we present results for the spreading widths $\Gamma^{\downarrow}_m$ and the squared matrix elements $V^2_{m,m+1}$ required for the solution of the master equation Eq. (D.3). We have already demonstrated the behavior of $\Gamma^{\downarrow}_{m\to m+1}(k)$ for the constant spacing in Fig. III.2. Fig. III.6 shows $\Gamma^{\downarrow}_{m\to m+1}(k)$ as functions of energy for the case of linear dependence of single-particle density on energy. A very strong dependence on energy can be observed. This happens due to the large values of the level densities and quadratic dependence of the optical potential W. At the upper ends of the curves numerical artifacts are observed. They are caused by high oscillations of the level densities at the ends of the spectrum. However, as we show further in Chapter IV, the nucleus does not reach this region of excitation energy (see Fig. IV.9). Fig. III.7 and Fig. III.8 show the squared matrix elements entering the matrix M as functions of energy. In semilogarithmic axes both of them resemble the inverse of plots for the level densities. We can conclude that the level densities play a crucial role in determination of matrix elements of nucleon-nucleon interaction and, thus, the description of the nuclear equilibration process.

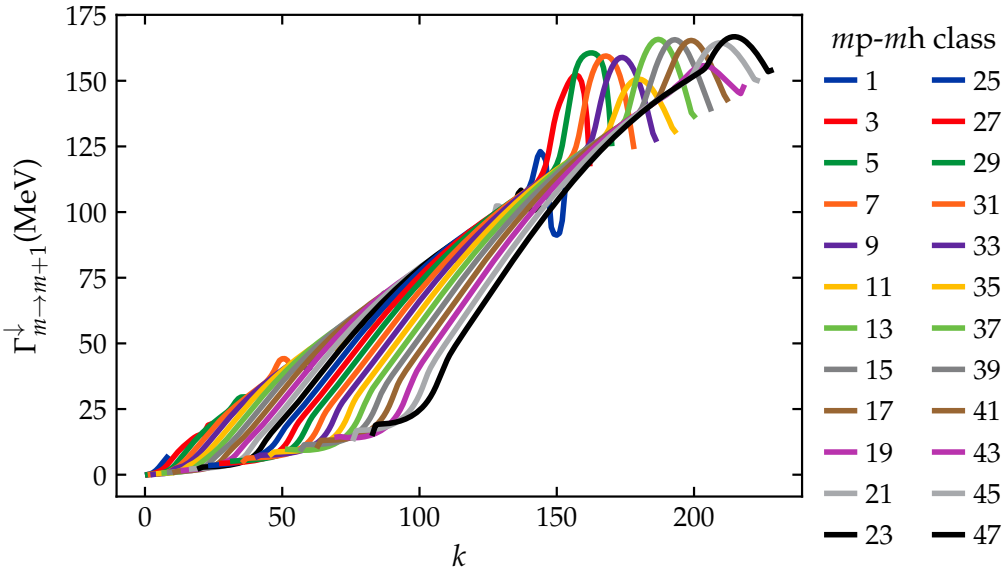

FIGURE III.6: Spreading width as a function of energy for different particle-hole classes m with linear dependence of single-particle density on energy. $A = 100, B = 148$. We plot the spreading width for every second transition. The low left part of the figure corresponds to small m numbers. The colors repeat every 12 curves.

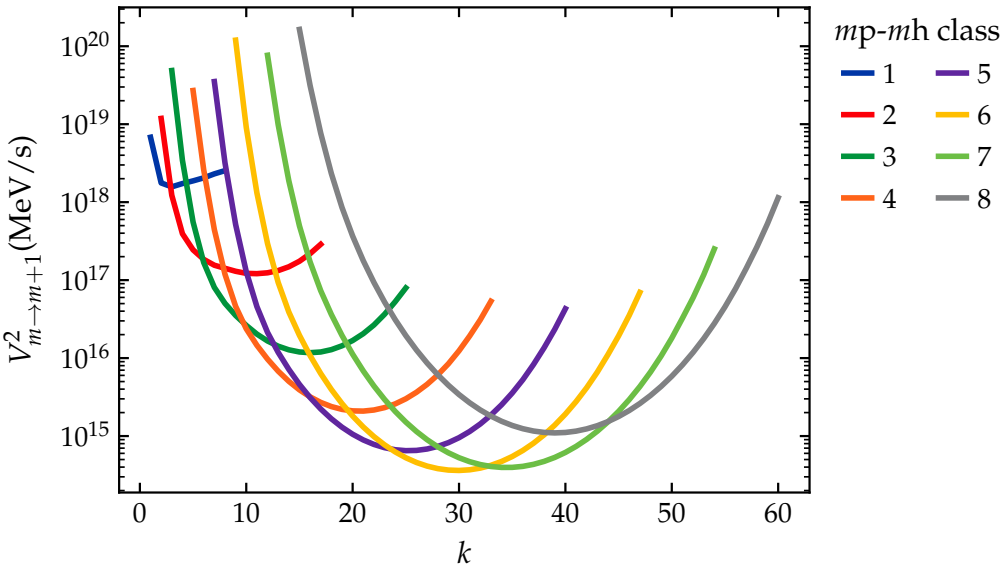

FIGURE III.7: Squared matrix element $V^2_{m\to m+1}$ for different particle-hole classes m as functions of energy for constant spacing. $A = 42, B = 51$.

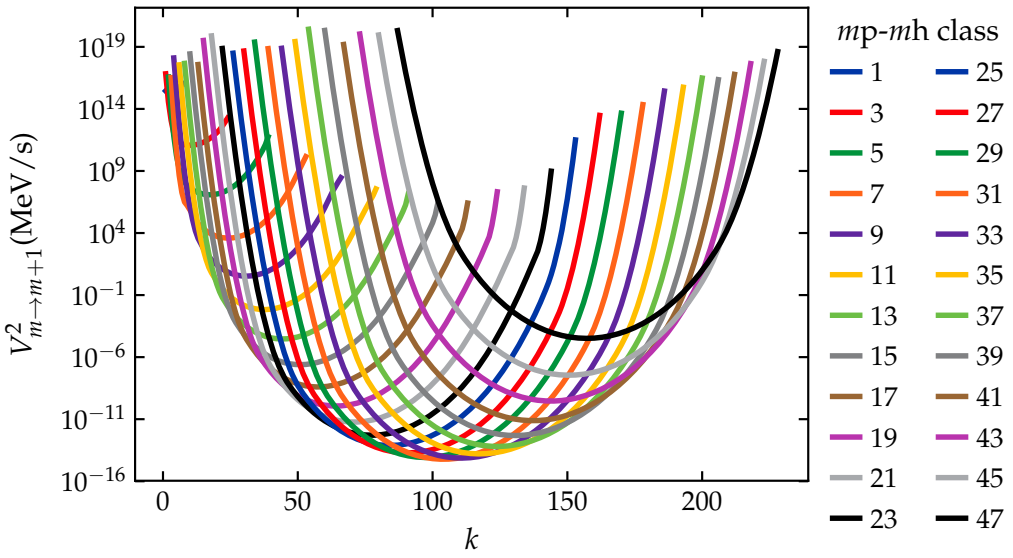

FIGURE III.8: Same as Fig. III.7 but for the linear dependence of single-particle density on energy. $A = 100$, $B = 148$.

Fig. III.9 and Fig. III.10 demonstrate the dependence of $\Gamma^{\downarrow}_m$ on class number m for constant spacing, and linear dependence of single-particle density on energy. The linear case displays artifacts caused by the strong oscillations of the level densities on the edges of the spectrum. Nevertheless similarities exist in the behavior of two cases, such as broad minimum and higher right ends of the curves compared to the left ends. The linear case shows higher values than the constant one due to the higher values of the level densities.

In Fig. III.11 and Fig. III.12 we show the dependence of the matrix elements on the class number m. Here the minima signify the preferable classes at corresponding excitation energy k. Small transition rates indicate that if the class is occupied, the transition from it is less probable. Since we show transitions $m \to m+1$ at the same energy, we can move along the curves from left to right (increasing number of m). This suggests that once the minimum is reached, it is very unlikely that another particle-hole pair will be created by means of nucleon-nucleon interaction. As a result, the areas beyond the minima can be accessed only via photon emission.

In summary, we calculated the spreading width $\Gamma^{\downarrow}_m$ and showed how it determines the attainment of the nuclear equilibrium. In turn, the properties of the spreading width and the squared matrix elements strongly depend on the level densities. The obtained matrix elements complete the specification of the transition rates for the matrix M the master equation Eq. (D.3). The full calculation taking into account the nucleon-nucleon interaction, laser-nucleus interaction, and neutron evaporation can now be performed to obtain the occupation probabilities.

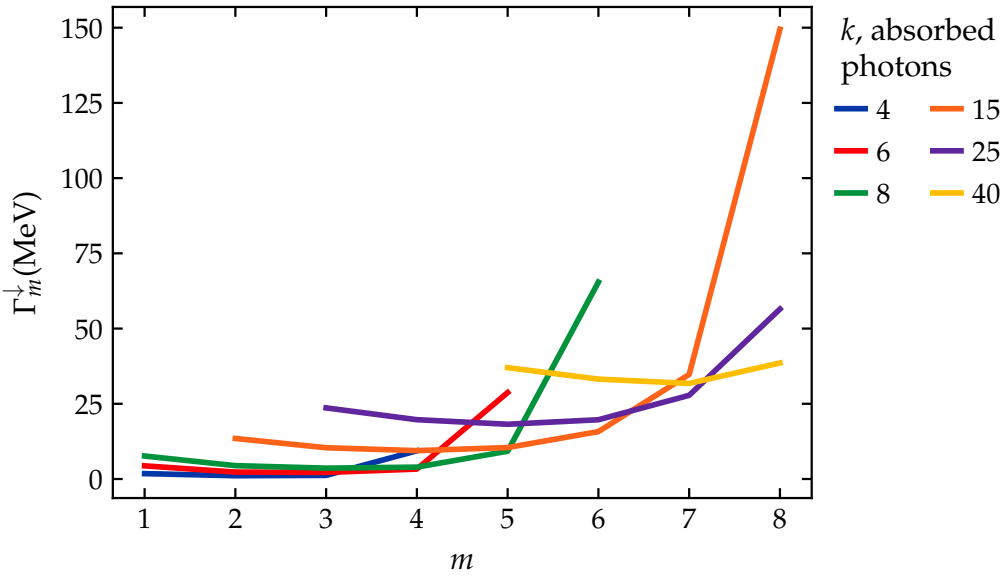

FIGURE III.9: Spreading width as a function of particle-hole class m at different excitation energies illustrated as the number of absorbed photons k for the constant spacing. $A = 42, B = 51$.

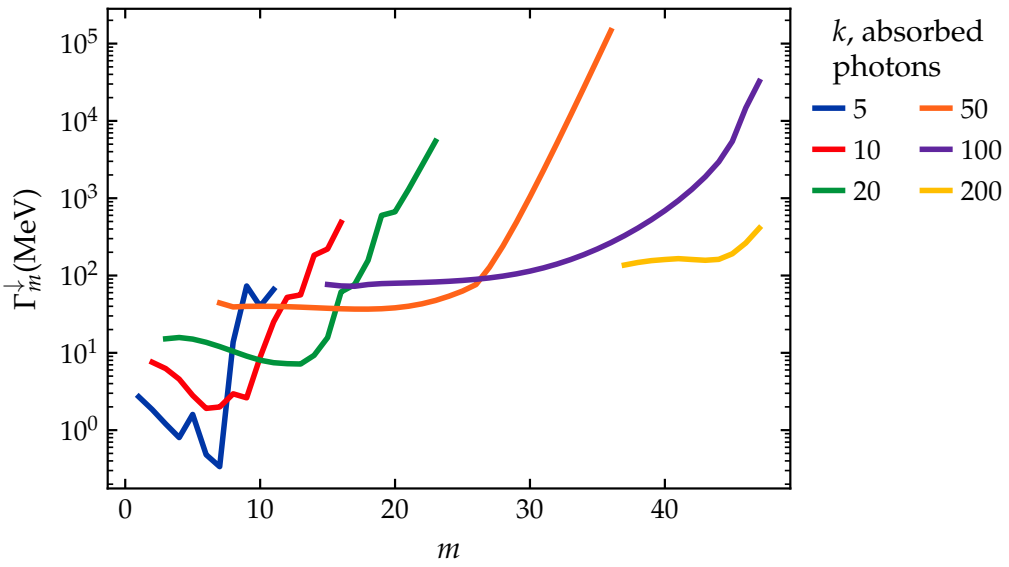

FIGURE III.10: Same as Fig. III.9 but for the linear dependence of single-particle density on energy. $A = 100, B = 148$.

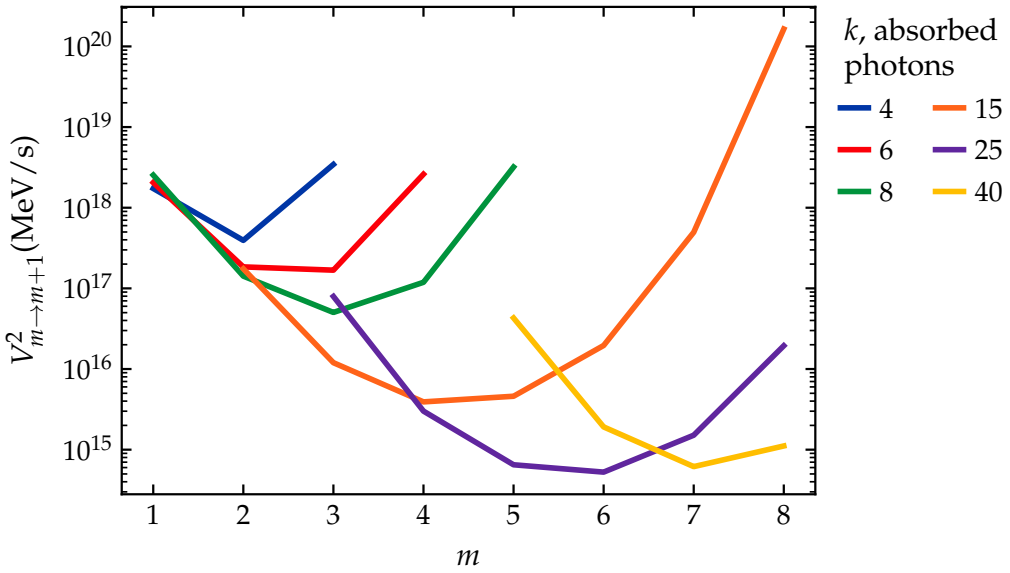

FIGURE III.11: Squared matrix element $V^2_{m\to m+1}$ as a function of particle-hole class m at different excitation energies expressed as the number of absorbed photons k for the constant spacing. $A = 42, B = 51$.

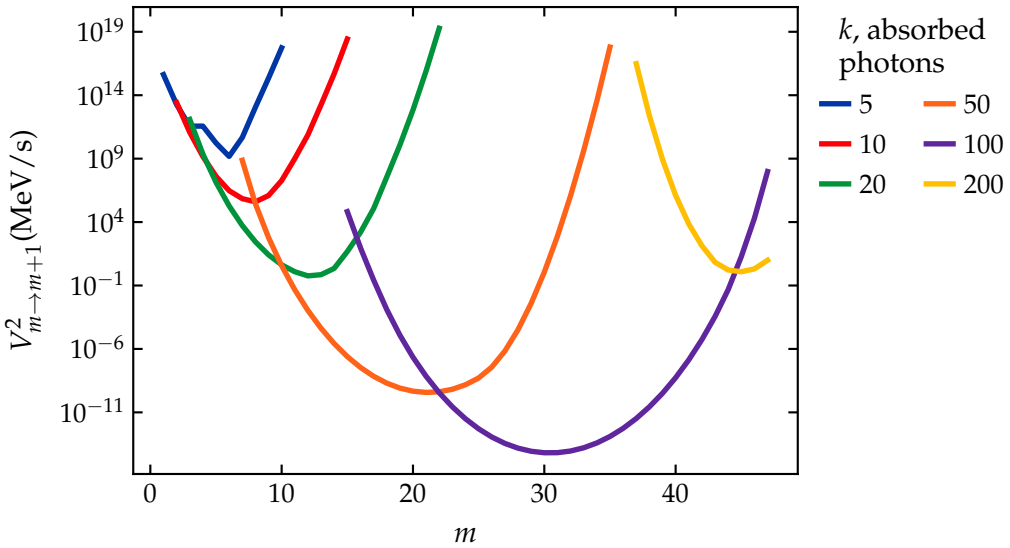

FIGURE III.12: Same as Fig. III.11 but for the linear dependence of single-particle density on energy. $A = 100, B = 148$.

CHAPTER IV
Numerical Results

In this Chapter we present numerical results for the time-dependent occupation probabilities $P_m(i,k,t)$. First, we investigate the behavior of the system and its saturation, we consider only a target nucleus, in which neutron evaporation does not take place. Later, we proceed to include neutron evaporation and investigate the excitation and production of target nucleus and three generations of daughter nuclei.

We use the generalized matrix master equation Eq. (D.6) written for all generations

$$\begin{aligned} \dot{\mathcal{P}}(t) &= \mathcal{M}\mathcal{P}(t) \\ \mathcal{P}(0) &= \mathcal{P}_0, \end{aligned} \tag{IV.1}$$

where the elements of vector-column $\mathcal{P}$ contain the occupation probabilities $\mathcal{P}_j = \rho_m^{-1/2}(i,k)P_m(i,k,t)$. The index j depends on the nuclear species i, number of absorbed photons k, and particle-hole class m. The initial condition corresponds to the ground state of the target nucleus.

The matrix $\mathcal{M}$ contains level densities $\rho_m(i,k)$ and time-independent transition rates. The derivation of the level densities from the cumulants of single-particle density $\bar{\rho}_1(\varepsilon)$ is described in Appendices A to C. The level density $\rho_m(i,k)$ also defines the transition rates. Hence, choosing a model for the single-particle density affects all entries of the matrix M. The specification for transition rates is given in Section I.5 and Chapter III. In summary, we defined the

- dipole absorption rate $W^2_{m,m+1}(i,k)$ in Eq. (I.12), which couples states at energy k in class m to states at energy $k+1$ in neighboring class $m+1$, and is calculated according to the procedure described in Section I.5.1;
- neutron evaporation rate $\Gamma_N(i,k,m)$ in Eq. (I.14), which couples states in generation i to states in the next generation $i+1$ within the same class m, and is calculated according to the procedure described in Section I.5.2;
- nuclear equilibration rate $V^2_{m,m+1}(i,k)$ in Eqs. (I.16) and (III.3), which couples neighboring classes m and $m+1$ at the same energy k, and is calculated according to the procedure described in Section I.5.3 and Chapter III.

The elements of the matrix can differ by 8 orders for nuclei with mass number $A = 42$ and by 70 orders for nuclei with mass number $A = 100$. All

elements play a crucial role in transferring occupation probability from classes with small number of the particle-hole pairs to classes with large ones. Their different magnitude comes mainly from the range of values that the level density can take. Diagonalizing this matrix, therefore, poses a stiff problem. The number of elements in our matrix ranges from 670 for $A = 42$ to ~ 10000 for $A = 100$. These numbers become even greater when several generations are considered: each generation contributes approximately an equal number of elements. Thus, we deal with huge matrices where elements range over many orders of magnitude. This poses some challenges for the numerical calculation.

Several numerical solvers have been used to solve Eq. (IV.1). We have found out that adopting the Chebyshov rational approximation method (CRAM) works best for our needs while common solvers, e.g., Runge-Kutta, Adams/BDF etc., fail and produce significant numerical artifacts. A descriptive application of CRAM for burnup equations via matrix exponential was presented in Ref. [34]. Burnup equations are first order differential equations, describing change of nuclide concentration $\boldsymbol{n}(t)$ due to various decays and transmutations

$$\frac{\mathrm{d}\boldsymbol{n}(t)}{\mathrm{d}t} = \boldsymbol{A}\boldsymbol{n}(t) \ . \tag{IV.2}$$

The transition matrix $\boldsymbol{A}$ contains decay and transmission coefficients of thousands different nuclides which can have timescales from seconds to thousands of years, with the problem of stiffness arising there as well. The solution of such equation can be described via the matrix exponential

$$\boldsymbol{n}(t) = \mathrm{e}^{\boldsymbol{A}t}\boldsymbol{n}(0) \ , \tag{IV.3}$$

where $\mathrm{e}^{\boldsymbol{A}t} = \sum_{k=0}^{\infty} \frac{(\boldsymbol{A}t)^k}{k!}$ and $\boldsymbol{A}^0 = \boldsymbol{I}$. Then a rational approximation to the matrix exponential is proposed and CRAM performs the best among other approximations [34], yielding high accuracy and fast speeds of calculation. Similarities between our problem and burnup equations, as well as their challenges, made CRAM a very attractive, fast and, as a result, a successful technique for the solution of our master equations. For all the calculations we used CRAM with partial fraction decomposition and an approximation of order 16 [34]. However, for the case of $\bar{\rho}_1(\varepsilon) \propto \varepsilon$ the calculation with neutron evaporation using the approximation of order 16 failed to give satisfactory results and we have used a more advanced CRAM with incomplete partial fractions and an approximation of order 32 [35].

To generate the results we use the following input data:

- mass number A
- number of single-particle states B
- Fermi level $F = 37$ MeV
- potential depth $V = 45$ MeV
- smooth single-particle density $\bar{\rho}_1(\varepsilon)$

- appropriate number of cumulants and orthogonal polynomials
- energy of a single photon $E_L = 5$ MeV
- duration of the laser pulse τ
- effective dipole rate $N\Gamma_{\text{dip}}$
- optical potential $W(\varepsilon) = 0.003\varepsilon^2$ (both W and ε are in units of MeV) .

The procedure of calculation is as follows:

- calculation of all the densities of states, namely:
  - $\rho_m(i,k)$ from the cumulants of $\bar{\rho}_1(\varepsilon)$,
  - $\rho_{\text{acc},m}(E)$ via Fermi-gas model, see Section II.3;
- calculation of all the transition rates via the densities, namely:
  - $W^2_{m,m+1}(i,k)$,
  - $\Gamma_N(i,k,m)$,
  - $V^2_{m,m+1}(i,k)$;
- construction of the matrix $\mathcal{M}$;
- solution of the master equation Eq. (IV.1).

IV.1 Constant spacing

First, we test and illustrate our approach and numerical calculation on a simple case for constant spacing $\bar{\rho}_1(\varepsilon) \equiv \text{const} = \frac{A}{F}$. We consider a nucleus with mass number $A = 42$ and $B = 51$ single-particle states. This yields in total 9 particle-hole classes. Further parameters are the Fermi energy $F = 37$ MeV and the depth of the potential well $V = 45$ MeV. We calculate all the required rates and solve the master equation with the initial condition corresponding to the populated ground state of the target nucleus.

The result of a calculation in the absence of neutron evaporation can be seen in Fig. IV.1 for laser pulse duration $\tau = 200$ zs, and effective dipole rate $N\Gamma_{\text{dip}} = 5$ MeV. The occupation probabilities are spread among different particle-hole classes. To populate classes with high numbers of particle-hole pairs, high excitation energy is required. This is seen in the figure as occupation probability goes higher with number of particle-hole pairs.

For better visualization, in Fig. IV.2 a vertical cut in all spectra of Fig. IV.1 showing the probabilities at the end of the laser pulse are presented. The system tends to reach the saturation regime in each particle-hole class, i.e. successive photon absorptions do not push occupation probabilities away from the region of maximum of each particle-hole class' level density, but rather induce photon emission. At the maxima the rates for photon absorption and stimulated emission become equal. This point is called 'saturation point'. The

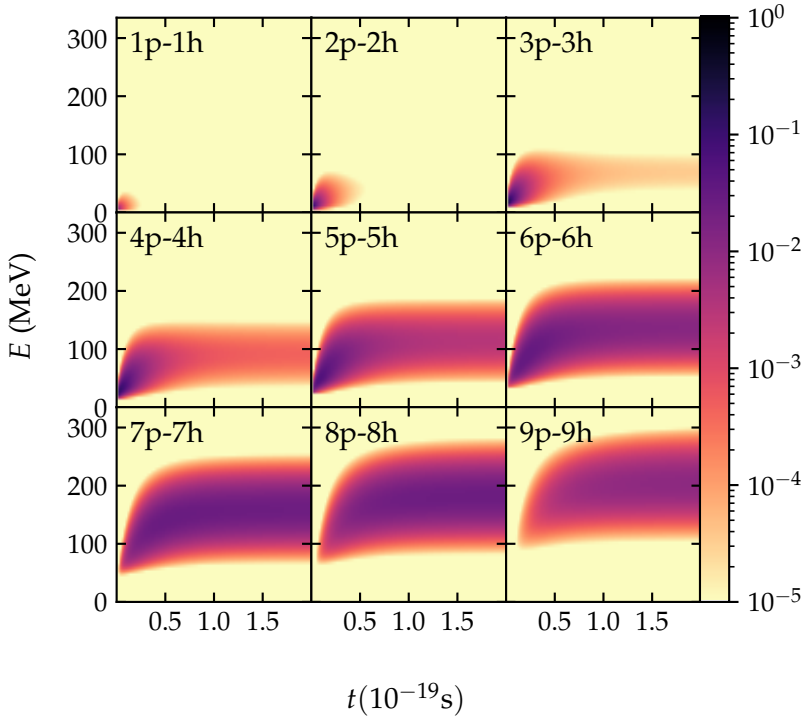

FIGURE IV.1: Distribution of occupation probabilities among different particle-hole classes. Constant spacing, $A = 42$, $N\Gamma_{\text{dip}} = 5$ MeV, $\tau = 200$ zs.

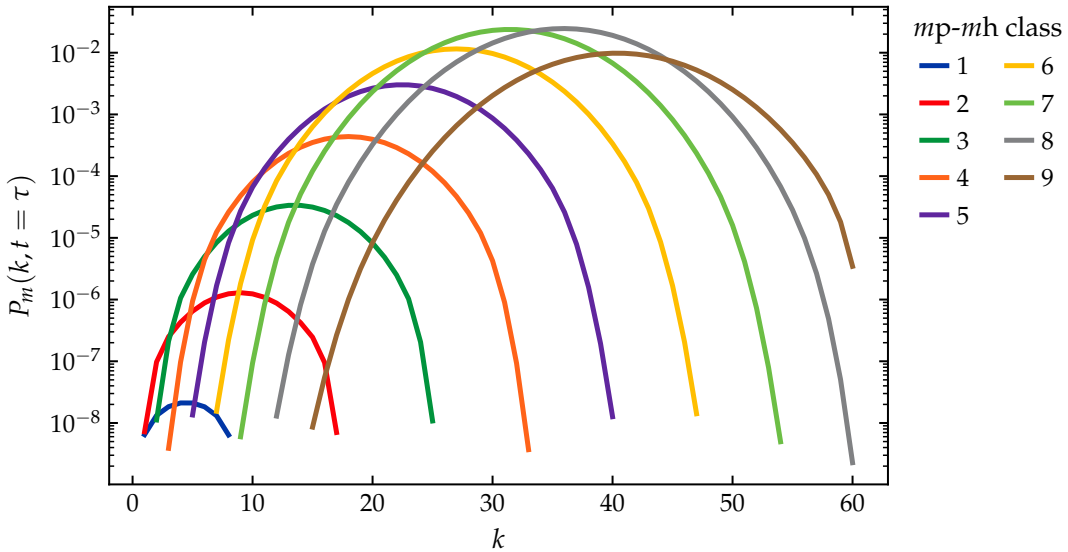

FIGURE IV.2: Occupation probabilities versus number of absorbed photons k for different particle-hole classes at the termination of the laser pulse with $t = 200$ zs. Constant spacing, $A = 42$, $N\Gamma_{\text{dip}} = 5$ MeV.

occupation probabilities' profiles for different classes approach the shape of the corresponding level densities, compare with Fig. II.2. During laser-nucleus interaction the total occupation probability summed over the particle-hole classes and energies is conserved, $\sum_{m,k} \dot{P}_m(0,k,t) = 0$. In the field of an infinitely long laser pulse the nucleus attains equilibrium. Eq. (I.5) turns into equilibrium distribution

$$P_{\mathrm{eq}}(0,k) = P_m(0,k,t \to \infty) \propto \rho_m(0,k) \,, \tag{IV.4}$$

for all energies below and around the saturation point.

Fig. IV.1 also shows that, e.g., classes 5p-5h and 6p-6h are more saturated on this timescale than classes with higher number of particle-hole pairs. For different classes saturation is achieved at different times, meaning that the system as a whole is saturated when the 'slowest' class is saturated.

We can sum the occupation probabilities over all classes. This gives the total occupation probability in Fig. IV.3. Due to the fact that particle-hole classes with high numbers $m > 6$ have not reached the saturation regime, the whole nucleus has not reached it.

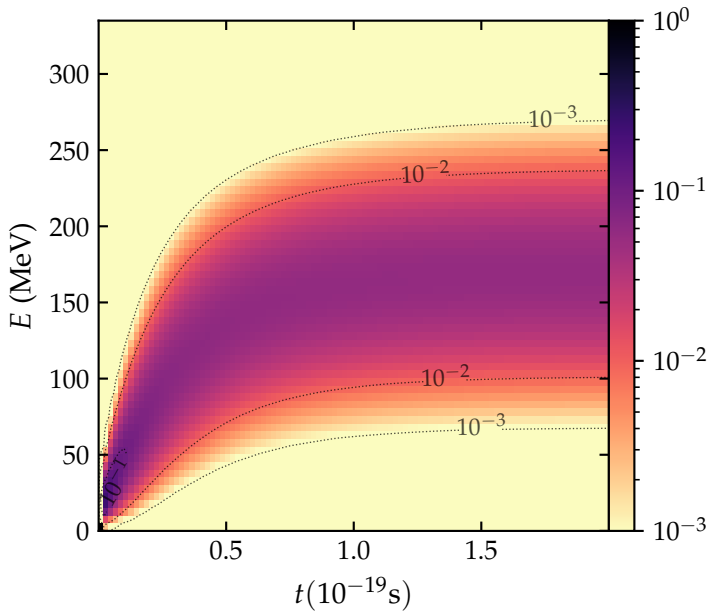

FIGURE IV.3: Total occupation probabilities summed over all particle-hole classes. $A = 42$, constant spacing, $N\Gamma_{\mathrm{dip}} = 5$ MeV, $\tau = 200$ zs.

Increasing $N\Gamma_{\mathrm{dip}}$ brings the system faster towards the saturation. Fig. IV.4 demonstrates this behavior on a shorter timescale $\tau = 100$ zs compared to the previous figures. For $N\Gamma_{\mathrm{dip}} = 20$ MeV the system reaches saturation at around 75 zs, while the cases for $N\Gamma_{\mathrm{dip}} = 5$ MeV and $N\Gamma_{\mathrm{dip}} = 8$ MeV show that the system is about to get into the saturation regime. Finally, the case for $N\Gamma_{\mathrm{dip}} = 1$ MeV is far from the saturation.

The next step is to include neutron evaporation. We consider a target nucleus with A particles (Gen 0), 2 daughter nuclei, with $A-1$ (Gen 1) and $A-2$ (Gen 2) nucleons respectively, and a dump nucleus with $A-3$ nucleons

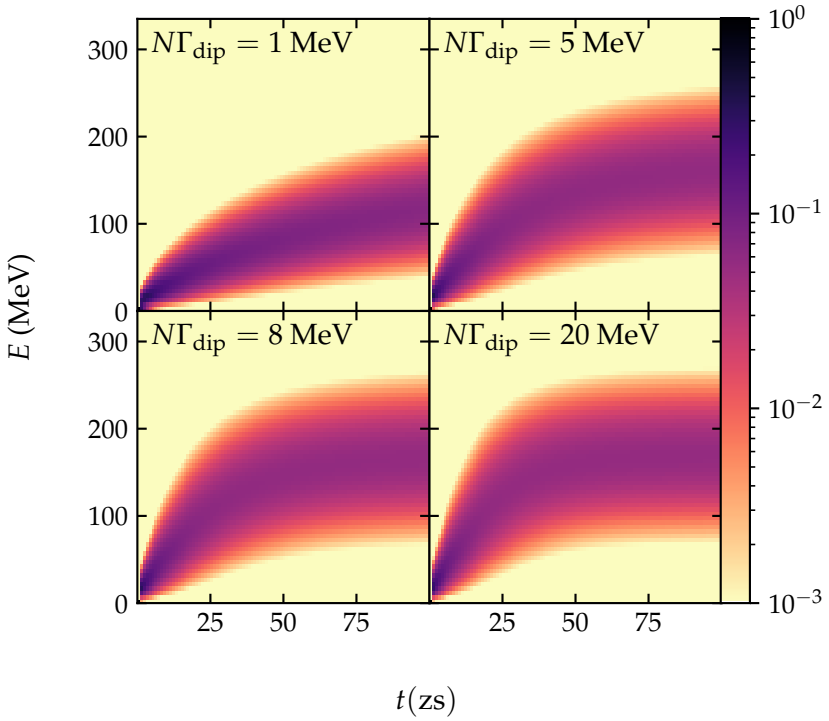

FIGURE IV.4: Total occupation probabilities summed over all particle-hole classes for different values of $N\Gamma_{\mathrm{dip}}$. $A = 42$, constant spacing, $\tau = 100$ zs.

(Gen 3), where we switch off neutron evaporation. The results are presented in Fig. IV.5. The plots confirm that the neutron evaporation can happen only after some number of photons is absorbed. The occupation probabilities for daughter nuclei lie below the energy of roughly 120 MeV. The photon absorption rate is significantly lower than the neutron evaporation at this energy. At 25 zs the occupation probability vanishes from the target nucleus while for the first generation and especially for the third one the probability exists at this time. Significant part of the occupation probability is dumped into the last nucleus. This happens via propagation of probability through all the previous generations, as they appear one after the other in a chain of reactions. The saturation is no longer achieved for the parent and daughter nuclei as neutron evaporation happens below their saturation points. On the other hand the final nucleus does go towards saturation regime. Because neutron evaporation is absent in the final nucleus, the photon excitation has no competing processes in pushing occupation probabilities towards the maxima of level densities. We expect a qualitatively similar picture if one considers more generations, where a chain of consecutive neutron evaporations drives the system towards a proton-rich region far from the valley of stability.

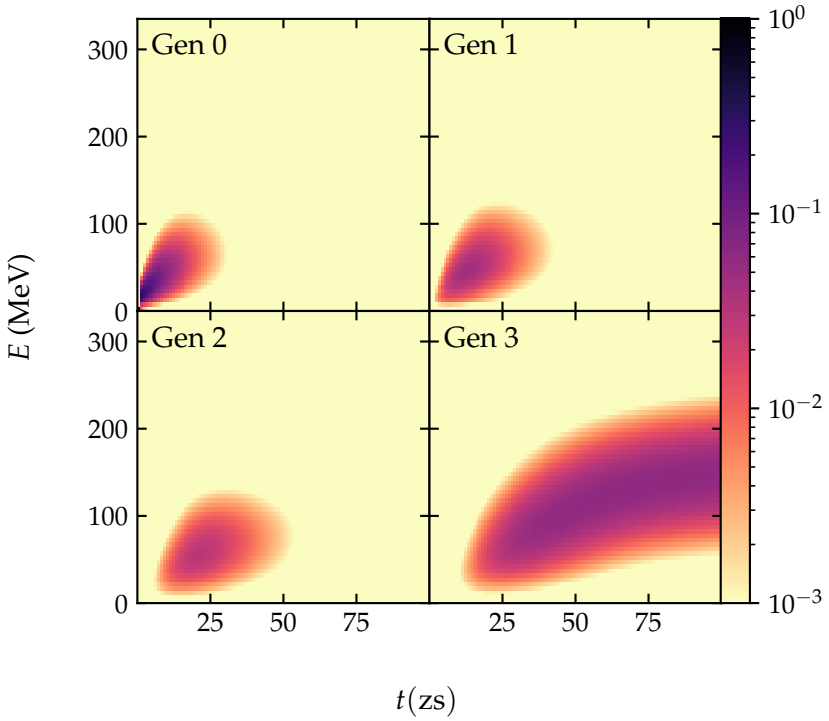

FIGURE IV.5: Total occupation probabilities summed over all particle-hole classes for 4 generations. Constant spacing, $A = 42$, $N\Gamma_{\text{dip}} = 5$ MeV, $\tau = 100$ zs.

IV.2 Medium-weight nuclei

The model of constant spacing is not realistic for medium-weight nuclei. In this section we consider the smooth single-particle density $\bar{\rho}_1(\varepsilon) = \frac{2A}{F^2}\varepsilon$ which approximates the single-particle energies for medium-weight nuclei. We study a system with $A = 100$ nucleons distributed over $B = 148$ single-particle states, with the depth of the potential well $V = 45$ MeV, and the Fermi energy $F = 37$ MeV. For the initial condition we assume that the target nucleus is in the ground state. $B = 148$ and $A = 100$ allow for 48 particle-hole classes in such nucleus. Generally, the results are qualitatively similar to constant spacing case, but in this case far more classes exist.

First, we address a case of photoexcitation in the absence of neutron evaporation for laser pulse duration $\tau = 200$ zs, and effective dipole rate $N\Gamma_{\text{dip}} = 5$ MeV. The result of this calculation is presented in Figs. IV.6 and IV.7. The population of both low and high numbers of the particle-hole classes are shown. For this the plotted range of values for occupation probabilities was increased from $[10^{-3}, 1]$ to $[10^{-7}, 1]$. At the beginning of the pulse the occupation probability is concentrated mostly in the classes with low particle-hole numbers, then it transits to the middle classes with particle-hole numbers between 20 to 35 and for the end of the pulse the probability is concentrated in the classes with high particle-hole numbers. This follows from the level density for different particle-hole classes, see Fig. II.5. The classes with small numbers of particle-hole pairs are concentrated at low excitation energies and

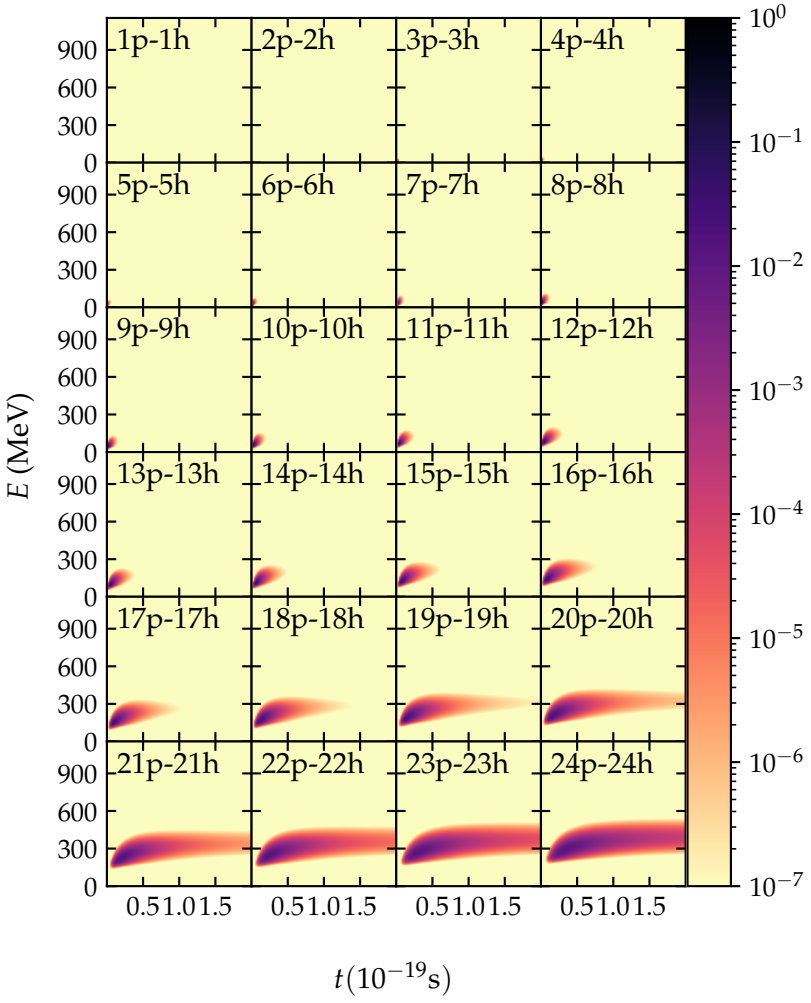

FIGURE IV.6: Distribution of occupation probabilities among the particle-hole classes from 1p-1h to 24p-24h. Medium-weight nucleus, $A = 100$, $N\Gamma_{\mathrm{dip}} = 5$ MeV, $\tau = 200$ zs.

are populated on the first stages of photoexcitation. The middle classes are spread across a significant part of the range of the excitation energy spectrum, starting almost from the origin and going beyond its middle. They are occupied from the first stages of the photoexcitation process and stay populated till the end of the laser pulse duration. The high classes are absent at the origin of the spectrum of the excitation energy and are populated later on when the photoexcitation had brought in enough energy to reach the excitation energy domain where the high classes exist.

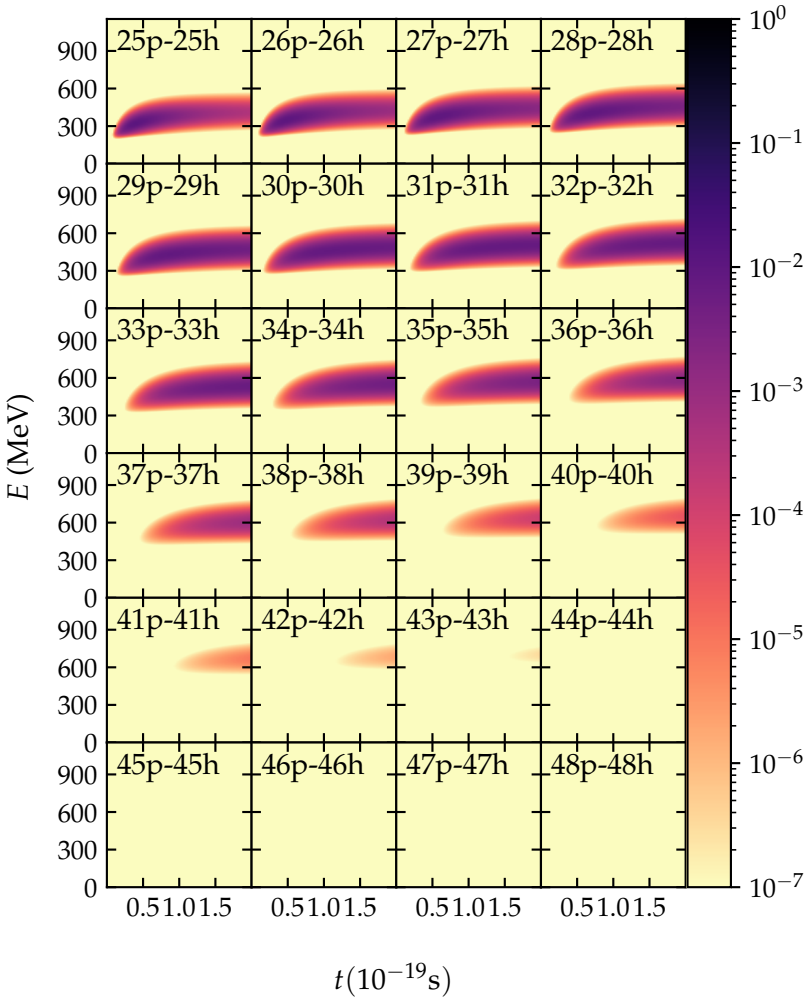

FIGURE IV.7: Distribution of occupation probabilities among the particle-hole classes from 25p-25h to 48p-48h. $A = 100$, $N\Gamma_{\text{dip}} = 5$ MeV, $\tau = 200$ zs.

Figs. IV.6 and IV.7 also demonstrate that the classes with high particle-hole numbers are poorly occupied. The reason for this is that the maxima of level densities of these particle-hole classes lie at higher excitation energies than the saturation point of the whole system. More to that, the level densities for high classes is lower than for the middle classes. Starting from the class with 32 particle-hole pairs the maxima of the following higher classes decreases. Even in the saturation regime, the classes with high particle-hole numbers are still poorly populated. This conclusion is harder to draw from the case of constant

spacing, see Fig. IV.1. There the maximum of level density for the ultimate class with 9 particle-hole pairs is not much smaller than the maximum for the class with 8 particle-hole pairs, hence the decrease in population probability just begins, see Fig. II.2.

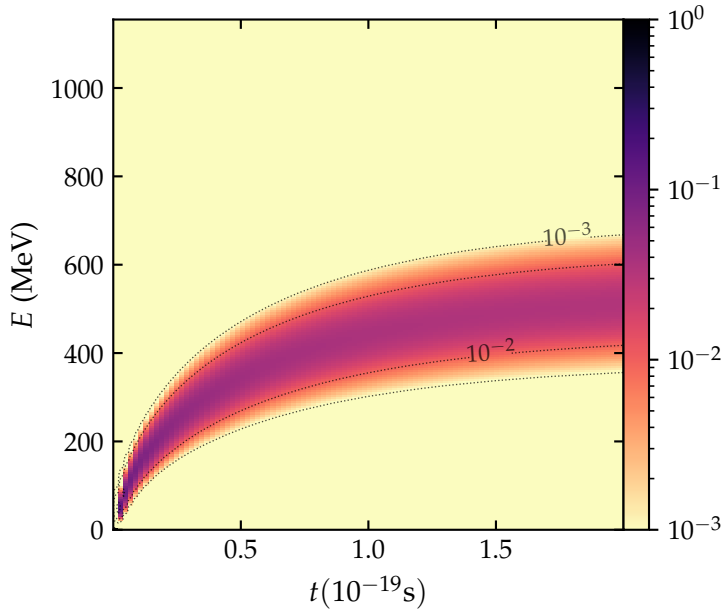

FIGURE IV.8: Total occupation probabilities summed over all particle-hole classes. $A = 100$, $N\Gamma_{\mathrm{dip}} = 5$ MeV, $\tau = 200$ zs.

Figs. IV.6 and IV.7 show several classes reach the saturation regime (approximately up to class with 24 particle-hole pairs). However, the saturation is not reached in all the classes. Hence, in Fig. IV.8 the occupation probability summed over all particle-hole classes demonstrates that the system is not yet in the saturation regime, i.e. the total occupation probability still appears to ascend at the end of the laser pulse duration, it has not attained the shape of the total level density up to the saturation point.

A comparison for increasing $N\Gamma_{\mathrm{dip}}$ similar to the case of constant spacing is presented in Fig. IV.9 for $\tau = 100$ zs. The case for $N\Gamma_{\mathrm{dip}} = 20$ MeV is close to the saturation regime, while $N\Gamma_{\mathrm{dip}} = 8$ MeV, $N\Gamma_{\mathrm{dip}} = 5$ and $N\Gamma_{\mathrm{dip}} = 1$ MeV are not in the saturation regime. The saturation point for $A = 100$, linear case lies around 550 MeV versus 150 MeV for $A = 42$, constant spacing. Hence, for $A = 100$ the saturation is attained only for large $N\Gamma_{\mathrm{dip}}$ for the same duration of the laser pulse.

It is of interest to compare our results with the ones from Ref. [19]. The latter considers the quasi-adiabatic regime of laser-nucleus interaction: the time scales for photon absorption and nuclear relaxation happen on similar time scales, after each photon absorption nuclear equilibrium is assumed to take place and the particle-hole classes are not considered. First we compare the laser-nucleus interaction of both regimes in the absence of neutron decay. The dependence of occupation probabilities on the number of absorbed photons at different moments in time for different effective dipole rates $N\Gamma_{\mathrm{dip}}$ is presented in Figs. IV.10 to IV.12. At early times (blue and red curves in Fig. IV.11 and

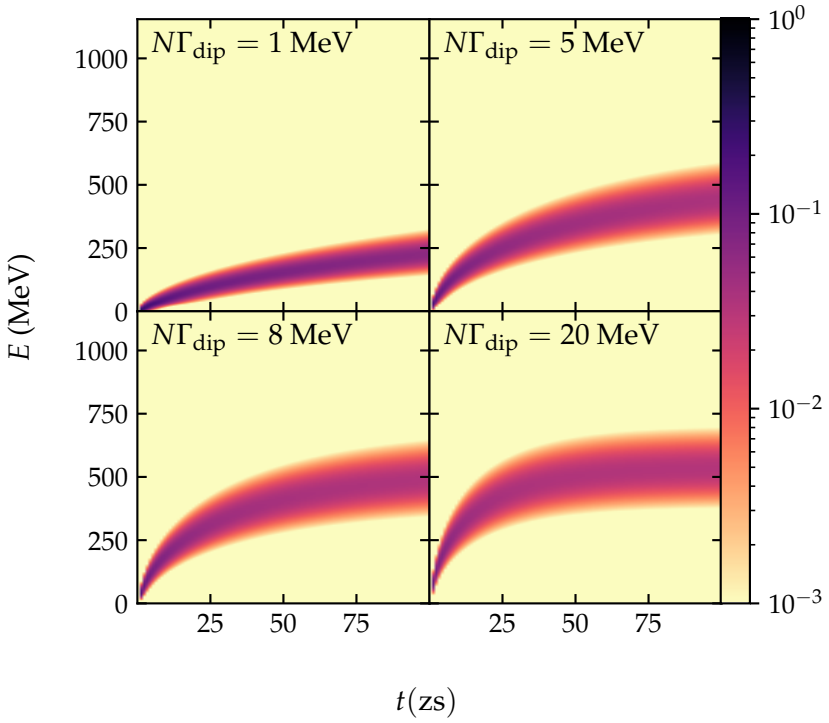

FIGURE IV.9: Total occupation probabilities summed over all particle-hole classes for different values of $N\Gamma_{\text{dip}}$. $A = 100$, $\tau = 100$ zs.

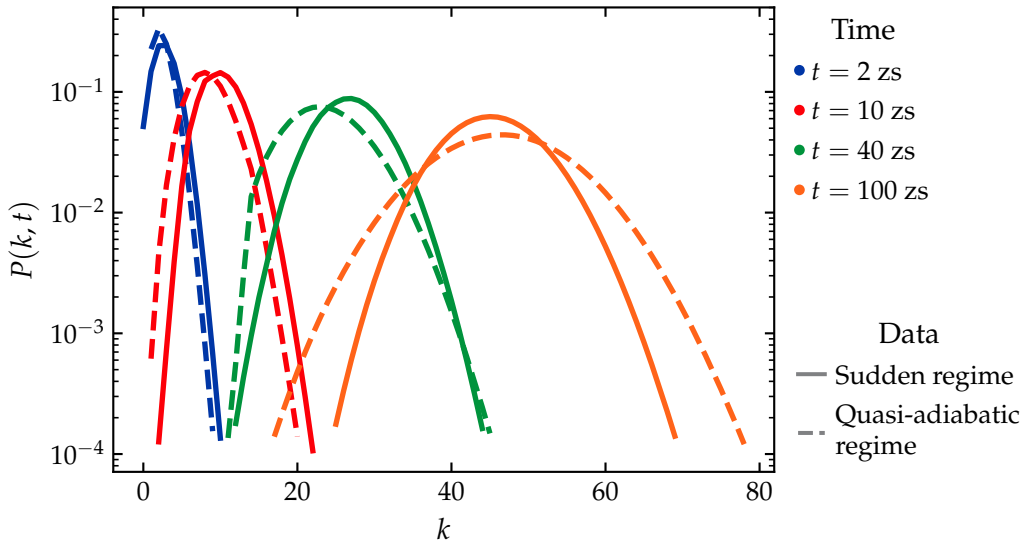

FIGURE IV.10: Total occupation probabilities summed over all particle-hole classes (solid line) compared with Ref. [19] (dashed line) versus number of absorbed photons k at different moments of laser-pules duration (coloring). $A = 100$, $N\Gamma_{\text{dip}} = 1$ MeV.

blue in Fig. IV.12) and for low $N\Gamma_{\text{dip}}$ (red and green curves in Fig. IV.10) in our calculation the occupation probability maxima are at slightly higher energies than the maxima of occupation probabilities yielded from the quasi-adiabatic regime calculations.

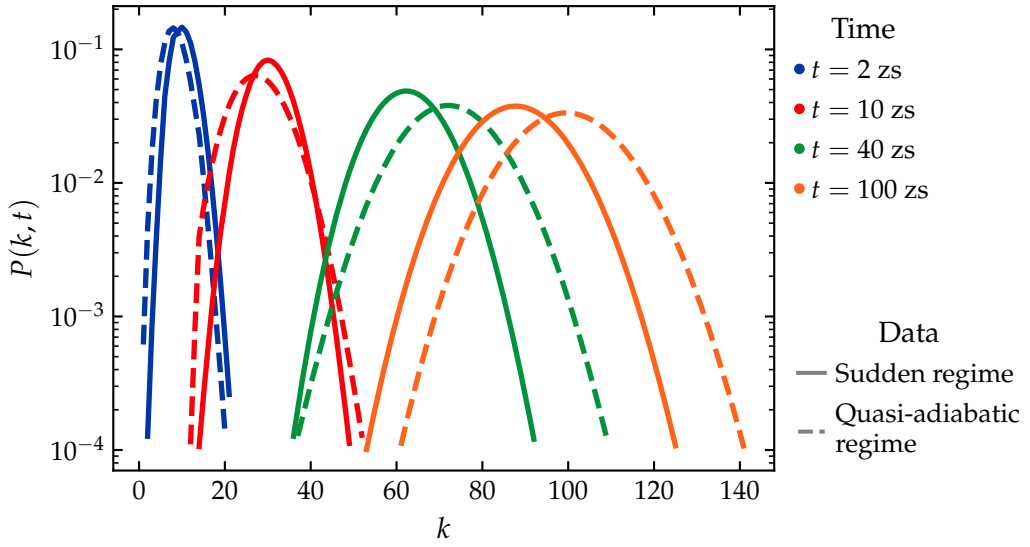

FIGURE IV.11: Same as Fig. IV.10, but $N\Gamma_{\text{dip}} = 5$ MeV.

On the other hand the results from our work do not show such a degree of saturation as the results in Ref. [19]. For high effective dipole rates and at late times our occupation probabilities reach lower energies in comparison to the quasi-adiabatic regime. Photon absorption may trigger a transition within the same particle-hole class or between two different classes, i.e. create an additional particle-hole pair. In the quasi-adiabatic calculation both of such scenarios are taken into account. However, our calculation assumes that absorbed photon can create an additional particle-hole pair only. Hence, omitting one of the transitions leads to lower excitation energies.

We also note that our results and the results from Ref. [19] for early times lie quite close to each other. On this timescale the excitation in both cases happens mostly via creation of a new particle-hole pairs. At low excitation energies most of the nucleons lie below the Fermi level, thus the first couple of dozens of photons have high probability to create a new particle-hole pair.

Fig. IV.12 shows that the orange curves are approaching each other. In the quasi-adiabatic calculation the saturation has already been reached and increasing $N\Gamma_{\text{dip}}$ or laser pulse duration further will not change the position of the orange dashed curve with respect to the number of absorbed photons k. Hence, it corresponds to the limit which the system will reach. What we see is that our occupation probability is approaching this limit. It is common for both calculations since the system that is considered is the same, and the processes are the same qualitatively though not quantitatively.

We mow proceed to include neutron evaporation for 3 generations, namely: target nucleus with A (Gen 0) nucleons, the first daughter with $A - 1$ (Gen 1) nucleons and the second daughter with $A - 2$ (Gen 2) nucleons. For the forth

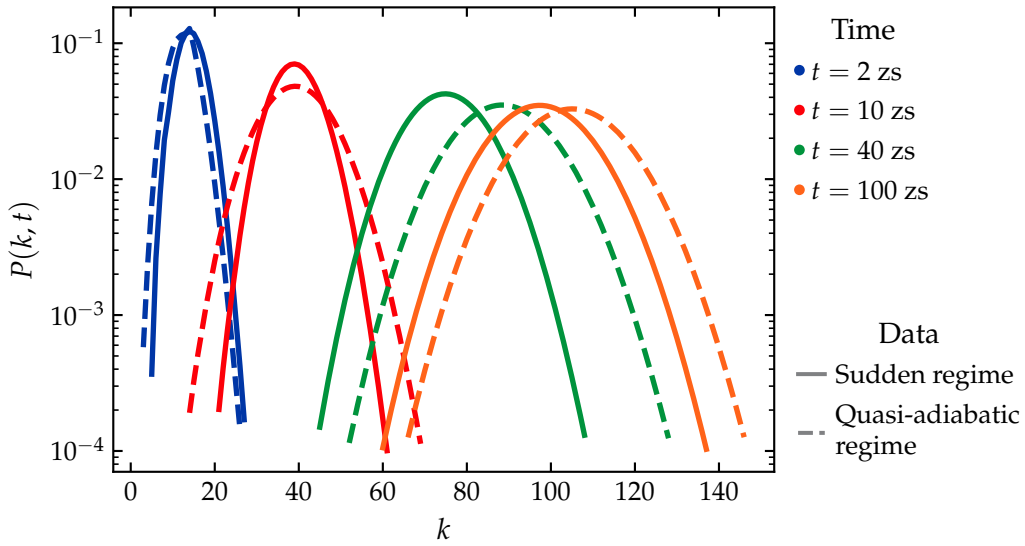

FIGURE IV.12: Same as Fig. IV.10, but $N\Gamma_{\text{dip}} = 8$ MeV.

generation with mass number $A - 3$ (Gen 3) we switch off neutron evaporation. Fig. IV.13 shows a qualitatively similar result to both constant spacing Fig. IV.13 and Ref. [19] calculations. Neutron evaporation does not take place unless several photons are absorbed. In the first three generations the saturation is not reached because the neutron evaporation prevents the probability flow towards the maximum of the total level density. The neutron evaporation dominates the photoexcitation of a given nucleus. After 20 zs the occupation probability of the target nucleus is lost to higher generations. We see that the dump nucleus approaches saturation regime since there is no competing mechanism for the photon absorption and the probability flows towards the maximum of the level density. One may expect qualitatively similar results for a chain of such reactions for many generations experiencing neutron evaporation. Such scenario may result in proton-rich medium-weight nuclei at high excitation energies.

We continue with the comparison of our results with the quasi-adiabatic regime investigated theoretically in Ref. [19]. The calculation for the quasi-adiabatic regime involves the target nucleus and four generations of daughter nuclei, where for the last one the neutron emission was switched off. In our work, we consider only three generations of daughter nuclei. Therefore, we can only compare the occupation probabilities for target nucleus and the first two generations, i.e., Gen 0, Gen 1 and Gen 2. The comparison for several values of time are presented in Figs. IV.14 to IV.16. At first sight suprisingly, for short times, the target nucleus gets much faster depleted in the quasi-adiabatic calculation. While for Gen 0 our results show that the target nucleus is still populated up to approx. 22 zs and reaches excitation energies of up to 250 MeV, this is not the case in the quasi-adiabatic case, where already for $t = 15$ zs the target nucleus is depleted. This original delay in depletion of the target nucleus can be also observed propagating through the following generations Gen 1 and Gen 2.

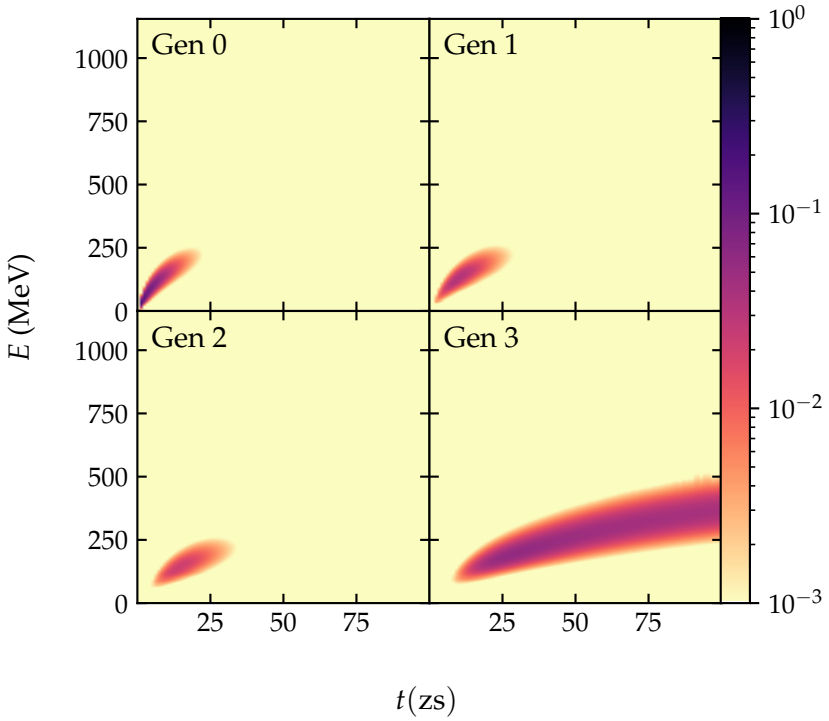

FIGURE IV.13: Total occupation probabilities summed over all particle-hole classes for 4 generations. $A = 100$, $N\Gamma_{\text{dip}} = 5$ MeV, $\tau = 100$ zs.

Prior to neutron decay, similar features to the comparison presented in Fig. IV.11 can be observed. We first note that for small excitation energies, the level densities used for the two regimes are calculated using different methods. In Ref. [19], the Bethe formula Eq. (II.1) is used for energies smaller than 68 MeV. This point corresponds to the kink at approx. $k = 13$ that can be observed in all three graphs in Figs. IV.14 to IV.16. Our calculation on the other hand uses extrapolations of the level densities at higher energies. A direct comparison between the quasi-adiabatic and sudden regimes at small energies is therefore only qualitatively possible.

However, this does not alter our observation that neutron emission appears to be stronger in the quasi-adiabatic calculation. Although a direct comparison between the neutron emission rates for the two cases is yet to be performed, we can speculate on important differences between the two approaches. First, it is clear that at short times and small excitation energies, the sudden regime system is rather far from equilibrium—since equilibration itself requires some time. In the quasiadiabatic calculation, it is assumed that complete equilibration takes place after every photon absorption. Second, neutron evaporation is assumed to take place only into the same particle-hole class in the sudden regime calculation. Since the particle-hole classes are not considered at all in the quasi-adiabatic approach, this restriction does not appear there. Finally, as we have already pointed out in the discussion around the comparison in Fig. IV.11, we did not take into account the absorption of a photon while remaining in the same class. However, since the neutron emission chains that we

investigate are already depleted at energies much smaller than the saturation energy and at short times, this aspect is less likely to play an important role in the differences shown in Figs. IV.14 to IV.16.

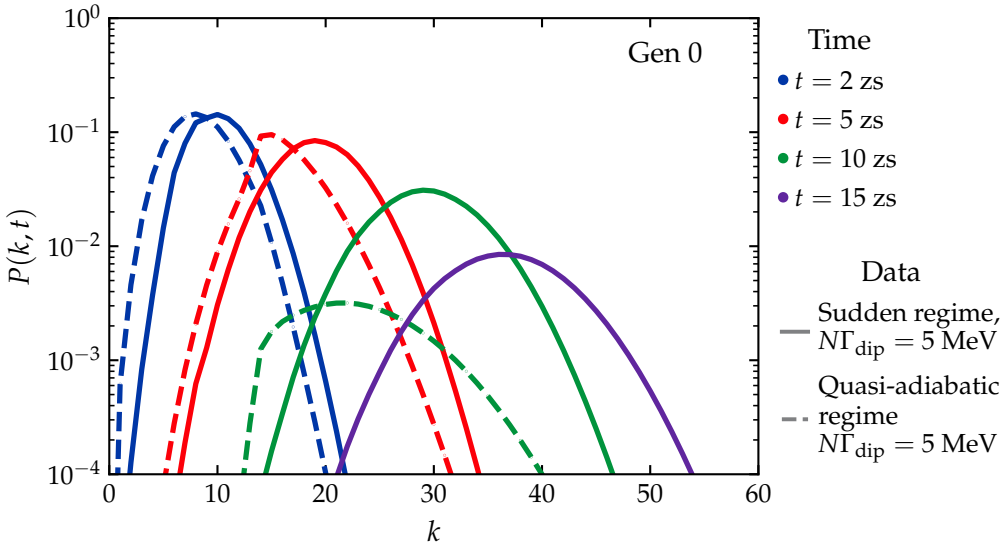

FIGURE IV.14: Comparison of occupation probabilities for target nucleus (Gen 0) calculated in the sudden regime (solid lines) and in the quasi-adiabatic regime Ref. [19] (dashed lines) as a function of number of absorbed photons for several time instants. $A = 100$, $N\Gamma_{\text{dip}} = 5$ MeV.

IV.3 Nuclear equilibration

We devote this short section to the demonstration of the way the nuclear equilibration between different particle-hole classes takes place. For the sake of simplicity we address the constant spacing model with $A = 42$, $B = 51$.

We consider only the target nucleus in the absence of neutron decay and laser field. Such a set up is described with the help of the master equation Eq. (I.4). The process of nuclear equilibration conserves the total excitation energy and the total occupation probability. This yields the result in Eq. (IV.4). The equilibrium distribution at energy E is achieved also in the absence of the laser pulse.

We solve the master equation Eq. (I.4) with initial condition being an occupied state at k_0 absorbed photons in class m_0. Since the laser pulse is switched off the nucleus relaxes via nucleon-nucleon interaction redistributing the initial excitation among other particle-hole classes. Ratios of occupation probabilities to level densities in Fig. IV.17 illustrate this relaxation process and eventual equilibrium distribution. The timescales of all four cases are of the order of 1 zs which corresponds to the characteristic time of interaction between the nucleons [25].

First, we compare initial configurations at the same energy, e.g., $k_0 = 15$ absorbed photons. Class $m_0 = 2$ (see Fig. II.2) is at lower level density and

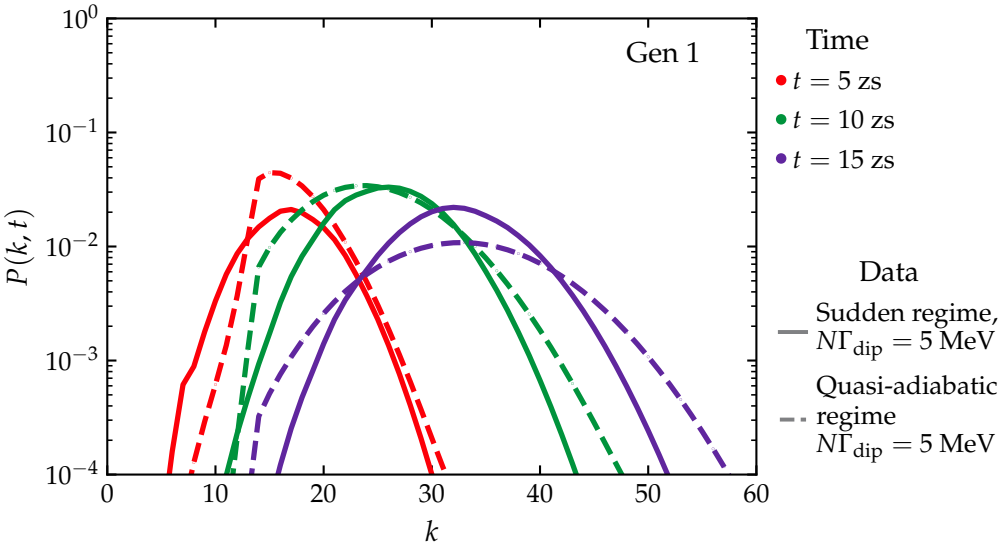

FIGURE IV.15: Same as Fig. IV.14 for the first daughter nucleus (Gen 1).

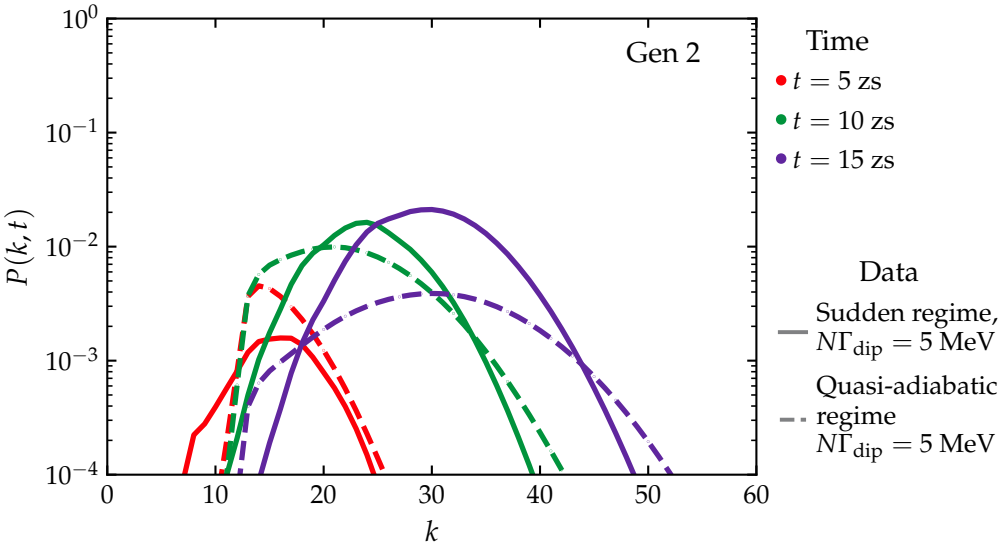

FIGURE IV.16: Same as Fig. IV.14 for the second daughter nucleus (Gen 2).

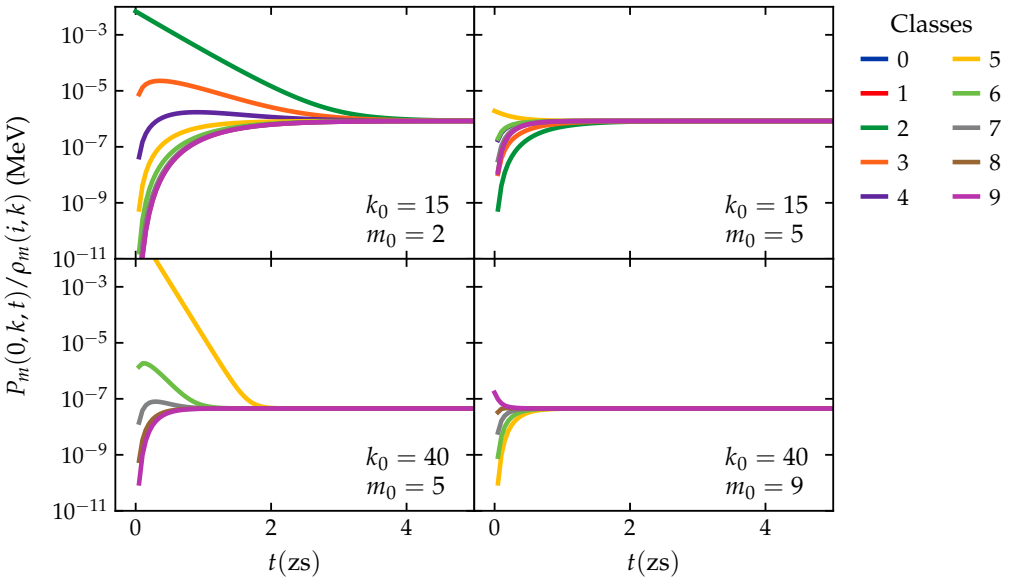

FIGURE IV.17: Equilibration between different particle-hole classes in the absence of neutron decay and laser field. Ratio of occupation probabilities in different particle-hole classes (coloring) to corresponding level densities as a function of time. k_0 and m_0 correspond to the initial condition.

populated by the same amount of occupation probability in comparison to class at $m_0 = 5$, i.e. $m_0 = 2$ is farther from the equilibrium distribution than $m_0 = 5$. Class $m_0 = 2$ at $k_0 = 15$ can transit only into class $m_0 = 3$ while $m_0 = 5$ at the same energy can transit to both $m_0 = 4$ and $m_0 = 6$. For class $m_0 = 2$ the probability has to be transfered over 8 classes subsequently, while for class $m_0 = 5$ the transitions can happen in both directions $5 \to 2$ and $5 \to 9$ simultaneously. More to that, the transition rates depend strongly on the level density, and transitions $2 \to 3$ are slower than transitions $5 \to 4$ and $5 \to 6$. Hence, slower transition rates, lower level density and smaller number of available transitions result in the initial class $m_0 = 2$ achieving equilibrium distribution slower than $m_0 = 5$ at energy $k_0 = 15$ absorbed photons. On the other hand, in the same initial class ($m_0 = 5$ in Fig. IV.17) in state $k_0 = 40$ the level density is lower and the number of available transitions is smaller, while the transition rate is faster than at $k_0 = 15$. Still $(m_0 = 5, k_0 = 40)$ attains equilibrium distribution slower than $(m_0 = 5, k_0 = 15)$. Hence, we can conclude that the equilibrium distribution $P_m(0,k,t \to \infty) \propto \rho_m(0,k)$ is attained via a complex interplay between the speed of transitions, the number of available transitions and the level densities.

Summary and Outlook

We have investigated theoretically the sudden regime of laser-nucleus interaction, in which multiple photon absorptions happen faster than nuclear nuclear relaxation processes. This work presents a follow up to works on the two other regimes: perturbative [17] and quasi-adiabatic regime [18, 19]. In our study we have considered the interplay between photoexcitation, equilibration and neutron evaporation. We have used master equations for the description of these competing process.

In the sudden regime the nucleus does not attain full equilibrium, hence, treatment of different particle-hole classes is required. The relaxation of the nucleus happens via nucleon-nucleon collisions in which different particle-hole classes redistribute initial excitation energy among all the other particle-hole classes. Hence, the particle-hole framework is essential for the description on the nuclear relaxation and its rate. We have described the rates for the dipole absorption and neutron evaporation as well in Section I.5 and Chapter III. All of them require densities for particle-hole classes. We have have derived the corresponding densities for particle-hole classes in Chapter II.

We have considered two models of single-particle densities: constant spacing model and linear dependence of single-particle density on energy. While the first one describes approximately single-particle levels distribution in light nuclei, the second one describes medium-weight nuclei. The constant spacing model was used only to illustrate the approach and calculations, as it is not realistic for medium-weight nuclei.

We use state-of-the-art matrix exponential solvers based on the Chebyshov rational approximation method to solve numerically the master equation.

The master equation describing the laser nucleus interaction in the sudden regime poses a stiff problem. The elements of the transition matrix can differ by 70 orders for nuclei with mass number $A = 100$. To numerically solve this problem, we use state-of-the-art matrix exponential solvers based on the Chebyshov rational approximation method Ref. [34, 35]. In Chapter IV we have first addressed a simpler case where neutron evaporation is disregarded and only two processes are considered: nuclear equilibration and photoexcitation. We have investigated the distribution of excitation among different particle-hole classes. The numerical calculation shows that saturation can be achieved in many particle-hole classes lying below the saturation point of the whole nucleus (the point where dipole absorption becomes less probable than stimulated dipole emission). The saturation in different particle-hole classes occurs at different times, hence, the saturation of the nucleus as a whole can not take place unless all the classes that can be populated below the

saturation point are saturated. By summing the occupation probabilities over the particle-hole classes we arrive at the total occupation probability.

We have compared the total occupation probabilities to the quasi-adiabatic regime from Ref. [19]. For the very early stages of photo-excitation up to 10 zs the occupation probabilities for both regimes have very similar values. At these times almost any incoming photon will trigger production of a particle-hole pair. For higher energies though, it appears that in our calculation the saturation is reached slower. We believe that this occurs due to our requirement that each photon absorption leads to the production of a new particle-hole pair, i.e., we do not account for transitions within the same particle-hole class. This limitation lowers the efficiency of attaining high excitation energies and, hence, the saturation happens slower in our calculations. As predicted in quasi-adiabatic regime, larger absorption rates lead to faster saturation.

The investigation of the laser-nucleus interaction taking into account neutron evaporation shows that the latter smears out the excitation among several generations of nuclei. The results show that neutron evaporation dominates photon absorption at energies lower than the saturation point. The target nucleus experiences neutron decay at early stages of excitation at low excitation energies (around 250 MeV for $A = 100$) and does not reach the saturation. This results in production of new daughter nuclei. Neutron evaporation can happen throughout the decay chain until the laser pulse terminates. This shows the same qualitative result that is yielded in the quasi-adiabatic regime. However, the comparison between the two regimes shows that the neutron decay happens slower in the sudden regime on the early stages of excitation. This calls for a more quantitative comparison between neutron decay rates from equilibrated and non-equilibrated particle-hole configurations.

Finally, in Section IV.3 we have briefly touched the topic of nuclear equilibration. For this we have considered the equilibration process starting from a certain excitation energy and initial particle-hole configuration. We have shown how different initial states can result in the total picture of nuclear equilibration. The total equilibration rate is of the order of 1 zs which corresponds to the characteristic time of nucleon collisions.

In conclusion, the novel theoretical, experimental and numerical developments in the direction of zeptosecond MeV pulses promise to open new avenues for the exploration of so far unexplored energy domain for compound nucleus. Multi-photon absorptions induced by a such pulse will bring the nucleus to the states far above the yrast line. The sudden regime of laser-nucleus interaction will allow a unique opportunity to study the decay mechanisms and nuclear reactions at high excitation energies. It is expected that such interaction will result in the production of nuclei in the proton-rich region of the chart of isotopes. Our approach is yet to be tested by the future experiments in the laser-nucleus field.

There is still room for further investigation and improvements of our work. Certain restrictions that we have used in our approach have turned out to limit the "sudden" character of the investigated regime. First, we have connected dipole absorption with the generation of a particle-hole pair. This will mostly be the case for small excitation energies, but with absorptions of more photons,

the competing dipole absorption without changing the particle-hole class becomes stronger. We believe that the inclusion of dipole transitions within the same particle-hole classes will allow to reach higher excitation energies and the saturation point faster.

Second, we have restricted the process of neutron evaporation to states in the same particle-hole class. This disregards the even-odd stagerring of nuclear binding energies and might have an influence on the magnitude of the neutron decay rate. Since the comparison between the sudden and quasi-adiabatic regimes has brought up surprising results, the exact magnitude of neutron decay rates from equilibrated and non-equilibrium configurations should be further investigated.

Another processes taking place in the nucleus, such as fission, nucleon excitation into continuum, pion production, could also be included. In principle, the investigation can be conducted for a model of single-particle density for heavy-weight nuclei ($A = 200$), though the numerical problem is expected to be even more challenging there. A comparison with quasi-adiabatic regime can be extended, i.e. taking into account more daughters, establishing the connection with the neutron decay rate for particle-hole classes and utilization of the level densities calculated in the same manner.

We hope that this work will help with further study of nuclear equilibration process and will be relevant for the layout of future experiments of laser-nucleus interactions.

APPENDIX A
Calculation of the level densities

Here we briefly present the method from Ref. [24] for the calculation of the nuclear level densities. A system of A noninteracting spinless fermions with total excitation energy E is considered. The fermions can occupy B non-degenerate single-particle levels $\varepsilon_1 < \varepsilon_2 < \cdots < \varepsilon_B$. The distribution of the levels is described by the single-particle density $\rho_1(\varepsilon)$. Such system can occupy

$$N = \binom{B}{A} \tag{A.1}$$

eigenstates. The energy of the ground state E_1 and the highest state E_N are introduced

$$E_1 = \sum_{j=1}^{A} \varepsilon_j \,, \tag{A.2}$$

$$E_N = \sum_{j=B+1-A}^{B} \varepsilon_j \,. \tag{A.3}$$

Then the Fermi-gas model is used to for the calculation of mean energy E_0. The Fermi distribution corresponding to the occupation probability of a single-particle state is

$$n_{A,E}\left(\varepsilon_j\right) = \frac{1}{1 + \exp\left\{\beta\varepsilon_j + \alpha\right\}} \,, \tag{A.4}$$

with α and β obtained as solutions of the equations

$$A = \sum_j n_{A,E}\left(\varepsilon_j\right), \quad E = \sum_j \varepsilon_j n_{A,E}\left(\varepsilon_j\right) \,, \tag{A.5}$$

where E is the total energy of the system. The mean energy is obtained by setting the temperature in the Fermi-distribution Eq. (A.4) to infinity

$$E_0 = \frac{A}{B} \sum_j \varepsilon_j \,. \tag{A.6}$$

The level density can be written in the following form

$$\rho_A(E) = \sum_{i=1}^{N} \delta\left(E - E_j\right) \,. \tag{A.7}$$

This can be written as

$$\rho_A(E) = \binom{B}{A} R_A(E) \ . \tag{A.8}$$

$R_A(E)$ is normalized to unity and differs from zero only in the interval $\{E_1, E_N\}$. It is then expanded in terms of orthogonal polynomials in this interval

$$R_A(E) = \sum_{n=1}^{\infty} r_A(n) T_n(E) \tag{A.9}$$

where the polynomials are

$$\begin{aligned} T_n(E) &= \sqrt{\frac{2}{L}} \sin\left\{\frac{1}{L}\pi n \left(E - E_c\right)\right\} \quad \text{for } n \text{ positive and even} \\ T_n(E) &= \sqrt{\frac{2}{L}} \cos\left\{\frac{1}{L}\pi n \left(E - E_c\right)\right\} \quad \text{for } n \text{ positive and odd} \end{aligned} \tag{A.10}$$

with the following definitions

$$L = E_N - E_1, \quad E_c = \frac{1}{2}\left(E_1 + E_N\right) \ . \tag{A.11}$$

And the coefficients are

$$\begin{aligned} r_A(n) &= \frac{1}{i}\sqrt{\frac{1}{2L}} \exp\left\{i\pi n \left(E_0 - E_c\right)/L\right\} \mathcal{F}_A(\pi n/L) + c.c. \quad \text{for } n \text{ positive and even} \\ r_A(n) &= \sqrt{\frac{1}{2L}} \exp\left\{i\pi n \left(E_0 - E_c\right)/L\right\} \mathcal{F}_A(\pi n/L) + c.c. \quad \text{for } n \text{ positive and odd} \end{aligned} \tag{A.12}$$

The Fourier transform $\mathcal{F}_A(\tau)$ is expressed via the moments $M_A(k)$ or cumulants $\kappa_A(k)$.

$$\mathcal{F}_A(\tau) = \exp\left\{\ln\left(1 + \sum_{k=2}^{\infty} \frac{i^k \tau^k}{k!} M_A(k)\right)\right\} = \exp\left\{\sum_{k=2}^{\infty} \frac{i^k \tau^k}{k!} \kappa_A(k)\right\} \tag{A.13}$$

These moments are the normalized moments of $\rho_A(k)$

$$M_A(k) = \int \mathrm{d}E \left(E - E_0\right)^k \rho_A(E)/N \ . \tag{A.14}$$

It turns out that it is possible to express them via the moments $\sum_{j=1}^{B} \left(\tilde{\varepsilon}_j\right)^l$ with $l < k$. Here

$$\tilde{\varepsilon}_j = \varepsilon_j - \Delta \ , \tag{A.15}$$

with

$$\Delta = \frac{1}{B}\sum_{j=1}^{B} \varepsilon_j = \frac{E_0}{A} \ . \tag{A.16}$$

From this point smooth single-particle density approximation $\bar{\rho}_1(\varepsilon)$ is

introduced to calculate the moments $\sum_{j=1}^{B}\left(\tilde{\varepsilon}_j\right)^l$. The single particle density is defined in the interval $0 \leq \varepsilon \leq V$. $\bar{\rho}_1(\varepsilon)$ defines the single-particle energies $\int_0^{\varepsilon_j} \mathrm{d}\varepsilon\bar{\rho}_1(\varepsilon) = j, \quad j = 1, \ldots, B$ From here the Fermi energy and the spectrum values can be obtained

$$\int_0^F \mathrm{d}\varepsilon\bar{\rho}_1(\varepsilon) = A \ , \tag{A.17}$$

$$E_1 = \int_0^F \mathrm{d}\varepsilon\varepsilon\bar{\rho}_1(\varepsilon), \quad E_N = \int_{E_{\mathrm{sup}}}^V \mathrm{d}\varepsilon\varepsilon\bar{\rho}_1(\varepsilon) \ , \tag{A.18}$$

where E_sup is defined by

$$A = \int_{E_{\mathrm{sup}}}^V \mathrm{d}\varepsilon\bar{\rho}_1(\varepsilon) \ . \tag{A.19}$$

The mean energy from Eq. (A.6) will turn into

$$E_0 = \frac{A}{B}\int_0^V \mathrm{d}\varepsilon\varepsilon\bar{\rho}_1(\varepsilon) \ . \tag{A.20}$$

Finally, the moments are expressed as

$$\sum_j \varepsilon_j^k = \int_0^V \mathrm{d}\varepsilon\varepsilon^k\rho_1(\varepsilon) \tag{A.21}$$

Now the single-particle density $\bar{\rho}_1(\varepsilon)$ can be used to calculate the total level density $\rho_A(E)$.

Th choice of the single-particle level density dictates the relation between A, B, F and V. We will consider

- constant spacing $\bar{\rho}_1(\varepsilon) = A/F$
- linear dependence $\bar{\rho}_1(\varepsilon) = 2A/F^2\varepsilon\varepsilon$

The total number B of single-particle levels is given by

$$B = \int_0^V \mathrm{d}\varepsilon\bar{\rho}_1(\varepsilon) \ . \tag{A.22}$$

For the constant spacing this gives

$$B = A\frac{V}{F} \tag{A.23}$$

and for the linear model

$$B^{(1)} = A\frac{V^2}{F^2} \ , \tag{A.24}$$

where the superscript '1' is used to distinguish from the constant spacing model.

APPENDIX B

Particle-hole level densities for constant spacing

As mentioned inSection II.2 the level density of a particle-hole class is a convolution of corresponding densities Eq. (II.3). With equal number of particles and equal number of holes in the framework of the method of Ref. [24] this would correspond to the convolution of two Fourier transforms

$$\mathcal{F}_{A-p,p}(\tau) = \mathcal{F}_{A-p}(\tau)\mathcal{F}_{p}(\tau) \,, \tag{B.1}$$

From this point the moments and the spectrum are needed to obtain the level densities ρ_m.

We consider the single-particle density $\bar{\rho}_1 = A/F$, where F is the Fermi energy for A particles, such that the energy level with number A corresponds to the Fermi energy. The single-particle density remains the same also for particles above Fermi-level, since it dictates the distribution of single-particle levels, regardless of their position with respect to F. From here on in this Appendix, since we are dealing with p particles and p holes, a subscript $A-p$ will signify that we are talking about a value for holes and a subscript p will signify that we are talking about particles above Fermi level.

II.1 Holes

First we carry out the calculation for the holes. We consider $A-p$ particles distributed over A levels with single-particle energies ranging from 0 to F.

We start with the spectrum range. A state with the highest excitation energy has all levels from E_{sup} to F populated

$$A - p = \int_{E_{sup}}^{F} \mathrm{d}\varepsilon\, \bar{\rho}_1(\varepsilon) = \frac{A}{F}(F - E_{sup}) \,, \tag{B.2}$$

$$E_{sup} = F - \frac{A-p}{A}F = \frac{p}{A}F \,, \tag{B.3}$$

$$E_{A-p,N} = \int_{E_{sup}}^{F} \mathrm{d}\varepsilon\, \varepsilon\bar{\rho}_1(\varepsilon) = \frac{A}{F}\frac{F^2 - E_{sup}^2}{2} \,, \tag{B.4}$$

where $E_{A-p,N}$ is the energy of the highest state of $A-p$ particles. The 'ground state' with states populated from 0 to F_h is described by

$$A-p=\int_0^{F_h}\mathrm{d}\varepsilon\,\bar{\rho}_1(\varepsilon)=\frac{A}{F}F_h\,, \tag{B.5}$$

$$F_h=\frac{A-p}{A}F\,, \tag{B.6}$$

$$E_{A-p,1}=\int_0^{F_h}\mathrm{d}\varepsilon\,\varepsilon\bar{\rho}_1(\varepsilon)=\frac{A}{F}\frac{F_h^2}{2}\,, \tag{B.7}$$

where $E_{A-p,1}$ is the ground state energy of $A-p$ particles. The Fermi distribution

$$n_{A-p,E}(\varepsilon)=\frac{\Theta(F-\varepsilon)}{1+\exp\left\{\beta_E\varepsilon+\alpha_{A-p,E}\right\}} \tag{B.8}$$

allows to calculate the mean energy $E_{A-p,0}$ of a Fermi gas with $A-p$ particles. First, the number of particles and total energy can be expressed as

$$A-p=\int_0^{F}\mathrm{d}\varepsilon\,n_{A-p,E}(\varepsilon)\bar{\rho}_1(\varepsilon),\quad E=\int_0^{F}\mathrm{d}\varepsilon\,\varepsilon n_{A-p,E}(\varepsilon)\bar{\rho}_1(\varepsilon)\,, \tag{B.9}$$

Setting $\beta_E=0$ (the temperature of the Fermi-gas is infinite) gives the energy

$$A-p=\int_0^{F}\mathrm{d}\varepsilon\,\frac{1}{1+\exp\{\alpha\}}\bar{\rho}_1(\varepsilon)=A\frac{1}{1+\exp\{\alpha\}}\,, \tag{B.10}$$

$$E_{A-p,0}=\frac{A-p}{A}\int_0^{F}\mathrm{d}\varepsilon\,\varepsilon\bar{\rho}_1(\varepsilon)=\frac{A-p}{A}\frac{A}{F}\frac{F^2}{2}=\frac{A-p}{2}F\,. \tag{B.11}$$

At this point we can calculate the moments for single-particle density, which can be evaluated for continuous approximation of single-particle density

$$\sum_{j=1}^{A}\varepsilon_j^l=\int_0^{F}\mathrm{d}\varepsilon\,\varepsilon^l\bar{\rho}_1(\varepsilon)=\frac{A}{F}\frac{F^{l+1}}{l+1}\,. \tag{B.12}$$

We proceed with the mean energy

$$E_0=\frac{A-p}{A}\int_0^{F}\mathrm{d}\varepsilon\,\varepsilon\bar{\rho}_1(\varepsilon)=\frac{A-p}{2}F \tag{B.13}$$

and

$$\Delta_h=\frac{1}{A}\sum_{j=1}^{A}\varepsilon_j=\frac{1}{A}\int_0^{F}\mathrm{d}\varepsilon\,\varepsilon\bar{\rho}_1(\varepsilon)=\frac{E_0}{A-p}=\frac{F}{2}\,. \tag{B.14}$$

Then we calculate the following moments

$$\sum_{j=1}^{A}(\tilde{\varepsilon}_j)^l = \sum_{j=1}^{A}(\varepsilon_j - \Delta_h)^l = \sum_{j=1}^{A}\sum_{m=0}^{l}(-1)^{l-m}\binom{l}{m}(\varepsilon_j)^m \Delta_h^{l-m} =$$

$$= \sum_{m=0}^{l}(-1)^{l-m}\binom{l}{m}\frac{AF^m}{m+1}\left(\frac{F}{2}\right)^{l-m} =$$

$$= AF^l \sum_{m=0}^{l}(-1)^{l-m}\binom{l}{m}\left(\frac{1}{2}\right)^{l-m}\frac{1}{m+1} =$$

$$= \frac{A}{F}F^{l+1}\sum_{m=0}^{l}(-1)^{l-m}\binom{l}{m}\int_0^1 \mathrm{d}x\, x^m \left(\frac{1}{2}\right)^{l-m} =$$

$$= \frac{A}{F}F^{l+1}\int_0^1 \mathrm{d}x\,(x-\frac{1}{2})^l = \frac{A}{F}F^{l+1}\left[\frac{1}{l+1}y^{l+1}\right]\Bigg|_{y=-\frac{1}{2}}^{y=+\frac{1}{2}}. \quad \text{(B.15)}$$

Thus, all ingredients for the calculation of the level density of $A-p$ particles distributed over A levels with single-particle energies from 0 to F are available.

II.2 Particles

In this case p particles above the Fermi level are distributed over $B-A$ single-particle levels with single particle energies form F to V. Here the same formalism presented above with corresponding replacement of the limits in the integrals for moments and spectrum values is applied. First we obtain the spectrum values

$$p = \int_{E_{sup}}^{V}\mathrm{d}\varepsilon\,\bar{\rho}_1(\varepsilon) = \frac{A}{F}(V - E_{sup})\,, \quad \text{(B.16)}$$

$$E_{sup} = V - \frac{p}{A}F\,; \quad \text{(B.17)}$$

$$p = \int_{F}^{F_p}\mathrm{d}\varepsilon\,\bar{\rho}_1(\varepsilon) = \frac{A}{F}(F_p - F)\,, \quad \text{(B.18)}$$

$$F_p = \left(1+\frac{p}{A}\right)F\,; \quad \text{(B.19)}$$

$$E_{p,1} = \int_{F}^{F_p}\mathrm{d}\varepsilon\,\varepsilon\bar{\rho}_1(\varepsilon) = \frac{A}{F}\frac{F_p^2 - F^2}{2}\,, \quad \text{(B.20)}$$

$$E_{p,N} = \int_{E_{sup}}^{V}\mathrm{d}\varepsilon\,\varepsilon\bar{\rho}_1(\varepsilon) = \frac{A}{F}\frac{V^2 - E_{sup}^2}{2}\,, \quad \text{(B.21)}$$

where $E_{p,1}$ is the energy of p particles occupying all states from F to F_p and $E_{p,N}$ is the energy of the highest state of p particles. The Fermi distribution of

a gas of p particles above the Fermi level F of the system of A particles reads

$$n_{p,E}(\varepsilon) = \frac{\Theta(\varepsilon - F)}{1 + \exp\left\{\beta_E \varepsilon + \alpha_{p,E}\right\}} \,. \tag{B.22}$$

We arrive to the expressions for the number of particles and total energy of p particles

$$p = \int_F^V \mathrm{d}\varepsilon \, n_{p,E}(\varepsilon)\bar{\rho}_1(\varepsilon), \quad E = \int_F^V \mathrm{d}\varepsilon \, \varepsilon n_{p,E}(\varepsilon)\bar{\rho}_1(\varepsilon) \,. \tag{B.23}$$

Applying the limit of infinite temperature $\beta_E = 0$ of this Fermi gas we can obtain the mean energy $E_{p,0}$

$$p = \int_F^V \mathrm{d}\varepsilon \, \frac{1}{1 + \exp\{\alpha\}} \bar{\rho}_1(\varepsilon) = \frac{A}{F}(V - F)\frac{1}{1 + \exp\{\alpha\}} \,, \tag{B.24}$$

$$E_{p,0} = \frac{p}{A}\frac{F}{V - F}\int_F^V \mathrm{d}\varepsilon \, \varepsilon\bar{\rho}_1(\varepsilon) = \frac{p}{A}\frac{F}{V - F}\frac{V^2 - F^2}{2} = p\frac{V + F}{2} \,. \tag{B.25}$$

The moments of the level density are

$$\sum_{j=A+1}^{B} \varepsilon_j^l = \int_F^V \mathrm{d}\varepsilon \, \varepsilon^l \bar{\rho}_1(\varepsilon) = \frac{A}{F}\frac{V^{l+1} - F^{l+1}}{l + 1} \,; \tag{B.26}$$

$$\Delta_p = \frac{1}{B - A}\sum_{j=A+1}^{B} \varepsilon_j = \frac{1}{B - A}\int_F^V \mathrm{d}\varepsilon \, \varepsilon\bar{\rho}_1(\varepsilon) = \frac{V + F}{2} \,, \tag{B.27}$$

where $B = A\frac{V}{F}$ (Eq. (A.23)) is taken into account.

Now we can calculate the following moments

$$\sum_{j=A+1}^{B}(\tilde{\varepsilon}_j)^l = \sum_{j=A+1}^{B}(\varepsilon_j-\Delta_p)^l = \sum_{j=A+1}^{B}\sum_{m=0}^{l}(-1)^{l-m}\binom{l}{m}(\varepsilon_j)^m\Delta_p^{l-m} =$$

$$= \sum_{m=0}^{l}(-1)^{l-m}\binom{l}{m}\frac{A}{F}\frac{V^{m+1}-F^{m+1}}{m+1}\left(\frac{V+F}{2}\right)^{l-m} =$$

$$= \frac{A}{F}V\sum_{m=0}^{l}(-1)^{l-m}\binom{l}{m}V^m\int_0^1 \mathrm{d}x\, x^m\left(\frac{V+F}{2}\right)^{l-m} -$$

$$- A\sum_{m=0}^{l}(-1)^{l-m}\binom{l}{m}F^m\int_0^1 \mathrm{d}x\, x^m\left(\frac{V+F}{2}\right)^{l-m} =$$

$$= \frac{AV}{F}\int_0^1 \mathrm{d}x\left(Vx-\frac{V+F}{2}\right)^l - A\int_0^1 \mathrm{d}x\left(Fx-\frac{V+F}{2}\right)^l =$$

$$= \frac{A}{F}\int_0^V \mathrm{d}Vx\left(Vx-\frac{V+F}{2}\right)^l - \frac{A}{F}\int_0^F \mathrm{d}Fx\left(Fx-\frac{V+F}{2}\right)^l =$$

$$= \frac{A}{F}\int_F^V \mathrm{d}y\left(y-\frac{V+F}{2}\right)^l = \frac{A}{F}\frac{1}{l+1}\left[\left(\frac{V-F}{2}\right)^{l+1} - \left(-\frac{V-F}{2}\right)^{l+1}\right] =$$

$$= \frac{A}{F}(V-F)^{l+1}\left[\frac{1}{l+1}y^{l+1}\right]\Bigg|_{y=-\frac{1}{2}}^{y=+\frac{1}{2}}. \quad \text{(B.28)}$$

Thus, all ingredients for the particle-hole density are obtained and we can write

$$\rho_{A-p,p}(E) = N_{A-p}N_p\sum_1^\infty r_{A-p,p}(n)T_n(E), \quad \text{(B.29)}$$

where (cf. Eq. (A.12))

$$r_{A-p,p}(n) = \frac{1}{i}\sqrt{\frac{1}{2L}}\exp\{i\pi n(E_0-E_c)/L\}F_{A-p,p}(\frac{\pi n}{L}) + c.c. \quad \text{for } n>0, \text{ even},$$

$$r_{A-p,p}(n) = \sqrt{\frac{1}{2L}}\exp\{i\pi n(E_0-E_c)/L\}F_{A-p,p}(\frac{\pi n}{L}) + c.c. \quad \text{for } n>0, \text{ odd}.$$

APPENDIX C
Linear model

The calculations follow exactly the same steps as in Appendix B up to the replacement of single-patricle density by $\bar{\rho}_1^{(1)}(\varepsilon)$ (where superscript '1' is used to distinguish from the constant spacing model) and the relation between A, B, F and V is Eq. (A.24). Here we just list the relevant quantities.

III.1 Holes

Values for the spectrum are

$$E_{sup}^{(1)} = \left(\frac{p}{A}\right)^{\frac{1}{2}} F \,, \tag{C.1}$$

$$F_h^{(1)} = \left(\frac{A-p}{A}\right)^{\frac{1}{2}} F \,, \tag{C.2}$$

$$E_1^{(1)} = \frac{2}{3}\frac{A}{F^2}(F_h^{(1)})^3 \,, \tag{C.3}$$

$$E_N^{(1)} = \frac{2}{3}\frac{A}{F^2}(F^3 - (E_{sup}^{(1)})^3) \,. \tag{C.4}$$

$$E_{A-p,0}^{(1)} = \frac{2}{3}(A-p)F \,. \tag{C.5}$$

The moments are

$$\sum_{j=1}^{A}(\varepsilon_j^{(1)})^l = \frac{2A}{F^2}\frac{F^{l+2}}{l+2} \,, \tag{C.6}$$

$$\Delta_h^{(1)} = \frac{2}{3}F \,, \tag{C.7}$$

$$\sum_{j=1}^{A}(\tilde{\varepsilon}_j^{(1)})^l = \frac{2A}{F^2}F^{l+2}\left[\frac{y^{l+2}}{l+2} + \frac{2}{3}\frac{y^{l+1}}{l+1}\right]\Bigg|_{y=-\frac{2}{3}}^{y=+\frac{1}{3}} \,. \tag{C.8}$$

III.2 Particles

The same as in previous Section but for particles. Values for the spectrum and the moments are

$$E_{sup}^{(1)} = \left(V^2 - \frac{p}{A}F^2\right)^{\frac{1}{2}} \; ; \tag{C.9}$$

$$F_p^{(1)} = \left(\frac{A+p}{A}\right)^{\frac{1}{2}} F \; ; \tag{C.10}$$

$$E_1^{(1)} = \frac{2}{3}\frac{A}{F^2}\left[(F_p^{(i)})^3 - F^{i+2}\right] \; , \tag{C.11}$$

$$E_N^{(1)} = \frac{2}{3}\frac{A}{F^2}\left[V^3 - (E_{sup}^{(1)})^{i+2}\right] \; . \tag{C.12}$$

$$E_{p,0}^{(1)} = p\frac{2}{3}\frac{V^3 - F^3}{V^2 - F^2} \; . \tag{C.13}$$

$$\Delta_p^{(1)} = \frac{2}{3}\frac{V^3 - F^3}{V^2 - F^2} \; . \tag{C.14}$$

$$\sum_{j=A+1}^{B} (\tilde{\varepsilon}_j^{(1)})^l = \frac{2A}{F^2}\left[\frac{y^{l+2}}{l+2} + \Delta_p^{(1)}\frac{y^{l+1}}{l+1}\right]\Bigg|_{y=F-\Delta_p^{(1)}}^{y=V-\Delta_p^{(1)}} \; . \tag{C.15}$$

APPENDIX D
Symmetric form of master equation

To get a more convenient form of the master equation for all generations of nuclei we need to symmetrize it. We start from Eq. (I.10) and introduce the following notations

$$
\begin{aligned}
X_{mm'}(i;k) &= V^2_{mm'}\rho^{1/2}_m(i,k)\rho^{1/2}_{m'}(i,k)\ , \\
Y_{mm'}(i;k,k') &= W^2_{mm'}\rho^{1/2}_m(i,k)\rho^{1/2}_{m'}(i,k')\ ; \\
\tilde{M}_{k,m;k'm'}(i) &= \delta_{kk'}\left\{ X_{mm'}(i;k) - \delta_{mm'}\sum_{m''}\rho^{-1/2}_m(i,k)X_{mm''}(i;k)\rho^{1/2}_{m''}(i,k)\right\} \\
&\quad + \Theta(1/\sigma - t)\Big\{(1-\delta_{kk'})Y_{mm'}(i;k,k') \\
&\quad - \delta_{kk'}\delta_{mm'}\sum_{k''\neq k}\sum_{m''}\rho^{-1/2}_m(i,k)Y_{mm''}(i;k,k'')\rho^{1/2}_{m''}(i,k'')\Big\}\ .
\end{aligned}
$$

We rewrite the master equation (I.10)

$$
\begin{aligned}
&\left[\rho^{-3/2}_m(i,k)\dot{\Pi}_m(i,k,t)\right] = \sum_{k',m'}\tilde{M}_{k,m;k',m'}(i)\left[\rho^{-3/2}_{m'}(i,k')\Pi_{m'}(i,k',t)\right] \\
&+ \sum_{k',m'}\Gamma_N(i-1,k'\to k,m')\rho^{-1/2}_{m'}(i-1,k')\rho^{-1/2}_m(i,k) \\
&\times\left[\rho^{-3/2}_{m'}(i-1,k')\Pi_{m'}(i-1,k',t)\right] \\
&-\Gamma_N(i,k,m)\left[\rho^{-3/2}_m(i,k)\Pi_m(i,k,t)\right]\ .
\end{aligned}
\tag{D.1}
$$

Introducing the following substitution

$$
M_{k,m;k',m'}(i) = \tilde{M}_{k,m;k',m'}(i) - \delta_{mm'}\delta_{kk'}\Gamma_N(i,k,m)\ , \tag{D.2}
$$

and omitting the i dependence of the matrix for brevity we come to the following matrix equation

$$
\dot{\tilde{R}}(t) = M\tilde{R}(t) + C(t)\ , \tag{D.3}
$$

where $\tilde{R}(t)$ is a column vector which determines the occupation probabilities and $C(t)$ is a column vector corresponding to the feeding term

$$\begin{aligned}
\tilde{R}_{k,m,i}(t) =& \rho_m^{-3/2}(i,k)\Pi_m(i,k,t), \\
C_{k,m,i}(t) =& \sum_{k',m'} \Gamma_N(i-1,k' \to k, m' \to m) && \text{(D.4)} \\
& \times \left[\rho_{m'}^{-3/2}(i-1,k')\Pi_{m'}(i-1,k',t)\right] && \text{(D.5)} \\
& \times \rho_{m'}^{-1/2}(i-1,k')\rho_m^{-1/2}(i,k)\ .
\end{aligned}$$

This expression can be generalized further for all generations of nuclei, more to that, it yields matrix $\mathcal{M}$ which is time-independent:

$$\dot{\mathcal{P}}(t) = \mathcal{M}\mathcal{P}(t)\ , \tag{D.6}$$

where the elements of vector-column $\mathcal{P}$ contain the occupation probabilities $\mathcal{P}_j = \rho_m^{-1/2}(i,k)P_m(i,k,t)$. The index j depends on the nuclear species i, number of absorbed photons k, and particle-hole class m. An initial condition can be introduced at this point, completing the statement of the problem.

Bibliography

[1] *Extreme light infrastructure nuclear physics*, https://www.eli-np.ro (2020 (accessed April 8, 2020)).

[2] *Zetta- and exawatt science and technology*, https://portail.polytechnique.edu/izest (2020 (accessed April 8, 2020)).

[3] W. Płaczek et al., Acta Physica Polonica B **50**, 1191 (2019).

[4] D. Budker et al., *Atomic physics studies at the Gamma Factory at CERN*, arxiv:2003.03855 [atom-ph], Mar. 2020.

[5] A. Einstein, Annalen der Physik **322**, 891 (1905).

[6] D. Kiefer et al., Nature Communications **4** (2013).

[7] J. Mu et al., Applied Physics Letters **103**, 261114 (2013).

[8] G. Mourou and T. Tajima, Science **331**, 41 (2011).

[9] S. V. Bulanov et al., Physics-Uspekhi **56**, 429 (2013).

[10] D. Kiefer et al., The European Physical Journal D **55**, 427 (2009).

[11] J. Meyer-ter-Vehn and H.-C. Wu, The European Physical Journal D **55**, 433 (2009).

[12] T. Z. Esirkepov et al., The European Physical Journal D **55**, 457 (2009).

[13] F. Y. Li et al., Applied Physics Letters **105**, 161102 (2014).

[14] A. Pálffy, P.-G. Reinhard, and H. A. Weidenmüller, Physical Review C **101** (2020).

[15] D. Agassi, Physics Reports **22**, 145 (1975).

[16] M. Herman, G. Reffo, and H. Weidenmüller, Nuclear Physics A **536**, 124 (1992).

[17] H. A. Weidenmüller, Physical Review Letters **106** (2011).

[18] A. Pálffy and H. Weidenmüller, Physical Review Letters **112** (2014).

[19] A. Pálffy, O. Buss, A. Hoefer, and H. A. Weidenmüller, Physical Review C **92** (2015).

[20] H. A. Bethe, Physical Review **50**, 332 (1936).

[21] T. Ericson, Advances in Physics **9**, 425 (1960).

[22] P. Obložinský, Nuclear Physics A **453**, 127 (1986).

[23] A. Pálffy and H. A. Weidenmüller, Physics Letters B **718**, 1105 (2013).

[24] A. Pálffy and H. A. Weidenmüller, Nuclear Physics A **917**, 15 (2013).

[25] J. M. Blatt and V. F. Weisskopf, *Theoretical nuclear physics* (Springer Science and Business Media, New York, 2012).

[26] M. G. Mayer and J. H. D. Jensen, *Elementary theory of nuclear shell structure* (Wiley, New York, 1955).

[27] N. Bohr, Nature **137**, 344 (1936).

[28] A. Pálffy and H. Weidenmüller, "Compound nucleus formation by irradiation of nuclei with a multi–mev femtosecond laser pulse", Unpublished draft, 2012.

[29] G. F. Bertsch et al., Phys. Rev. C **79**, 034306 (2009).

[30] C. Bloch, Physique Nucleaire, Ecole d'Eté des Houches, 303 (1968).

[31] J. Jeukenne, A. Lejeune, and C. Mahaux, Physics Reports **25**, 83 (1976).

[32] C. Mahaux, P. Bortignon, R. Broglia, and C. Dasso, Physics Reports **120**, 1 (1985).

[33] C. Kalbach-Cline, Nuclear Physics A **210**, 590 (1973).

[34] M. Pusa, Nuclear Science and Engineering **169**, 155 (2011).

[35] M. Pusa, Nuclear Science and Engineering **182**, 297 (2016).

Acknowledgements

In this last page I would like to express my gratitude to people which contributed, directly or indirectly, to my work and helped me to adapt and experience a new cultural environment here in Germany.

First and foremost, I am grateful to PD Dr. Adriana Pálffy-Buß, my supervisor. I would like to thank her especially for her patience, time and support that she contributed while guiding me through this project. I can hardly imagine completing this work without her professional scientific advice and her skill in keeping things in order.

I am also greatly indebted to Professor Emeritus Hans-Arwed Weidenmüller, my second supervisor. He shared his wisdom and knowledge through countless discussions and comments. His expertise, intuitions and insight in physics contributed greatly to this work. I thank him for his patience, time and support as well.

I want to thank my third supervisor Prof. Dr. Selim Jochim and his group. My visits to the journal club of his group were always warmly welcomed. The interaction and discussions on potential collaboration helped me get a glimpse of the state of the art experiments in ultracold quantum gases.

I am thankful to apl. Prof. Dr. Georg Wolschin for his time and willingness to review this thesis.

I would like to thank Prof. Dr. Werner Aeschbach and Prof. Dr. Selim Jochim for their time and eagerness to be my examiners.

I thank Honorarprofessor Dr. Christoph H. Keitel for providing me with the opportunity to work in his division and the MPIK, as well as all of my colleagues and, especially Sibel Babacan. I am thankful to the administration of MPIK who created a stimulating working environment.

I am grateful to SFB1225 ISOQUANT for the financial support of this work and the granting of an extension.

I acknowledged countless useful discussions with Prof. Dr. Nikolay Minkov, Dr. Oleg Skoromnik, Dr. Sergey Bragin, Dr. Alessandro Angioi, Dr. Salvatore Castrignano, Dr. André Gontijo Campos.

I am greatly thankful to my friend Archana Sampath, whom I got to know very well, not only did she share an office with me but also many discussions, jolly moments and dilemmas.

Similarly, I would like to express my gratitude to other friends. Thank you to Dominik Lentrodt, Maitreyi Sangal, Daniel Bakucz-Canário, Dr. Fabien Niel, Kamil Dzikowski, Petar Andrejić, Halil Cakir, Igor Valuev, Dr. Erez Raicher, Dr. Pavlo Bilous, Dr. Xiangjin Kong, Janko Nauta, Jullian Stark for sharing not only working environment but also free time. I am especially grateful to Petar Andrejić, Kamil Dzikowski, Daniel Bakucz-Canário, and Dominik Lentrodt for reading and giving their feedback on some parts of my thesis.

I am extremely thankful to my mother and my father for everything they did for me.